PROGRESS REPORT TO THE NATIONAL AERONAUTICS

AND SPACE ADMINISTRATION

FACILITY FORM 602

N64 28891 (ACCESSION NUMBER)	(THRU)
200 (PAGES)	1 (CODE)
CR 58625 (NASA CR OR TMX OR AD NUMBER)	23 (CATEGORY)

Research Grant No. NsG 239-62

August, 1964

Prepared by the
Texas Engineering Experiment Station
Space Technology Division

Texas A&M University
College Station, Texas

OTS PRICE

XEROX $ 13.50ph

MICROFILM $ ______

REPORTS CONTROL No.

PROGRESS REPORT TO THE NATIONAL AERONAUTICS AND SPACE ADMINISTRATION

Research Grant No. NsG 239-62

August, 1964

Report submitted by

ORIGINAL SIGNED BY
H. E. WHITMORE

Harry E. Whitmore
Head, Space Technology Division

Prepared by the

Texas Engineering Experiment Station
Space Technology Division

Texas A&M University
College Station, Texas

INDEX

SUMMARY

Research at Texas A&M University under NASA Grant NsG 239-62 now consists of eight major projects which are covered in this report. All of these projects were being pursued at the time of the last semi-annual report.

This report contains only a technical presentation on the various projects. The fiscal report is submitted quarterly on NASA forms 1030 and 1031.

It should be mentioned here that a new building to house Activation Analysis and the Space Technology Division is to be built on the campus in the near future. This building, having a total gross area in excess of 30,000 square feet, will permit the physical consolidation of the various Space Technology research projects and will lead to a considerable expansion of space-oriented research. Space and equipment will be provided initially for research in activation analysis, space structures, applied plasma physics, space life sciences, and space electronics. The breadth of research will eventually be expanded to include most space oriented disciplines. In view of the new building and the additional research capabilities that will be provided, a new and expanded proposal for NASA sponsored research will be submitted prior to 1 November 1964.

SPACE TECHNOLOGY PROJECT NO. 2

STUDIES BASIC TO CLOSED MINIMUM VOLUME BIOLOGICAL WASTE UTILIZATION UNITS

STUDIES BASIC TO CLOSED MINIMUM VOLUME BIOLOGICAL WASTE UTILIZATION UNITS

Project Investigators

Joseph H. Sorrels, Professor of Sanitary Engineering and Research Engineer

W. W. Meinke, Associate Professor of Chemical Engineering and Head of the Chemurgic Research Laboratory

I. Introduction

Prior research data obtained for this investigation have indicated the merits of an activated sludge system for the stabilization of body wastes voided by man. The data of this report represent an extension of the activated sludge investigation - an extension directed toward an evaluation of the response of the sludge to continuous increased loading with a blend of feces and urine.

Conventional activated sludge installations of municipal sewage treating plants attempt to maintain around 0.2% sludge solids in the aeration chambers receiving the settled sewage influent with a BOD value which may range from 150 to 300 ppm. To achieve the desired level of sludge in the aeration chambers it is necessary to remove excess sludge and either discard or process the excess - or utilize it in "modified" activated sludge processes.

The earlier studies with activated sludge - as well as the results of this report - are in reality not a true "activated sludge" system. However, for ease of terminology in presenting the findings of the research, the term activated sludge has been employed in investigations involving the aeration of mixtures of body wastes and preformed sludge.

II. Experimental Approachs and Materials

A. Activated Sludge Preparation

The activated sludge used in these investigations has the same origin as that used in experiments reported in earlier reports; namely, the sludge preparation was started with material taken from the secondary settling tank following a standard rate trickling filter of a municipal sewage treatment plant. The sludge or material taken from the settling tank was fed for 15 days with settled sewage influent and then maintained with daily additions of 50 ml of a feces-urine (F-U) blend containing 50 grams of feces per 50 ml of urine. At the start of the experiments of this report the sludge contained approximately one per cent dry suspended solids. This value was ascertained by centrifuging 200 ml of the sludge suspension at 1500 RPM for 10 minutes. The supernatant was decanted and the solids were then dried - yielding approximately 2 grams of dry solids per 200 ml of sludge suspension. The centrifuged supernatant provided a 5-day BOD value of 90 ppm.

B. Experimental Feces-Urine (F-U) Blend

Feces and Urine were collected and maintained in the deep freeze until preparation for the investigation. In the preparation of the experimental F-U blend, feces and urine - in the ratio of 50 grams of moist feces and 500 ml of urine - were blended in a Waring Blender. Measured volumes of the blend were then measured into containers, sealed and placed in the the deep freeze for future use. Five-day BOD was run on the blend as well as on a centrifuged - 1500 RPM for 15 minutes - supernatant of the blend. The blend and the supernatant gave 5-day BOD values of 18,500 and 14,300 ppm, respectively.

C. Experimental Approach

Seven liters of sludge - as described under A above - was available at the start of the investigation. The sludge was allowed to settle and 100 ml of the supernatant was removed and centrifuged (1500 RPM for 10 minutes). The supernatant was stored in the deep freeze for BOD assay and the small amount of solids collected in the centrifuge bottles were returned to the remaining 6.9 liters of sludge along with 100 ml of the F-U blend described in B above. Aeration of the 7 liters of sludge and F-U blend mixture was provided by pulling laboratory air through the mixture with a water aspirator connected to a tap of the water supply of the laboratory. Adequate air was pulled through the mixture to provide turbulent motion to the sludge and F-U blend mixutre. The experiment was run at room temperature - essentially 25°C.

At the end of a 24 hour aeration period, aera-aion was stopped to allow the sludge to settle. One hundred (100) ml of the supernatant was removed and centrifuged. The centrifuged liquid was stored in the deep freeze for subsequent BOD assay whereas the solids were returned to the aeration chamber with 100 ml of feces-urine blend. Air flow through the sludge-body waste mixture was again started and continued for 24 hours. The above cycle of procedures was employed with additions of the same volume of F-U blend for three days. Following three days of the addition of a given volume of F-U blend, the volume of feces-urine blend addition was increased or the volume of sludge was reduced so as to provide another specific volume ratio of F-U blend to total aeration volume. Details of the experimental design are presented by Table I.

III. Discussion of Results

Figures 1 and 2 represent the resulting BOD of an effluent from an activated sludge system receiving different concentrations

FIGURE 1 - FIVE DAY BOD VALUES OF THE SUPERNATANT OF 24 HOUR DIGESTS OF A FECES-URINE BLEND WITH ACTIVATED SLUDGE (2)

(1) F-U - FECES-URINE BLEND CONTAINING 50 GRAMS OF FECES AND 500 ML. URINE

(2) SEE "EXPERIMENTAL APPROACH" SECTION FOR OTHER DETAILS

A AVERAGE OF B, C & D

B 24 HOUR AERATION FOLLOWING ADDITION OF FIRST F-U BLEND AT A GIVEN RATIO

C 24 HOUR AERATION FOLLOWING ADDITION OF SECOND F-U BLEND AT A GIVEN RATIO

D 24 HOUR AERATION FOLLOWING ADDITION OF THIRD F-U BLEND AT A GIVEN RATIO

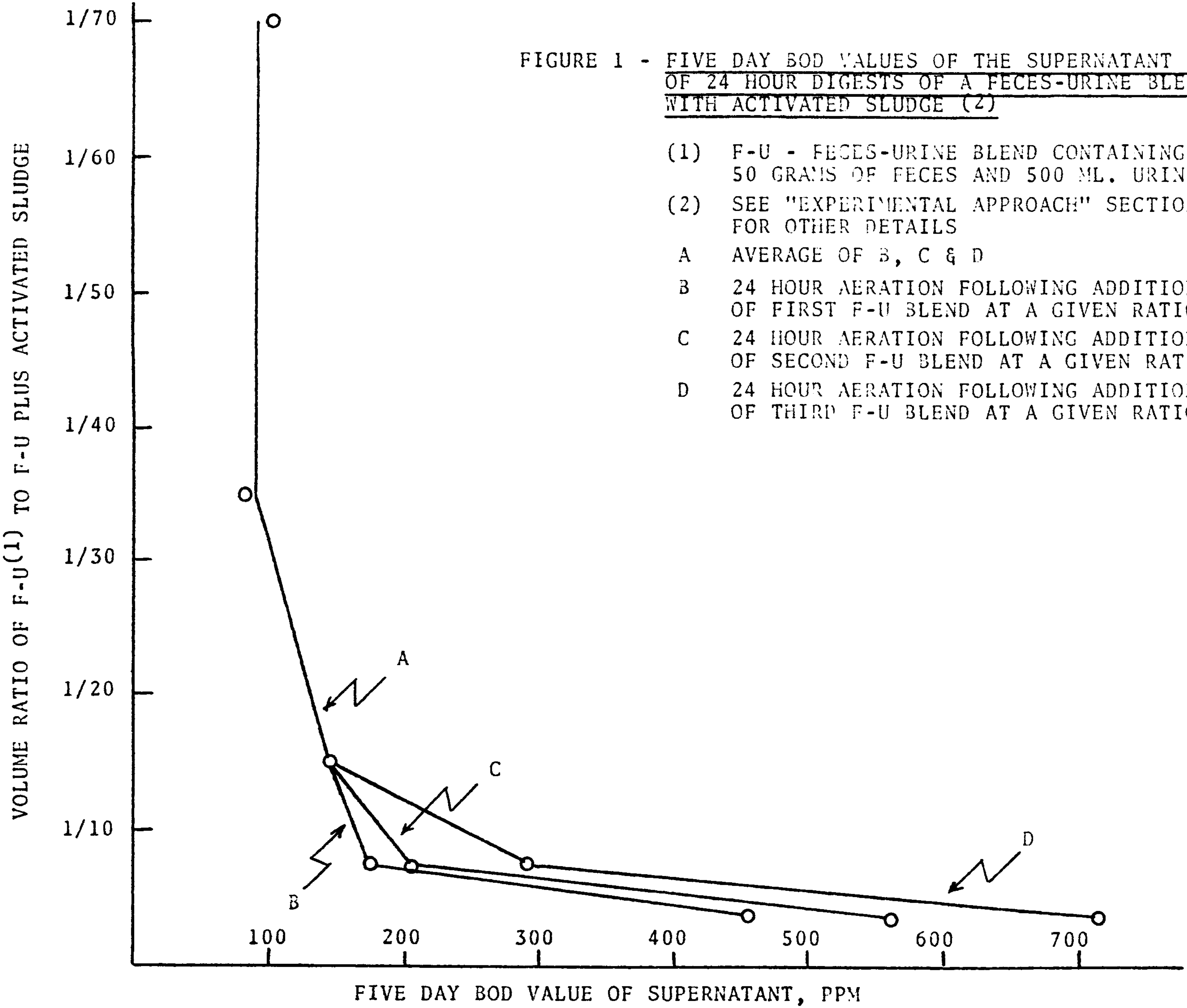

FIGURE 2 - BOD OF SUPERNATANT OF AN AERATED MIXTURE OF ACTIVATED SLUDGE AND A FECES-URINE BLEND

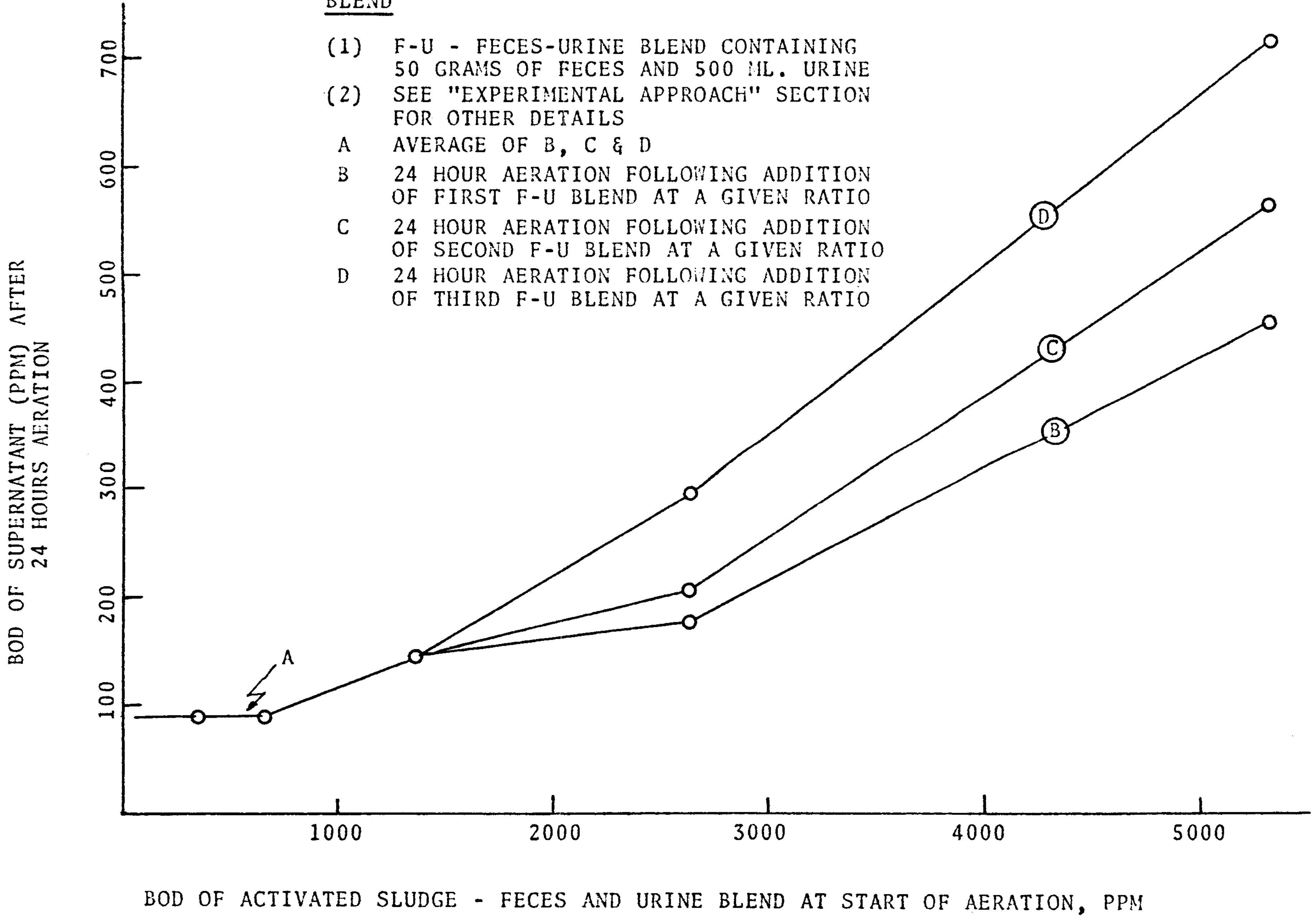

TABLE I

EXPERIMENTAL PROCEDURE EMPLOYED

Volume of Aerated Mixture(1) ml	F-U Blend Added(2) ml	Volume-Ratio of F-U Blend To Mixture ml/ml	Volume % of F-U Blend To Mixture %	Days of Addition
7000	100	1/70	1.43	3
7000	200	1/35	2.86	3
3000	200	1/15	6.67	3
1500	200	1/7.5	13.34	3
750	200	1/3.75	26.68	3

(1) Mixtures aerated for 24 hours at room temperature - essentially 25°C.

(2) Addition made after the removal of same volume supernatant for BOD evaluations. See text for other details.

of a feces-urine (F-U) blend. The system was operated for a total of 15 continuous days - starting with a 1/70 mixture (1 part F-U blend + 69 parts of activated sludge) of feces-urine blend and sludge. This volume ratio of F-U blend (1.43%) in the aeration mixture - added daily over a period of 3 days after the daily removal of 100 ml of settled supernatant - caused no BOD build-up in the supernatant. Likewise the addition of a 1/35 volume ratio (2.86%) provided the same results - that is, a residual BOD of 90 ppm in the centrifuged effluent from the aerated mixture.

When the F-U blend concentration was increased to 6.67% (volume ratio of 1/15) the residual BOD rose to 144 ppm - however, the rise was not regular over the 3 successive days of addition of this level of F-U. At higher concentrations of F-U, 13.34 and 26.68% (1/7.5 & 1/3.75 volume ratio), each successive day of addition provided for a build-up of BOD in the supernatant or effluent from the aerated mixture of sludge and F-U blend. All these results were obtained in 24 hour aeration tests.

These data could be of value in planning for future space programs - such as space stations - employing both biological and physical processes for the recovery of water from body waste and waste sanitary water. As envisioned from these results, the sanitary water would be isolated from the body wastes - feces and urine and as such be subjected to a physical method of treatment - evaporation following pretreatment. The concentrated feces and urine mixture would be diverted to a small volume activated sludge system. The effluent from the sludge digestion would be blended with the sanitary water for processing. This system would obviate the need for storage of the feces and would permit their conversion.

The true significance of these data - both for space exploration and for earth based stabilization of concentrated wastes - is indicated by Figure 3. These data indicated that approximately 91.3% of the BOD value of feces-urine can be satisfied by an activated sludge system in 24 hours up to a concentration of 26.68% of F-U blend in the aeration mixture. These data demonstrate that, starting with an activated sludge containing approximately one % dry solids, it is possible to destroy or oxidize a great deal of organic matter in a small volume if the nutrient (F-U blend) is of sufficient concentration. For example, in a one liter system which had been fed an F-U blend supplying 300 ppm of oxidizable matter only 274 mg of this material will be removed in 24 hours. However, in the same volume the amount of BOD satisfaction is 4,639 ppm when the F-U blend supplied 5,285 ppm of BOD. For earth based operations producing a concentrated waste of relatively small volume, these observations may have a significant impact. That is, these concentrated wastes may be treated in a "small volume" system and the effluent then diluted with very dilute

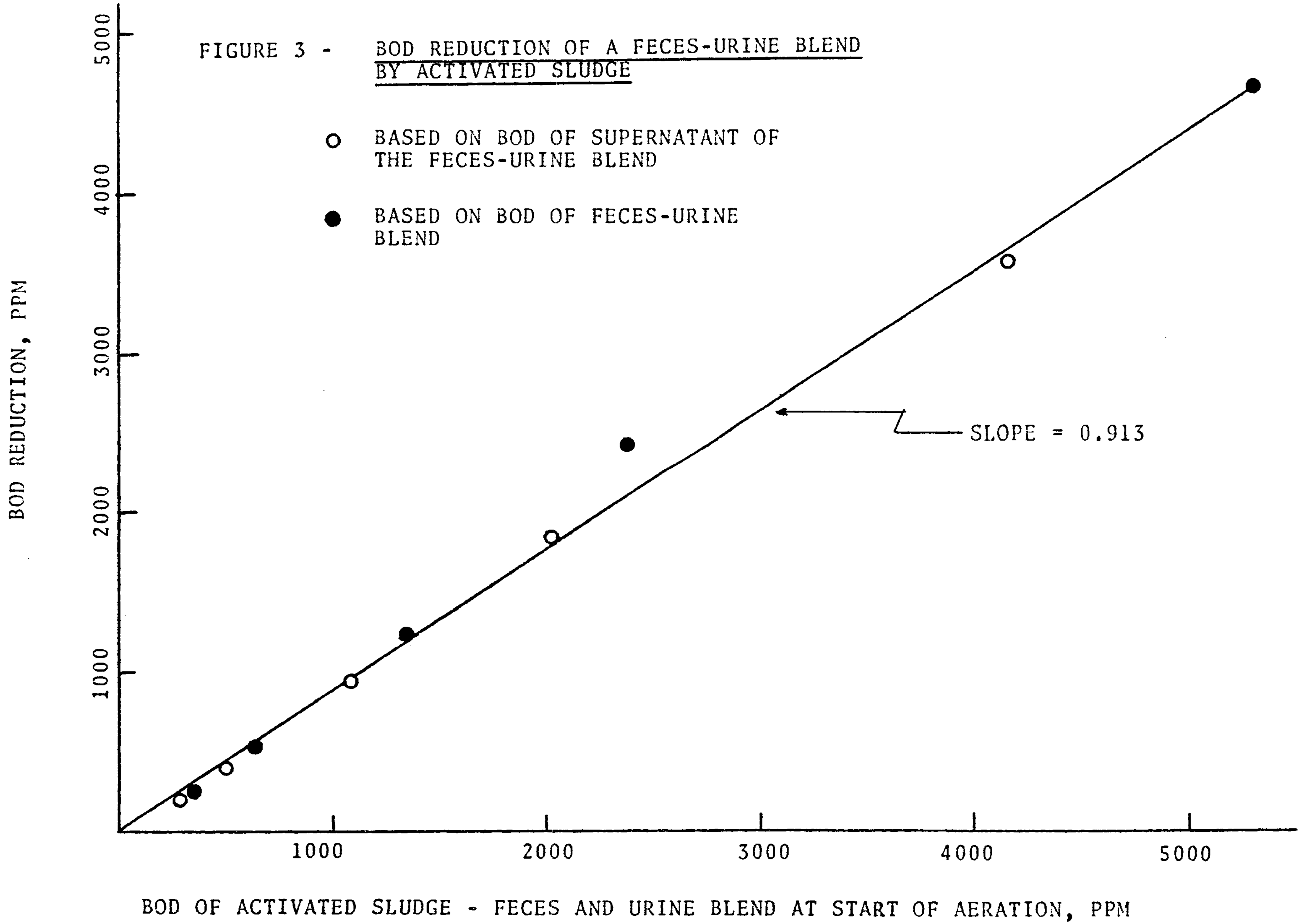

FIGURE 3 - BOD REDUCTION OF A FECES-URINE BLEND BY ACTIVATED SLUDGE

effluent from other areas of the plant operation. This procedure would reduce the BOD load on the streams receiving the plant effluent and would present a more economical approach for plant management to install - in essence the suggestion would be "treat and then dilute" as opposed to "dilute and treat".

The "dilute and treat" aspect is imposed on our municipal plants by the fact that essentially every voiding of waste - feces and urine - by man is diluted with 4 gallons of water from the commode. Perhaps in the establishment of military bases or in the development of under-developed countries consideration should be given to the possibility of sewage systems which provide small quantities of flush water. The above data suggest that not only would water be saved but the treatment plant would be smaller for the BOD load.

IV. Conclusions and Future Research Approaches Needed

The above data are preliminary and require further research. Such continuing research could be carried out at a significant rate with an annual budget of $12,000 per year for a two year period. The research approaches would be as follows:

1. An evaluation of the BOD reduction achieved by activated sludge systems of known sludge content - that is, activated sludge contents of from 0.2 to 4.0%.

2. An evaluation of the oxygen (pure) and air requirements for different systems containing known levels of sludge solids.
3. An evaluation of continuous versus periodic BOD addition on concentrated activated sludge systems.
4. An evaluation of the level of BOD fed to an activated sludge where the organic solid in the system remains constant. That is, formation of active sludge solids and digestion of old solids (dead bacteria, etc.) at the same rate.
5. An expansion of the program to concentrated industrial wastes.

TABLE II

EXPERIMENTAL AND CALCULATED DATA

Feces-Urine Blend Concentration	Addition No.	BOD of Mixture			BOD Reduction	
		Supernatant (2) Start	Supernatant (3) Plus Solids Start	Supernatant Final	Supernatant (2)	Supernatant (3) Plus Solids
Vol. %	day	ppm	ppm	ppm	ppm	ppm
1.43	Av. (1)	293	353	90	203	263
2.86	Av. (1)	495	615	90	405	525
6.67	Av. (1)	936	1344	144	792	1200
13.34	1st	2026	2610	175	1851	2435
	2nd	2073	2617	204	1869	2413
	3rd	2098	2662	293	1805	2369
	Av.	2066	2630		1842	2406
26.68	1st	4054	5182	456	3598	4626
	2nd	4175	5303	566	3609	4637
	3rd	4252	5370	716	3536	4654
	Av.	4160	5285		3581	4639

(1) Average of 1st, 2nd & 3rd day additions - all average values underlined.

(2) Based on BOD value of centrifuged F-U blend.

(3) Based on BOD value of F-U blend.

SPACE TECHNOLOGY PROJECT NO. 3

HEAT TRANSFER FROM PLASMA JETS

HEAT TRANSFER FROM PLASMA JETS

Project Investigators:

Dr. P. T. Eubank
Department of Chemical Engineering

Mr. J. R. Johnson
Graduate Assistant

Since January 1964 work in the field of plasma heat transfer has been carried out on two fronts:

Preparation and initiation of final data taken on the experimental apparatus and library research for improved technical methods and models by which to treat the data.

I. Experimental

Much of the time covered by this report has been spent debugging the experimental apparatus. Attempts to begin the accumulation of heat transfer data began in January 1964; however, some of the extensive instrumentation equipment failed to function as expected when used in conjunction with the entire system. These difficulties have now been corrected, and heat transfer data on a nitrogen plasma is proceeding satisfactorily.

II. Data Correlation

The major modes for this type of plasma heat transfer are radiation and forced convection. While radiation can be treated by standard methods, forced convection correlation is more difficult, because of the ionization-recombination reactions occuring in the flowing plasma. The problem is similar to heat transfer from a flowing gas undergoing a chemical reaction, which has been widely researched, except the reaction is one of ionization. This literature is being accumulated and should provide several models for treatment of the forced convection contributions for plasmas.

Because all such models require information concerning the physical properties of the system, literature on the thermal conductivity, electrical conductivity, heat capacity, and viscosity of partially ionized nitrogen, argon, and helium are sought. In many cases data does not exist at sufficiently high temperatures. Here it is necessary to estimate the thermodynamic properties by statistical methods and the transport coefficients by the simple kinetic energy theory.

SPACE TECHNOLOGY PROJECT NO. 5

A MATHEMATICAL INVESTIGATION OF THE

STRUCTURE OF LIGHT METALS

A MATHEMATICAL INVESTIGATION OF THE STRUCTURE OF LIGHT METALS

Project Investigator

Dr. E. R. Keown, Professor of Mathematics

I. Introduction

This is the final report of research performed under Project 5, NsG 239-62 which began February 1, 1963. Previous work having been fully reported in Supplementary Report to Project 5, HARTREE-FOCK SOLUTIONS WITHOUT EXCHANGE FOR BERYLLIUM, August, 1963 . This report will cover only research performed since September 1, 1963. It is expected that this summary report will be followed by a more detailed supplement.

The three most significant results of this research were: (1) the calculation of the energy bands of the diamond crystal for 256 points in the first Brillouin zone, (2) the preparation of specifications of diamond type for Augmented Plane Wave Calculations[1,2,6], and (3) the development of an IBM program which permits the plane wave analysis of any type of crystal when given the matrices of the irreducible representations of the group of wave vectors for all symmetry points of interest in the first Brillouin zone. The program permits the use of Slater Representation Matrices in reducing Wigner plane (augmented) wave representations.

The energy bands of diamond are presented in Figures 1 and 2. A list of all the specifications is too lengthy to be presented in this summary report. It is anticipated that such a list will appear in the supplementary report. The plane-wave-symmetrizing program will probably be distributed through SHARE.

This report contains a discussion of the calculations and results in Section 2 where a tabulation of the calculated energy eigenvalues may be found in Table VI. A brief discussion of the diamond crystal is given in Section 3 which also contains diagrams of the crystal, the Wigner-Seitz Cell, and the first Brillouin zone of diamond in Figures 3, 4, and 5 respectively. Table VII contains a listing of the basic crystal potentials obtained from the $(1s)^2 (2s)^2 (2p)^2$ and $(1s)^2 (2s)(2p)^3$ configurations of the carbon atom. These potentials were calculated by the Herman-Skillman program[10] as modified by L. F. Mattheiss to include superposition of potentials from neighboring sites.

II. Details of the Calculation

The energy bands presented in this report were calculated by the Augmented Plane Wave Method[1,2] of J. C. Slater by means of a program coded by J. H. Wood with minor revisions by C. Nielson to permit running under Fortran Monitor control. The calculations were carried out for 20 points in the first Brillouin zone of the diamond lattice which, by symmetry considerations, lead to the energy eigenvalues of 256 equivalent points. The results of the calculation are presented graphically in Figures 1 and 2 and numerically in Table VI where the coordinates of the selected 20 points are listed along with the corresponding eigenvalues. The general locations of these symmetry points are shown pictorially in Figure 5.

The interior points of the first Brillouin zone were treated using their full symmetry under the group of the specific wave vector under consideration by means of the irreducible representations of the diamond crystal according to the scheme of J. C. Slater[5]. However, some of the boundary points of the first zone were treated with less than their full symmetry because of difficulties with complex coefficients in the symmetrized augmented waves associated with their irreducible representations. The present Augmented Plane Wave (hereafter written APW) programs are not designed to treat this case of complex coefficients.

The following sentences describe the use of symmetry on the zone boundary. The symmetry points K, L, and Q possess the property of having real coefficients for their symmetrized augmented plane waves so that they were calculated according to their full symmetry. The points X and Z were calculated with lower symmetry corresponding to that of an interior point on the axis of symmetry through X and of the symmetry plane through Z. The point U theoretically should have the same symmetry and same energy eigenvalues as the point K. Values were calculated for U with a smaller symmetry group, but, in Figure 2, the computed energy values at U were replaced by those computed at K which are quite similar as shown by a comparison of the computed values given in Table VI. The energy eigenvalues for the point W were obtained by extrapolation from neighboring points because of symmetry difficulties at the point W itself. For these reasons, the values at W and U are shown in Figure 2 without symmetry labels. The value of 1.52 Rydbergs assigned to Gamma 2' is an adaptation from the results presented by Bassani[8] for diamond. The eigenvalues are given in the form x.xxxx which indicates an accuracy the author does not assert. Results of the form x.xx00 were usually obtained by means of graphical interpolation to avoid rerunning the given point with a finer energy mesh. Such values are probably accurate to about 0.01 Rydbergs. Checks on convergence were made only for a few points along the direction from Gamma to X where there is evidence of convergence to a few thousandths of a Rydberg. The results are complete to within these limitations for 256 points in the first Brillouin zone.

It is anticipated that a few points will be checked for convergence and symmetry before the summer is ended. A density of states calculation is planned to be based on the eigenvalues arranged in Table VI in order of increasing value.

The energies presented in Figures 1 and 2 and in Table VI are as determined by the APW program. This program calculates energies with respect to a zero value for the potential between the APW spheres.

Some general conclusions to be drawn from the calculations are as follows: First, they indicate that the Augmented Plane Wave method of Slater is satisfactory in the case of a covalent crystal where the assumption of a "muffin-tin" potential is probably the least tenable. Second, they demonstrate the practicality of using the Slater Representation Theory[3,4,5] to reduce plane wave representations obtained by means of the Wigner Theory as applied in J. H. Wood's APW programs[6]. Third, they give computational support to the interpretation of the Slater Representation Theory given by E. R. Keown[7]. Fourth, they agree in general with the results obtained by F. Bassani and M. Yoshime[8] in their Orthogonal Plane Wave calculations for diamond (these results are presented in Figure 1). Fifth, they indicate that the use by Scop[9] of the constant potential between the sphere as a disposable parameter may be especially useful in cases where there is considerable variation in the crystal potential between the APW spheres. Sixth, they indicate a previously unsuspected gap in the conduction states of diamond.

III. The Diamond Crystal

The two distinct crystalline states of the element carbon are graphite and diamond which belong to the hexagonal and cubic sygonies respectively. Our principal interest lies with diamond whose crystalline structure may be described as composed of two interpenetrating face-centered-cubic lattices in which each point of the two lattices are occupied by a carbon atom. The lattices themselves are diaplaced, one to the other, along a body diagonal of the fundamental cell by a quarter of its length. A sketch of the structure is given in Figure 3 where the fundamental cubic cell is described as having a side of length $\underline{a}$. This so-called fundamental cell is not a primitive cell for the translational symmetry of the diamond lattice nor does it adequately denote its rotational symmetry. One

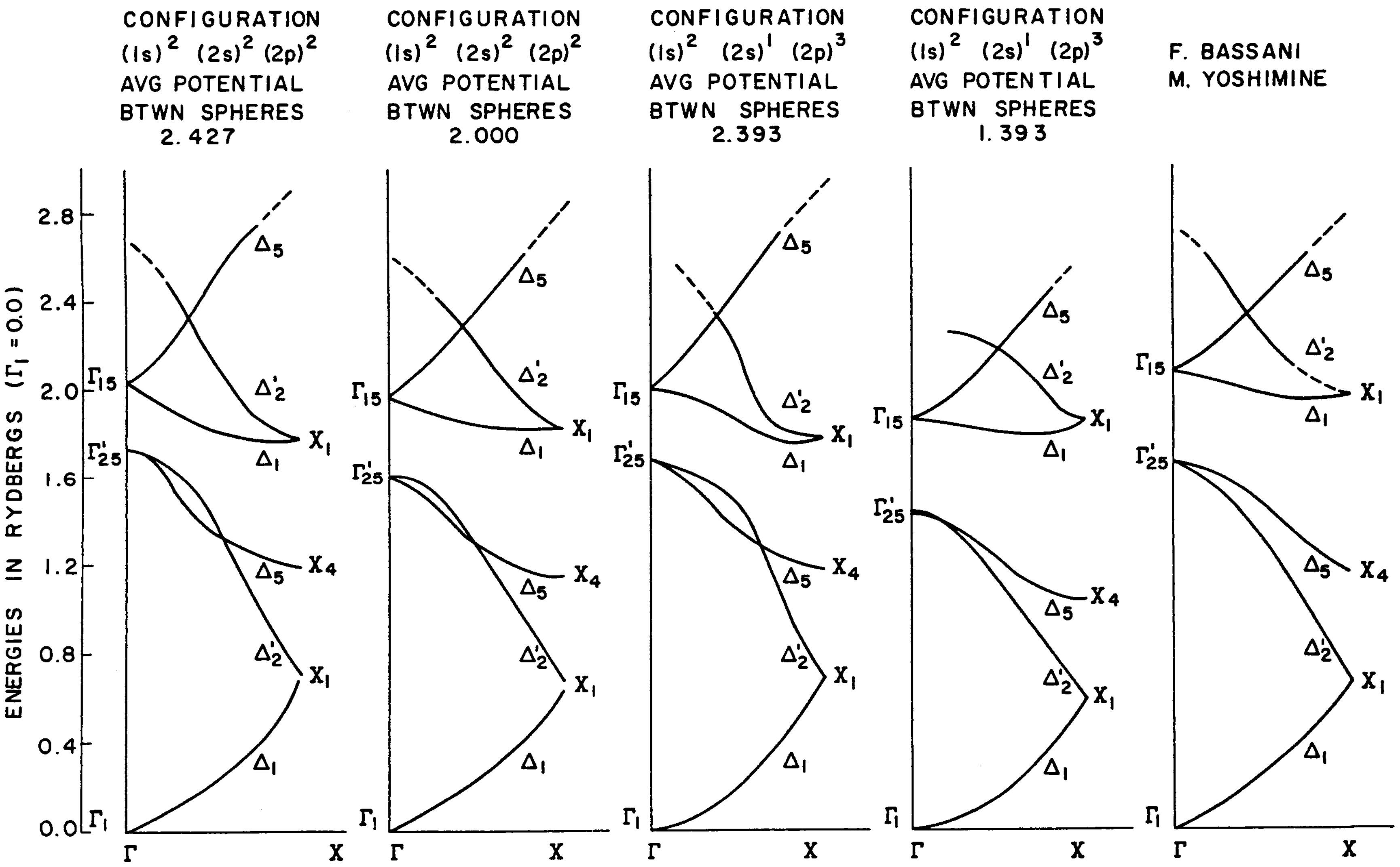
CONFIGURATION
$(1s)^2$ $(2s)^2$ $(2p)^2$
AVG POTENTIAL
BTWN SPHERES
2.427
CONFIGURATION
$(1s)^2$ $(2s)^2$ $(2p)^2$
AVG POTENTIAL
BTWN SPHERES
2.000
CONFIGURATION
$(1s)^2$ $(2s)^1$ $(2p)^3$
AVG POTENTIAL
BTWN SPHERES
2.393
CONFIGURATION
$(1s)^2$ $(2s)^1$ $(2p)^3$
AVG POTENTIAL
BTWN SPHERES
1.393
F. BASSANI
M. YOSHIMINE
ENERGIES IN RYDBERGS (Γ_1 = 0.0)
2.8
2.4
2.0
1.6
1.2
0.8
0.4
0.0
Γ_{15}
Γ'_{25}
Γ_1
Δ_5
Δ'_2
Δ_1
X_1
X_4
Γ
X

FIGURE 1

TABLE I

SUMMARY OF PRELIMINARY CALCULATIONS FOR DIAMOND

SYMMETRY		K	1	2	3	4	5
GAMMA	1	0004	-0.3581	-0.5601	-0.4073	-0.9200*	-0.3600*
GAMMA	25P	0004	1.3787	1.0517	1.2966	0.5108	1.3200*
GAMMA	15	0004	1.6689/	1.4037	1.6042	0.9398	1.7200*
DELTA	1	2004	1.6030	1.3576	1.5427	0.9203	1.6800*
DELTA	1	2004	2.4200*	2.2429	2.3726	2.0014	
DELTA	2P	2004	1.2767	0.9537	1.1956	0.4200	1.1800*
DELTA	2P	2004	2.1229	1.8584	2.0644	1.3201	2.2000*
DELTA	5	2004	1.2153	0.9195	1.1419	0.4200*	1.2400*
DELTA	5	2004	1.8623	1.5630	1.7872	1.0614	1.8500*
DELTA	1	4004			-0.2289	-0.7688	-0.1100*
DELTA	1	4004	1.4920	1.2778	1.4393	0.8892	1.6200*
DELTA	2P	4004	1.0299	0.7212	0.9526	0.2076	0.9500*
DELTA	2P	4004	1.7794	1.6406	1.7495	1.2654	1.9000*
DELTA	5	4004	1.0182	0.7433	0.9502	0.2689	1.0900*
DELTA	5	4004	2.1442	1.8207	2.0630	1.2819	2.0200*
DELTA	1	6004	0.0200*		-0.0103	-0.5805	0.0600*
DELTA	1	6004	1.4202	1.2320	1.3738	0.8860	1.6000*
DELTA	2P	6004	0.6932	0.4175	0.6253	0.5894	0.6800*
DELTA	2P	6004	1.5257	1.3889	1.4932	1.0884	1.7000*
DELTA	5	6004	0.8886	0.6232	0.8229	0.1635	0.9300*
DELTA	5	6004	2.3950*	2.0474	2.3072	1.4724	2.2400*
DELTA	1	8004	0.3429	0.0560*	0.2836	-0.3351	0.3000*
DELTA	2P	8004	0.3433	0.1250/	0.2841	-0.3334	0.3000*
DELTA	5	8004	0.8448	0.5826	0.7799	0.1281	0.8000*
DELTA	1	8004	1.4216	1.2591	1.3817	0.9479	1.6100*
DELTA	2P	8004	1.4218	1.2594	1.3819	0.9482	1.6100*

LEGEND AND REMARKS

* DENOTES AN APPROXIMATE VALUE FROM CURVE OR INTERPOLATION
/ DENOTES A VALUE WHICH IS PROBABLY INCORRECT

1 CONFIGURATION (1S)2 (2S)2 (2P)2 POTENTIAL AT SPHERE RADIUS IS 2.65 AVG POTENTIAL BETWN SPHERES IS 2.427

2 CONFIGURATION (1S)2 (2S)2 (2P)2 POTENTIAL AT SPHERE RADIUS IS 2.65 AVG POTENTIAL BETWN SPHERES IS 2.000

3 CONFIGURATION (1S)2 (2S)1 (2P)3 POTENTIAL AT SPHERE RADIUS IS 2.73 AVG POTENTIAL BETWN SPHERES IS 2.393

4 CONFIGURATION (1S)2 (2S)1 (2P)3 POTENTIAL AT SPHERE RADIUS IS 2.73 AVG POTENTIAL BETWN SPHERES IS 1.393

TABLE II

SUMMARY OF PRELIMINARY CALCULATIONS ZERO ENERGY AT GAMMA 1

SYMMETRY		K	1	2	3	4	5
GAMMA	1	0004	0.0000	0.0000	0.0000	0.0000	0.0000
GAMMA	25P	0004	1.7368	1.6118	1.7039	1.4508	1.6800
GAMMA	15	0004	2.0270	1.9638	2.0115	1.8598	2.0800
DELTA	1	2004	1.9111	1.9177	1.9500	1.8403	2.0400
DELTA	1	2004	2.7781	2.8030	2.7739	2.9214	
DELTA	2P	2004	1.6348	1.5138	1.6029	1.3400	1.5400
DELTA	2P	2004	2.4810	2.4185	2.4717	2.2401	2.5600
DELTA	5	2004	1.5734	1.4796	1.5492	1.3400	1.6000
DELTA	5	2004	2.2204	2.1231	2.1945	1.9814	2.2100
DELTA	1	4004			0.1784	0.1512	0.2500
DELTA	1	4004	1.8501	1.8379	1.8466	1.8092	1.9800
DELTA	2P	4004	1.3880	1.2813	1.4599	1.1276	1.3100
DELTA	2P	4004	2.1375	2.2007	2.1566	2.1854	2.2600
DELTA	5	4004	1.3763	1.3034	1.3575	1.1889	1.4500
DELTA	5	4004	2.5023	2.3808	2.4703	2.2019	2.3800
DELTA	1	6004	0.3781		0.3970	0.3395	0.4200
DELTA	1	6004	1.7783	1.7921	1.7811	1.8060	1.9600
DELTA	2P	6004	1.0513	1.6118	1.0326	1.5094	1.0400
DELTA	2P	6004	1.8838	1.9638	1.8005	2.0084	2.0600
DELTA	5	6004	1.2467	1.1833	1.2302	1.0835	1.2900
DELTA	5	6004	2.7531	2.6075	2.7145	2.3924	2.6000
DELTA	1	8004	0.7010	0.6161	0.6906	0.5649	0.6000
DELTA	2P	8004	0.7014	0.6851	0.6914	0.5866	0.6600
DELTA	5	8004	1.2029	1.1427	1.1872	1.0461	1.1600
DELTA	1	8004	1.7797	1.8192	1.7890	1.8679	1.9700
DELTA	2P	8004	1.7799	1.8195	1.7892	1.8682	1.9700

REMARKS

THESE VALUES WERE DETERMINED FROM TABLE I WHICH SHOULD BE CONSULTED IN CONNECTION WITH TABLE II

TABLE III

POTENTIAL FOR CONFIGURATION $(1S)^2(2S)^2(2P)^2$

RADIUS	POTENTIAL
0.00000000	UNDEFINED
0.00730833	1626.83896
0.01705277	688.13368
0.02679721	431.90047
0.03654166	312.22626
0.04628610	242.90414
0.06333887	172.91861
0.08282775	128.29834
0.10231663	100.78965
0.12180551	82.20031
0.14129439	68.84605
0.17539994	52.81996
0.21437770	40.98066
0.25335546	32.95802
0.29233322	27.19615
0.33131099	22.87865
0.39952207	17.50485
0.47747760	13.44263
0.55543312	10.71221
0.63338865	8.80585
0.71134418	7.41611
0.84776634	5.71933
1.00367738	4.44539
1.15958844	3.59290
1.31549948	3.01563
1.47141054	2.63258
1.62732159	2.39439

STARTING VALUES FOR INTEGRATING RADIAL WAVE EQUATIONS

	R = 0.002436	R = 0.004872
1	0.24007288E-02	0.47315914E-02
1	0.58914080E-05	0.23393882E-04
1	0.14387012E-07	0.11453320E-06
1	0.35090853E-10	0.55937833E-09
1	0.85547318E-13	0.27293534E-11
1	0.20850362E-15	0.13310806E-13
1	0.50811343E-18	0.64897713E-16
1	0.12381412E-20	0.31635869E-18
1	0.30168568E-23	0.15419860E-20
1	0.73505814E-26	0.75153000E-23
1	0.17909189E-28	0.36625782E-25
1	0.43633560E-31	0.17848781E-27
1	0.10630605E-33	0.86979240E-30

TABLE IV

POTENTIAL FOR CONFIGURATION $(1S)^{2}(2S)^{1}(2P)^{x}$

RADIUS	POTENTIAL
0.00000000	UNDEFINED
0.00730833	1626.98192
0.01705277	688.27858
0.02679721	432.04540
0.03654166	312.36971
0.04628610	243.04486
0.06333887	173.05232
0.08282775	128.42179
0.10231663	100.90172
0.12180551	82.30084
0.14129439	68.93559
0.17539994	52.89303
0.21437770	41.04068
0.25335546	33.01173
0.29233322	27.24984
0.33131099	22.93743
0.39952207	17.57945
0.47747760	13.53375
0.55543312	10.80682
0.63338865	8.89248
0.71134418	7.49242
0.84776634	5.78575
1.00367738	4.51213
1.15958844	3.66461
1.31549948	3.09251
1.47141054	2.71307
1.62732159	2.47629

STARTING VALUES FOR INTEGRATING RADIAL WAVE EQUATIONS

	R = 0.002436	R = 0.004872
1	0.24007282E-02	0.47315869E-02
1	0.58914085E-05	0.23393890E-04
1	0.14387015E-07	0.11453329E-06
1	0.35090861E-10	0.55937890E-09
1	0.85547341E-13	0.27293565E-11
1	0.20850368E-15	0.13310822E-13
1	0.50811359E-18	0.64897797E-16
1	0.12381416E-20	0.31635912E-18
1	0.30168578E-23	0.15419881E-20
1	0.73505838E-26	0.75153103E-23
1	0.17909196E-28	0.36625835E-25
1	0.43633576E-31	0.17848806E-27
1	0.10630609E-33	0.86979368E-30

TABLE V

VARIOUS CONSTANTS USED IN THE PROGRAM

A(LATTICE CONSTANT)	=	6.7406	A.U.
APW SPHERE RADIUS	=	1.4594	A.U.
NEAREST NEIGHBOR(4)	=	2.9188	A.U.
2ND NEAREST NEIGHBOR(12)	=	4.7734	A.U.
3RD NEAREST NEIGHBOR(12)	=	5.5890	A.U.

CALCULATION	MATTHEISS AVERAGING RADIUS	AVG POTENTIAL BETWEEN SPHERES	CONFIGURATION
1	2.6342 A.U.	2.4273 RYD.	$(1S)^2(2S)^2(2P)^2$
2	2.6342 A.U.	2.0000 RYD.	$(1S)^2(2S)^2(2P)^2$
3	2.0907 A.U.	2.3928 RYD.	$(1S)^2(2S)^1(2P)^3$
4	2.0907 A.U.	1.3928 RYD.	$(1S)^2(2S)^1(2P)^3$

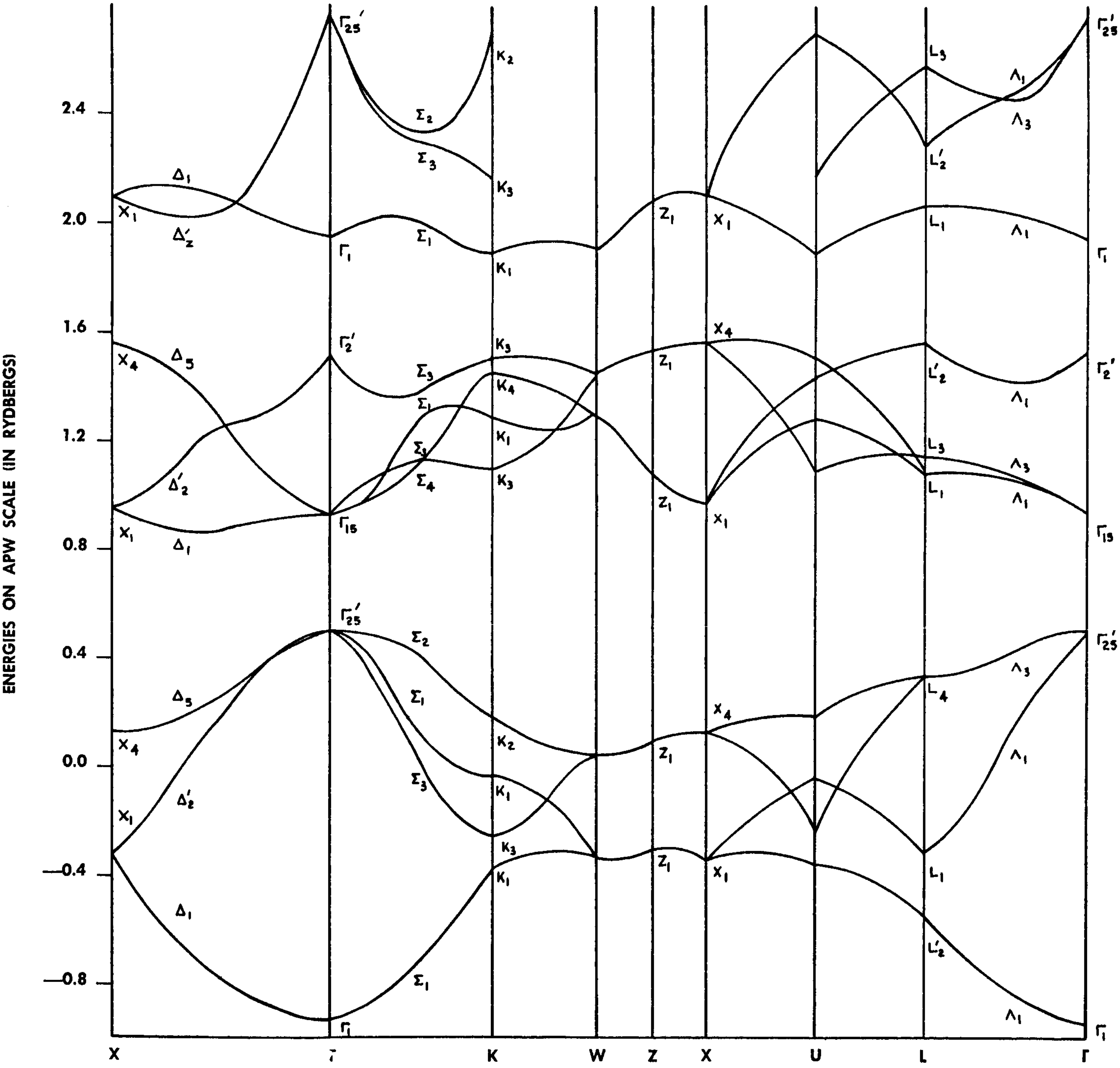
ENERGIES ON APW SCALE (IN RYDBERGS)
2.4
2.0
1.6
1.2
0.8
0.4
0.0
—0.4
—0.8
X
Γ
K
W
Z
X
U
L
Γ

Figure 2

TABLE VI

Table VI is made up of two distinct parts. The first is a tabulation of the energies into 20 sublists, each headed by a particular k-vector defining the translational symmetry of the wave function corresponding to the listed energy eigenvalue. The label of each k-vector is given in a form such as Sigma (4, 4, 0)/4 which gives the conventional name, Sigma, of the k-vector and its coordinates, (4/4, 4/4, 0/4) = (1, 1, 0), in units of π/a. The value of π/a was taken to be 0.46607 in the diamond calculation. Within each such sublist, the eigenvalues are further classified according to the various irreducible representations of the group of the wave vector k. The letter "P" is used in this list as a substitute for the symbol "," whenever it occurs. The second part is a listing of the energy eigenvalues in terms of increasing energy with each eigenvalue given its proper translational and rotational symmetry classification.

```
          ENERGIES ARRANGED ACCORDING TO SYMMETRY POINTS

GAMMA(0,0,0)/4                                              NRGE0010
                                                            NRGE0020
GAMMA   1       -0.9300                                     NRGE0030
GAMMA   25P      0.5108                                     NRGE0040
GAMMA   25P      0.5108                                     NRGE0050
GAMMA   25P      0.5108                                     NRGE0060
GAMMA   15       0.9398                                     NRGE0070
GAMMA   15       0.9398                                     NRGE0080
GAMMA   15       0.9398                                     NRGE0090
GAMMA   1        1.9545                                     NRGE0100
GAMMA   25P      2.7829                                     NRGE0110
GAMMA   25P      2.7829                                     NRGE0120
GAMMA   25P      2.7829                                     NRGE0130
                                                            NRGE0140
                                                            NRGE0150
DELTA(2,0,0)/4                                              NRGE0160
                                                            NRGE0170
DELTA   1       -0.8800                                     NRGE0180
DELTA   2 P      0.4200                                     NRGE0190
DELTA   5        0.4200                                     NRGE0200
DELTA   5        0.4200                                     NRGE0210
DELTA   1        0.9203                                     NRGE0220
DELTA   5        1.0614                                     NRGE0230
DELTA   5        1.0614                                     NRGE0240
DELTA   2 P      1.3200                                     NRGE0250
DELTA   1        2.0014                                     NRGE0260
DELTA   2 P      2.2932                                     NRGE0270
DELTA   1 P      2.8800                                     NRGE0280
                                                            NRGE0290
                                                            NRGE0300
DELTA(4,0,0)/4                                              NRGE0310
                                                            NRGE0320
DELTA   1       -0.7688                                     NRGE0330
DELTA   2 P      0.2076                                     NRGE0340
DELTA   5        0.2689                                     NRGE0350
DELTA   5        0.2689                                     NRGE0360
DELTA   1        0.8892                                     NRGE0370
DELTA   2 P      1.2654                                     NRGE0380
DELTA   5        1.2819                                     NRGE0390
DELTA   5        1.2819                                     NRGE0400
DELTA   2 P      2.0372                                     NRGE0410
DELTA   1        2.0938                                     NRGE0420
                                                            NRGE0430
                                                            NRGE0440
DELTA(6,0,0)/4                                              NRGE0450
                                                            NRGE0460
DELTA   1       -0.5835                                     NRGE0470
DELTA   2 P     -0.0589                                     NRGE0480
DELTA   5        0.1635                                     NRGE0490
DELTA   5        0.1635                                     NRGE0500
DELTA   1        0.8860                                     NRGE0510
DELTA   2 P      1.0884                                     NRGE0520
```

```
    DELTA  5        1.4724                                              NRGE0530
    DELTA  5        1.4724                                              NRGE0540
    DELTA  2 P      2.0394                                              NRGE0550
    DELTA  1        2.1397                                              NRGE0560
                                                                        NRGE0570
                                                                        NRGE0580
    XXXXX(8,0,0)/4                                                      NRGE0590
                                                                        NRGE0600
    DELTA  2 P     -0.3334                                              NRGE0610
    DELTA  1       -0.3351                                              NRGE0620
    DELTA  5        0.1281                                              NRGE0630
    DELTA  5        0.1281                                              NRGE0640
    DELTA  1        0.9479                                              NRGE0650
    DELTA  2 P      0.9482                                              NRGE0660
    DELTA  5        1.5580                                              NRGE0670
    DELTA  5        1.5580                                              NRGE0680
    DELTA  2 P      2.1063                                              NRGE0690
    DELTA  1        2.1126                                              NRGE0700
                                                                        NRGE0710
                                                                        NRGE0720
    SIGMA(2,2,0)/4                                                      NRGE0730
                                                                        NRGE0740
    SIGMA  1       -0.8400                                              NRGE0750
    SIGMA  3        0.2642                                              NRGE0760
    SIGMA  1        0.3293                                              NRGE0770
    SIGMA  2        0.4713                                              NRGE0780
    SIGMA  4        1.0196                                              NRGE0790
    SIGMA  1        1.0844                                              NRGE0800
    SIGMA  3        1.0800                                              NRGE0810
    SIGMA  3        1.3640                                              NRGE0820
    SIGMA  1        2.0258                                              NRGE0830
    SIGMA  2        2.3709                                              NRGE0840
    SIGMA  3        2.3973                                              NRGE0850
                                                                        NRGE0860
                                                                        NRGE0870
    SEVEN(4,2,0)/4                                                      NRGE0880
                                                                        NRGE0890
    SEVEN  1       -0.7272                                              NRGE0900
    SEVEN  2        0.1050                                              NRGE0910
    SEVEN  1        0.2050                                              NRGE0920
    SEVEN  2        0.3604                                              NRGE0930
    SEVEN  1        1.0350                                              NRGE0940
    SEVEN  2        1.2193                                              NRGE0950
    SEVEN  1        1.3189                                              NRGE0960
    SEVEN  2        1.3630                                              NRGE0970
    SEVEN  1        2.0808                                              NRGE0980
    SEVEN  2        2.1252                                              NRGE0990
    SEVEN  2        2.6228                                              NRGE1000
                                                                        NRGE1010
                                                                        NRGE1020
    EIGHT(6,2,0)/4                                                      NRGE1030
                                                                        NRGE1035
    EIGHT  1       -0.5400                                              NRGE1040
    EIGHT  2       -0.0900                                              NRGE1050
```

```
     EIGHT   1        0.1105                                          NRGE1060
     EIGHT   2        0.1762                                          NRGE1070
     EIGHT   1        1.0200                                          NRGE1080
     EIGHT   2        1.2100                                          NRGE1090
     EIGHT   2        1.3949                                          NRGE1100
     EIGHT   1        1.5010                                          NRGE1110
     EIGHT   1        2.0778                                          NRGE1120
     EIGHT   2        2.0918                                          NRGE1130
     EIGHT   2        2.8700                                          NRGE1140
                                                                      NRGE1150
                                                                      NRGE1160
     ZZZZZ(8,2,0)/4                                                   NRGE1170
                                                                      NRGE1180
     ZZZZZ   2       -0.3000                                          NRGE1190
     ZZZZZ   1       -0.3000                                          NRGE1200
     ZZZZZ   1        0.0898                                          NRGE1210
     ZZZZZ   2        0.0932                                          NRGE1220
     ZZZZZ   2        1.0854                                          NRGE1230
     ZZZZZ   1        1.0863                                          NRGE1240
     ZZZZZ   1        1.5278                                          NRGE1250
     ZZZZZ   2        1.5326                                          NRGE1260
     ZZZZZ   2        2.0816                                          NRGE1270
     ZZZZZ   1        2.0824                                          NRGE1280
                                                                      NRGE1290
                                                                      NRGE1300
                                                                      NRGE1310
     SIGMA(4,4,0)/4                                                   NRGE1320
                                                                      NRGE1330
     SIGMA   1       -0.6207                                          NRGE1340
     SIGMA   3       -0.0534                                          NRGE1350
     SIGMA   1        0.0538                                          NRGE1360
     SIGMA   2        0.3343                                          NRGE1370
     SIGMA   3        1.1200                                          NRGE1380
     SIGMA   4        1.2127                                          NRGE1390
     SIGMA   1        1.3393                                          NRGE1400
     SIGMA   3        1.4145                                          NRGE1410
     SIGMA   1        1.9651                                          NRGE1420
     SIGMA   3        2.2821                                          NRGE1430
     SIGMA   2        2.3453                                          NRGE1440
                                                                      NRGE1450
                                                                      NRGE1460
     ELEVN(6,4,0)/4                                                   NRGE1470
                                                                      NRGE1480
     ELEVN   1       -0.4500                                          NRGE1490
     ELEVN   2       -0.1600                                          NRGE1500
     ELEVN   1       -0.0095                                          NRGE1510
     ELEVN   2        0.2053                                          NRGE1520
     ELEVN   2        1.1700                                          NRGE1530
     ELEVN   1        1.3000                                          NRGE1540
     ELEVN   2        1.4119                                          NRGE1550
     ELEVN   1        1.4711                                          NRGE1560
     ELEVN   1        1.9028                                          NRGE1570
     ELEVN   2        2.1774                                          NRGE1580
     ELEVN   2        2.6345                                          NRGE1590
```

```
WWWWW(8,4,0)/4

WWWWW          -0.3400
WWWWW          -0.3400
WWWWW           0.0500
WWWWW           0.0500
WWWWW           1.2900
WWWWW           1.2900
WWWWW           1.4500
WWWWW           1.4500
WWWWW           1.9000
WWWWW           1.9000



KKKKK(6,6,0)/4

KKKKK  1       -0.3550
KKKKK  3       -0.2615
KKKKK  1       -0.0432
KKKKK  2        0.1905
KKKKK  3        1.1050
KKKKK  1        1.2869
KKKKK  4        1.4471
KKKKK  3        1.5021
KKKKK  1        1.8958
KKKKK  3        2.1879
KKKKK  2        2.6803


LAMDA(2,2,2)/4

LAMDA  1       -0.8000
LAMDA  1        0.0999
LAMDA  3        0.4100
LAMDA  3        0.4100
LAMDA  1        1.0700
LAMDA  3        1.0793
LAMDA  3        1.0793
LAMDA  1        1.4220
LAMDA  1        2.0337
LAMDA  3        2.4624
LAMDA  3        2.4624
LAMDA  1        2.4691



FIFTN(4,2,2)/4

FIFTN  1       -0.6800
FIFTN  1        0.0700
FIFTN  2        0.3246
FIFTN  1        0.3400
```

```
FIFTN 1     1.0900                                  NRGE2140
FIFTN 1     1.2000                                  NRGE2150
FIFTN 2     1.2459                                  NRGE2160
FIFTN 1     1.4684                                  NRGE2170
FIFTN 1     2.0500                                  NRGE2180
FIFTN 1     2.1958                                  NRGE2190
FIFTN 1     2.6219                                  NRGE2200
FIFTN 2     2.6943                                  NRGE2210
                                                    NRGE2220
SIXTN(6,2,2)/4                                      NRGE2230
                                                    NRGE2235
SIXTN 1    -0.5100                                  NRGE2240
SIXTN 1    -0.1700                                  NRGE2250
SIXTN 1     0.1184                                  NRGE2260
SIXTN 2     0.2476                                  NRGE2270
SIXTN 1     1.0400                                  NRGE2280
SIXTN 1     1.3270                                  NRGE2290
SIXTN 2     1.3942                                  NRGE2300
SIXTN 1     1.4533                                  NRGE2310
SIXTN 1     1.9900                                  NRGE2320
SIXTN 1     2.1840                                  NRGE2330
SIXTN 2     2.7573                                  NRGE2340
                                                    NRGE2350
                                                    NRGE2360
UUUUU(8,2,2)/4                                      NRGE2370
                                                    NRGE2380
UUUUU 1    -0.3495                                  NRGE2390
UUUUU 2    -0.2700                                  NRGE2400
UUUUU 1    -0.0259                                  NRGE2410
UUUUU 2     0.2157                                  NRGE2420
UUUUU 1     1.0200                                  NRGE2430
UUUUU 1     1.3000                                  NRGE2440
UUUUU 2     1.4791                                  NRGE2450
UUUUU 1     1.5412                                  NRGE2460
UUUUU 1     1.9100                                  NRGE2470
UUUUU 1     2.2221                                  NRGE2480
UUUUU 2     2.6979                                  NRGE2490
                                                    NRGE2500
                                                    NRGE2510
EGTEN(4,4,2)/4                                      NRGE2520
                                                    NRGE2530
EGTEN 1    -0.5900                                  NRGE2540
EGTEN 1    -0.2200                                  NRGE2550
EGTEN 1     0.2554                                  NRGE2560
EGTEN 2     0.3573                                  NRGE2570
EGTEN 1     1.1330                                  NRGE2580
EGTEN 2     1.2110                                  NRGE2590
EGTEN 1     1.2200                                  NRGE2600
EGTEN 1     1.5541                                  NRGE2610
EGTEN 1     2.2983                                  NRGE2620
EGTEN 1     2.3000                                  NRGE2630
EGTEN 2     2.4662                                  NRGE2640
                                                    NRGE2650
                                                    NRGE2660
```

QQQQQ(6,4,2)/4			NRGE2670
			NRGE2680
QQQQQ	2	-0.4700	NRGE2690
QQQQQ	1	-0.2600	NRGE2700
QQQQQ	1	0.1274	NRGE2710
QQQQQ	2	0.2498	NRGE2720
QQQQQ	2	1.1800	NRGE2730
QQQQQ	1	1.1900	NRGE2740
QQQQQ	1	1.3636	NRGE2750
QQQQQ	2	1.5106	NRGE2760
QQQQQ	1	1.9317	NRGE2770
QQQQQ	2	2.2105	NRGE2780
QQQQQ	1	2.6270	NRGE2790
QQQQQ	2	2.8800	NRGE2800
			NRGE2810
LLLLL(4,4,4)/4			NRGE2820
			NRGE2830
LLLLL	2 P	-0.5451	NRGE2840
LLLLL	1	-0.3409	NRGE2850
LLLLL	4	0.3364	NRGE2860
LLLLL	4	0.3364	NRGE2870
LLLLL	1	1.0928	NRGE2880
LLLLL	3	1.1462	NRGE2890
LLLLL	3	1.1462	NRGE2900
LLLLL	2 P	1.5616	NRGE2910
LLLLL	1	2.0679	NRGE2920
LLLLL	2 P	2.2871	NRGE2930
LLLLL	3	2.5814	NRGE2940
LLLLL	3	2.5814	NRGE2950

ENERGIES ARRANGED IN ORDER OF INCREASING ENERGY

GAMMA	1		-0.9300	DNST0010
DELTA	1		-0.8800	DNST0020
SIGMA	1		-0.8400	DNST0030
LAMDA	1		-0.8000	DNST0040
DELTA	1		-0.7688	DNST0050
SEVEN	1		-0.7272	DNST0060
FIFTN	1		-0.6800	DNST0070
SIGMA	1		-0.6207	DNST0080
EGTEN	1		-0.5900	DNST0090
DELTA	1		-0.5835	DNST0100
LLLLL	2	P	-0.5451	DNST0110
EIGHT	1		-0.5400	DNST0120
SIXTN	1		-0.5100	DNST0130
QQQQQ	2		-0.4700	DNST0140
ELEVN	1		-0.4500	DNST0150
KKKKK	1		-0.3550	DNST0160
UUUUU	1		-0.3495	DNST0170
LLLLL	1		-0.3409	DNST0180
WWWWW			-0.3400	DNST0190
WWWWW			-0.3400	DNST0200
DELTA	1		-0.3351	DNST0210
DELTA	2	P	-0.3334	DNST0220
ZZZZZ	2		-0.3000	DNST0230
ZZZZZ	1		-0.3000	DNST0240
UUUUU	2		-0.2700	DNST0250
KKKKK	3		-0.2615	DNST0260
QQQQQ	1		-0.2600	DNST0270
EGTEN	1		-0.2200	DNST0280
SIXTN	1		-0.1700	DNST0290
ELEVN	2		-0.1600	DNST0300
EIGHT	2		-0.0900	DNST0310
FIFTN	1		-0.0700	DNST0320
DELTA	2	P	-0.0589	DNST0330
SIGMA	3		-0.0534	DNST0340
KKKKK	1		-0.0432	DNST0350
UUUUU	1		-0.0259	DNST0360
ELEVN	1		-0.0095	DNST0370
WWWWW			0.0500	DNST0380
WWWWW			0.0500	DNST0390
SIGMA	1		0.0538	DNST0400
ZZZZZ	1		0.0898	DNST0410
ZZZZZ	2		0.0932	DNST0420
LAMDA	1		0.0999	DNST0430
SEVEN	2		0.1050	DNST0440
EIGHT	1		0.1105	DNST0450
SIXTN	1		0.1184	DNST0460
QQQQQ	1		0.1274	DNST0470
DELTA	5		0.1281	DNST0480
DELTA	5		0.1281	DNST0490
DELTA	5		0.1635	DNST0500
DELTA	5		0.1635	DNST0510
EIGHT	2		0.1762	DNST0520

KKKKK	2		0.1905	DNST0530
~~SEVEN~~	~~1~~		~~0.2050~~	~~DNST0540~~
ELEVN	2		0.2053	DNST0550
~~DELTA~~	~~2~~	~~P~~	~~0.2076~~	~~DNST0560~~
UUUUU	2		0.2157	DNST0570
~~SIXTN~~	~~2~~		~~0.2476~~	~~DNST0580~~
QQQQQ	2		0.2498	DNST0590
~~EGTEN~~	~~1~~		~~0.2554~~	~~DNST0600~~
SIGMA	3		0.2642	DNST0610
~~DELTA~~	~~5~~		~~0.2689~~	~~DNST0620~~
DELTA	5		0.2689	DNST0630
~~FIFTN~~	~~2~~		~~0.3246~~	~~DNST0640~~
SIGMA	1		0.3293	DNST0650
~~SIGMA~~	~~2~~		~~0.3343~~	~~DNST0660~~
LLLLL	4		0.3364	DNST0670
~~LLLLL~~	~~4~~		~~0.3364~~	~~DNST0680~~
FIFTN	1		0.3400	DNST0690
~~EGTEN~~	~~2~~		~~0.3573~~	~~DNST0700~~
SEVEN	2		0.3604	DNST0710
~~LAMDA~~	~~3~~		~~0.4100~~	~~DNST0720~~
LAMDA	3		0.4100	DNST0730
~~DELTA~~	~~2~~	~~P~~	~~0.4200~~	~~DNST0740~~
DELTA	5		0.4200	DNST0750
~~DELTA~~	~~5~~		~~0.4200~~	~~DNST0760~~
SIGMA	2		0.4713	DNST0770
~~GAMMA~~	~~25P~~		~~0.5108~~	~~DNST0780~~
GAMMA	25P		0.5108	DNST0790
~~GAMMA~~	~~25P~~		~~0.5108~~	~~DNST0800~~
DELTA	1		0.8860	DNST0810
~~DELTA~~	~~1~~		~~0.8892~~	~~DNST0820~~
DELTA	1		0.9203	DNST0830
~~GAMMA~~	~~15~~		~~0.9398~~	~~DNST0840~~
GAMMA	15		0.9398	DNST0850
~~GAMMA~~	~~15~~		~~0.9398~~	~~DNST0860~~
DELTA	1		0.9479	DNST0870
~~DELTA~~	~~2~~	~~P~~	~~0.9482~~	~~DNST0880~~
SIGMA	4		1.0196	DNST0890
~~EIGHT~~	~~1~~		~~1.0200~~	~~DNST0900~~
UUUUU	1		1.0200	DNST0910
~~SEVEN~~	~~1~~		~~1.0350~~	~~DNST0920~~
SIXTN	1		1.0400	DNST0930
~~DELTA~~	~~5~~		~~1.0614~~	~~DNST0940~~
DELTA	5		1.0614	DNST0950
~~LAMDA~~	~~1~~		~~1.0700~~	~~DNST0960~~
LAMDA	3		1.0793	DNST0970
~~LAMDA~~	~~3~~		~~1.0793~~	~~DNST0980~~
SIGMA	3		1.0800	DNST0990
~~SIGMA~~	~~1~~		~~1.0844~~	~~DNST1000~~
ZZZZZ	2		1.0854	DNST1010
~~ZZZZZ~~	~~1~~		~~1.0863~~	~~DNST1020~~
DELTA	2	P	1.0884	DNST1030
~~FIFTN~~	~~1~~		~~1.0900~~	~~DNST1040~~
LLLLL	1		1.0928	DNST1050
~~KKKKK~~	~~3~~		~~1.1050~~	~~DNST1060~~

SIGMA	3	1.1200	DNST1070
EGTEN	1	1.1330	DNST1080
LLLLL	3	1.1462	DNST1090
LLLLL	3	1.1462	DNST1100
ELEVN	2	1.1700	DNST1110
QQQQQ	2	1.1800	DNST1120
QQQQQ	1	1.1900	DNST1130
FIFTN	1	1.2000	DNST1140
EIGHT	2	1.2100	DNST1150
EGTEN	2	1.2110	DNST1160
SIGMA	4	1.2127	DNST1170
SEVEN	2	1.2193	DNST1180
EGTEN	1	1.2200	DNST1190
FIFTN	2	1.2459	DNST1200
DELTA	2 P	1.2654	DNST1210
DELTA	5	1.2819	DNST1220
DELTA	5	1.2819	DNST1230
KKKKK	1	1.2869	DNST1240
WWWWW		1.2900	DNST1250
WWWWW		1.2900	DNST1260
ELEVN	1	1.3000	DNST1270
UUUUU	1	1.3000	DNST1280
SEVEN	1	1.3189	DNST1290
DELTA	2 P	1.3200	DNST1300
SIXTN	1	1.3270	DNST1310
SIGMA	1	1.3393	DNST1320
SEVEN	2	1.3630	DNST1330
QQQQQ	1	1.3636	DNST1340
SIGMA	3	1.3640	DNST1350
SIXTN	2	1.3942	DNST1360
EIGHT	2	1.3949	DNST1370
ELEVN	2	1.4119	DNST1380
SIGMA	3	1.4145	DNST1390
LAMDA	1	1.4220	DNST1400
KKKKK	4	1.4471	DNST1410
WWWWW		1.4500	DNST1420
WWWWW		1.4500	DNST1430
SIXTN	1	1.4533	DNST1440
FIFTN	1	1.4684	DNST1450
ELEVN	1	1.4711	DNST1460
DELTA	5	1.4724	DNST1470
DELTA	5	1.4724	DNST1480
UUUUU	2	1.4791	DNST1490
EIGHT	1	1.5010	DNST1500
KKKKK	3	1.5021	DNST1510
QQQQQ	2	1.5106	DNST1520
ZZZZZ	1	1.5278	DNST1530
ZZZZZ	2	1.5326	DNST1540
UUUUU	1	1.5412	DNST1550
EGTEN	1	1.5541	DNST1560
DELTA	5	1.5580	DNST1570
DELTA	5	1.5580	DNST1580
LLLLL	2 P	1.5616	DNST1590
KKKKK	1	1.8958	DNST1600

WWWWW			1.9000	DNST1610
WWWWW			1.9000	DNST1620
ELEVN	1		1.9028	DNST1630
UUUUU	1		1.9100	DNST1640
QQQQQ	1		1.9317	DNST1650
GAMMA	1		1.9545	DNST1660
SIGMA	1		1.9651	DNST1670
SIXTN	1		1.9900	DNST1680
DELTA	1		2.0014	DNST1690
SIGMA	1		2.0258	DNST1700
LAMDA	1		2.0337	DNST1710
DELTA	2	P	2.0372	DNST1720
DELTA	2	P	2.0394	DNST1730
FIFTN	1		2.0500	DNST1740
LLLLL	1		2.0679	DNST1750
EIGHT	1		2.0778	DNST1760
SEVEN	1		2.0808	DNST1770
ZZZZZ	2		2.0816	DNST1780
ZZZZZ	1		2.0824	DNST1790
EIGHT	2		2.0918	DNST1800
DELTA	1		2.0938	DNST1810
DELTA	2	P	2.1063	DNST1820
DELTA	1		2.1126	DNST1830
SEVEN	2		2.1252	DNST1840
DELTA	1		2.1397	DNST1850
ELEVN	2		2.1774	DNST1860
SIXTN	1		2.1840	DNST1870
KKKKK	3		2.1879	DNST1880
FIFTN	1		2.1958	DNST1890
QQQQQ	2		2.2105	DNST1900
UUUUU	1		2.2221	DNST1910
SIGMA	3		2.2821	DNST1920
LLLLL	2	P	2.2871	DNST1930
DELTA	2	P	2.2932	DNST1940
EGTEN	1		2.2983	DNST1950
EGTEN	1		2.3000	DNST1960
SIGMA	2		2.3453	DNST1970
SIGMA	2		2.3709	DNST1980
SIGMA	3		2.3973	DNST1990
LAMDA	3		2.4624	DNST2000
LAMDA	3		2.4624	DNST2010
EGTEN	2		2.4662	DNST2020
LAMDA	1		2.4691	DNST2030
LLLLL	3		2.5814	DNST2040
LLLLL	3		2.5814	DNST2050
FIFTN	1		2.6219	DNST2060
SEVEN	2		2.6228	DNST2070
QQQQQ	1		2.6270	DNST2080
ELEVN	2		2.6345	DNST2090
KKKKK	2		2.6803	DNST2100
FIFTN	2		2.6943	DNST2110
UUUUU	2		2.6979	DNST2120
SIXTN	2		2.7573	DNST2130
GAMMA	25P		2.7829	DNST2140

```
GAMMA   25P     2.7829                                              DNST2150
GAMMA   25P     2.7829                                              DNST2160
EIGHT   2       2.8700                                              DNST2170
DELTA   1 P     2.8800                                              DNST2180
QQQQQ   2       2.8800                                              DNST2190
```

suitable choice of basic primitive cell for the translationas (there are infinitely-many others, of course) is the set of three vectors defined by $\underline{a}_1 = (0, a/2, a/2)$, $\underline{a}_2 = (a/2, 0, a/2)$, and $\underline{a}_3 = (a/2, a/2, 0)$. The set of all integral linear combinations of these three vectors describe the translational symmetry of the diamond crystal. The conventional Wigner-Seitz cell for such translational symmetry is drawn in Figure 4. The Wigner-Seitz cell does not describe the rotational symmetry of the diamond lattice to the same degree that it does the face-centered-cubic lattice determined by the set of three basic primitive translations given above. The reason for this failure is that the diamond lattice has non-trivial glide planes and screw axes of symmetry. One-half of the 48 elements of O_h, the symmetry group of the cube, must be accompanied by non-primitive translations in order to bring the Wigner-Seitz cell back into coincidence with itself as the diamond lattice is brought back into itself. The particular elements of O_h which are accompanied by non-primitive translation depend upon the choice of location of the origin of coordinates with respect to the position of the two face-centered-cubic lattices. In our particular case, one carbon atom is located at (a/8, a/8, a/8) while its partners in the same lattice are determined by displacements through primitive translations of the given atom. The "other atom" in the Wigner-Seitz cell is located at (-a/8, -a/8, -a/8) and its partners again by symmetry. This choice of origin is referred to as Case 2 in J. C. Slater's discussion of the symmetries of the diamond lattice[5].

The direct lattice spanned by $\underline{a}_1$, $\underline{a}_2$, and $\underline{a}_3$ has for its reciprocal lattice one which is spanned by vectors $\underline{b}_1$, $\underline{b}_2$, and $\underline{b}_3$. These vectors are defined by $\underline{b}_1 = (-2\pi/a, 2\pi/a, 2\pi/a)$, $\underline{b}_2 = (2\pi/a, -2\pi/a, 2\pi/a)$, and $\underline{b}_3 = (2\pi/a, 2\pi/a, -2\pi/a)$. The first Brillouin zone for the diamond lattice is really the Wigner-Seitz cell for the reciprocal lattice. A diagram for the first Brillouin zone of diamond is given in Figure 5.

Our notation for elements in the reciprocal space is somewhat special. We frequently denote such a "k-vector" in units of the quantity /a. Thus the basic primitive translation $\underline{b}_1 = (-2\pi/a, 2\pi/a, 2\pi/a)$ is denoted in these units merely by the symbol (-2,2,2). This practice, although confusing at first, has two advantages: (1) lattices with the same symmetry, but different values of π/a can be treated by changing a single constant in the data and (2) the input of data is largely limited to integer values which are easier to punch on IBM cards.

Figure 3

DIAMOND LATTICE

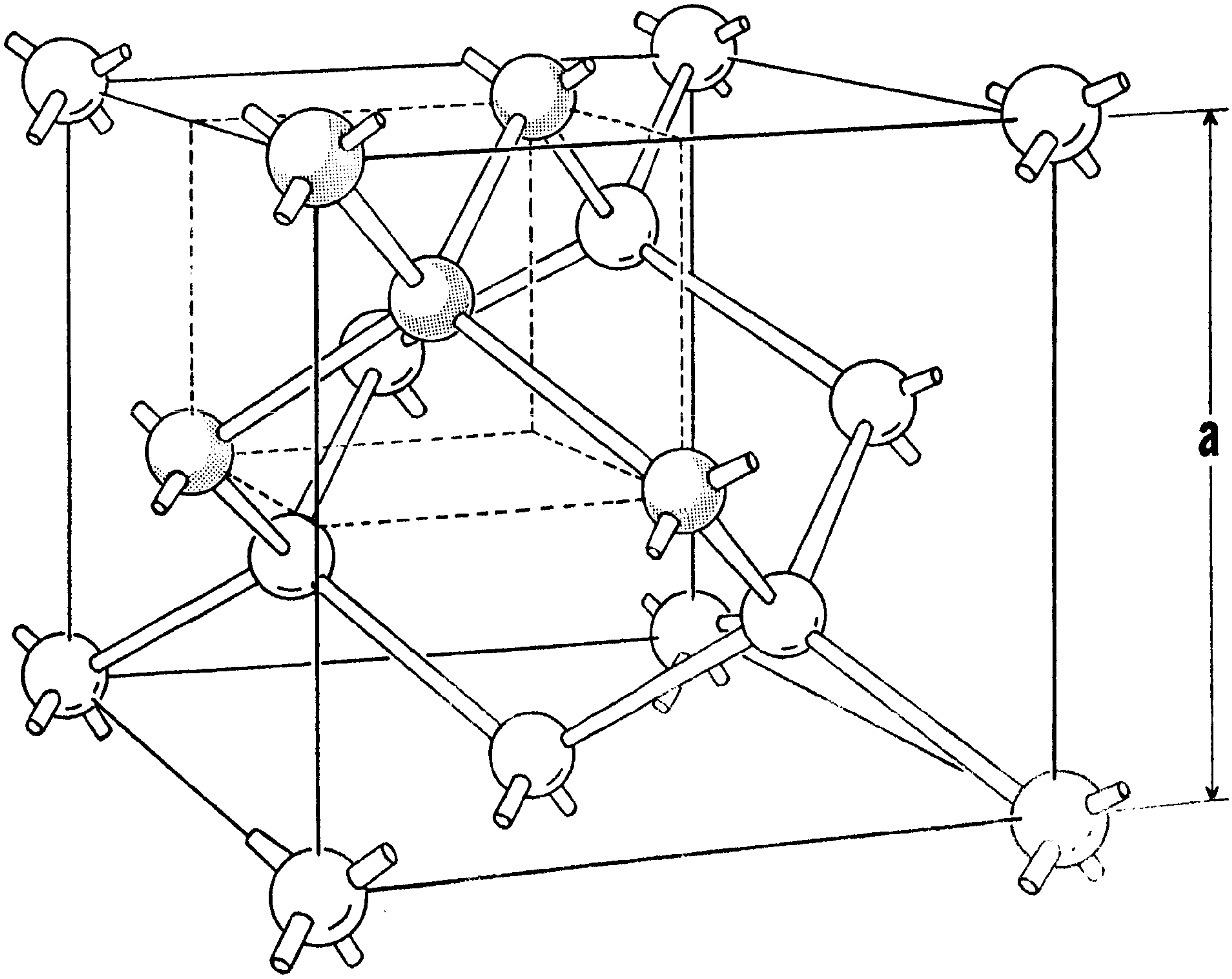

FIGURE 4

WIGNER-SEITZ CELL DIAMOND LATTICE

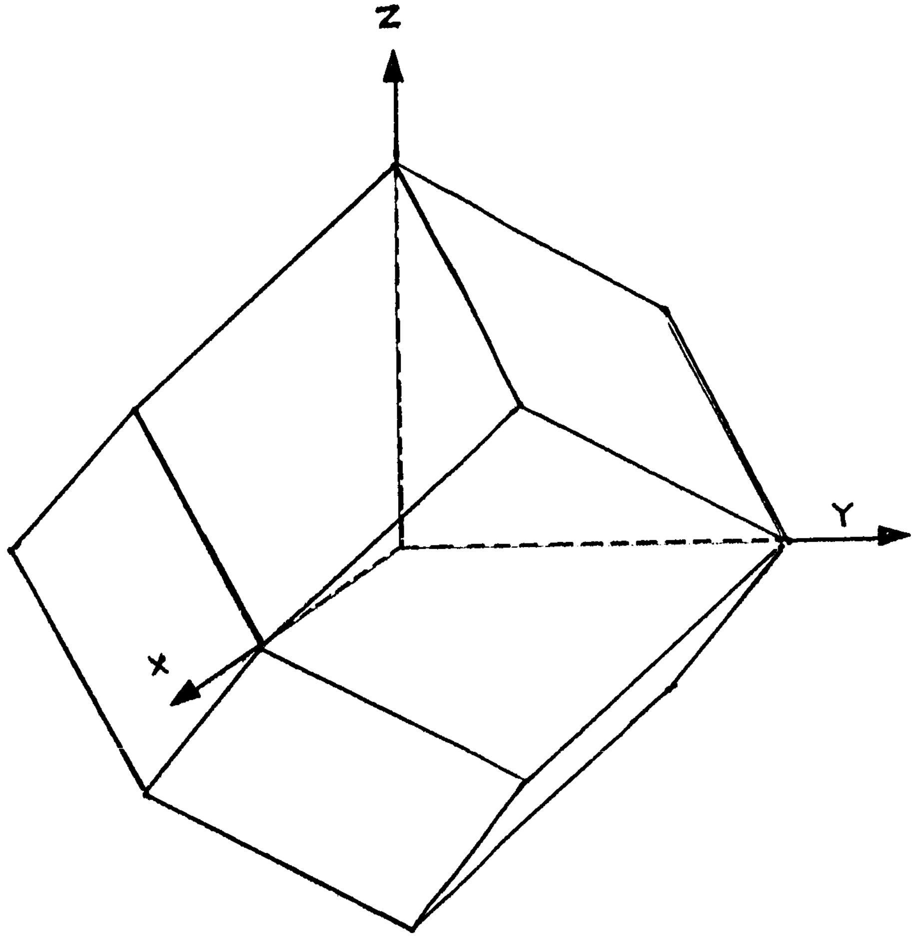

FIGURE 5

FIRST BRILLOUIN ZONE DIAMOND LATTICE

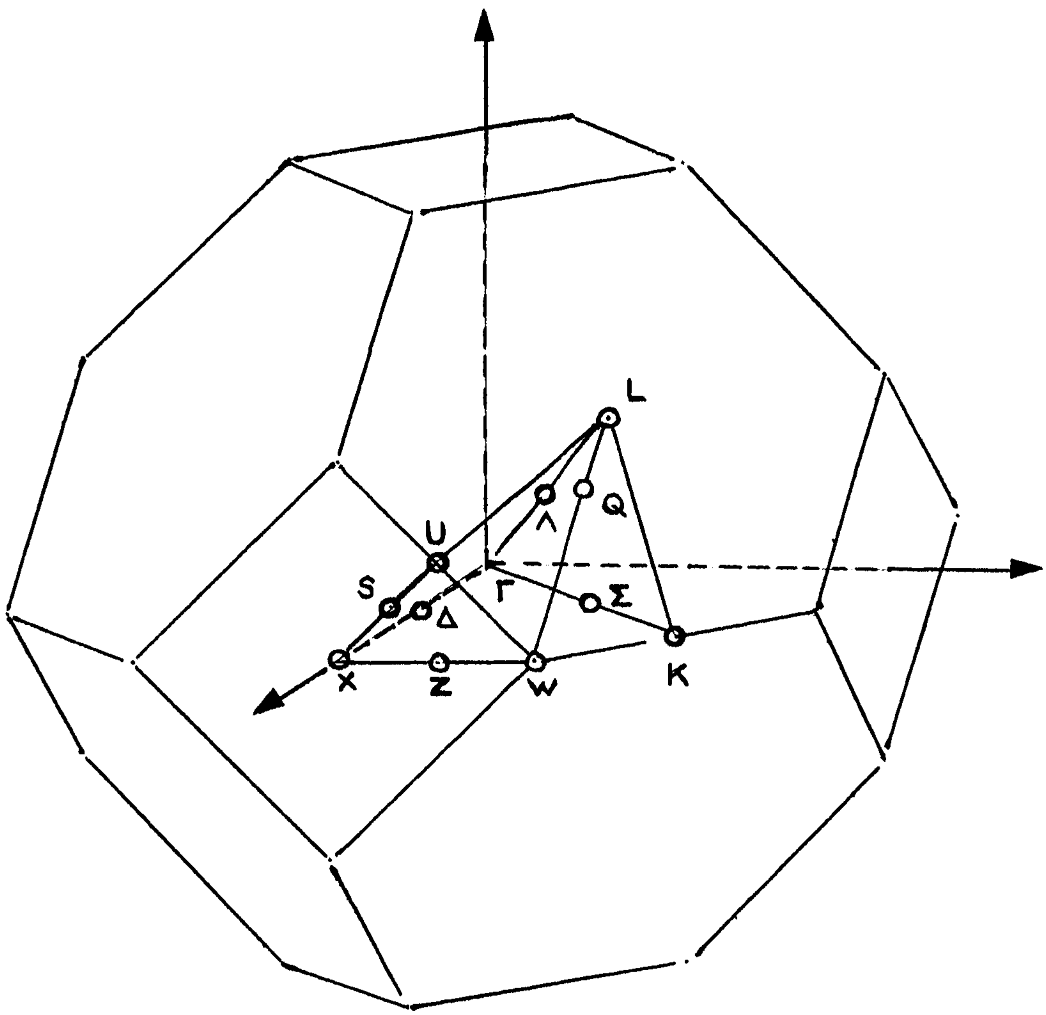

TABLE VII

This table consists of two parts. The first part is a crystal potential determined for the atomic configuration $(1s)^2$ $(2s)^2$ $(2p)^2$ of carbon together with the contributions from nearest neighbors as included by L. F. Mattheiss in one of the SSMTG versions of the Herman-Skillman program[10]. The second part is a similar potential calculated from a $(1s)^2$ $(2s)(2p)^3$ configuration for the atom. The first column of entries in each tabulation contains the entries for the radial distances measured in atomic units. The second column is the entries for the corresponding crystal potential measured in Rydbergs. More correctly, the values of the crystal potential are the negatives of the given numbers according to the usual custom. Each of these parts produced two potentials used in the preliminary calculations.

First Part

	Potential 1	Potential 2
Potential at APW sphere radius	-2.66	-2.66
Average Between Spheres	-2.43	-2.00
Jump	0.23	0.66

Second Part

	Potential 3	Potential 4
Potential at APW sphere radius	-2.73	-2.73
Average Between Spheres	-2.393	-1.393
Jump	0.337	1.337

All energies in these lists are in units of Rydbergs. One should keep in mind that in the APW calculations the energies are taken to be zero in the region between the APW spheres. The zero of potential in the above lists and in the tabulated potentials is at infinity as is the usual custom for atomic calculations.

THIS RUN CARBON AVG=2.427322 (1S)2 (2S)2 (2P)2 12/12/63

OTENTIAL FOR CARBON DETERMINED BY THE MATTHEISS VERSION OF H-F-S SCF CARB008
~~ECIMA CARB009~~
105 0.00243611 13 2.427322 1.459393 CARB010
~~20 40 60 80 CARB011~~
0.00243611 4911.02454 CARB012
~~0.00487222 2447.94733 CARB013~~
0.00730833 1626.83896 CARB014
~~0.00974444 1216.22809 CARB015~~
0.01218055 969.82029 CARB016
~~0.01461666 805.51719 CARB017~~
0.01705277 688.13368 CARB018
~~0.01948888 600.07706 CARB019~~
0.02192499 531.57349 CARB020
~~0.02436110 476.75861 CARB021~~
0.02679721 431.90047 CARB022
~~0.02923332 394.51105 CARB023~~
0.03166944 362.86784 CARB024
~~0.03410555 335.74036 CARB025~~
0.03654166 312.22626 CARB026
~~0.03897776 291.64872 CARB027~~
0.04141387 273.49014 CARB028
~~0.04384998 257.34791 CARB029~~
0.04628610 242.90414 CARB030
~~0.04872221 229.90452 CARB031~~
0.05359443 207.45138 CARB032
~~0.05846665 188.74350 CARB033~~
0.06333887 172.91861 CARB034
~~0.06821109 159.36058 CARB035~~
0.07308331 147.61737 CARB036
~~0.07795553 137.34981 CARB037~~
0.08282775 128.29834 CARB038
~~0.08769997 120.26101 CARB039~~
0.09257219 113.07823 CARB040
~~0.09744441 106.62227 CARB041~~
0.10231663 100.78965 CARB042
~~0.10718885 95.49561 CARB043~~
0.11206107 90.67012 CARB044
~~0.11693329 86.25473 CARB045~~
0.12180551 82.20031 CARB046
~~0.12667773 78.46528 CARB047~~
0.13154995 75.01414 CARB048
~~0.13642217 71.81648 CARB049~~
0.14129439 68.84605 CARB050
~~0.14616662 66.08006 CARB051~~
0.15591105 61.08460 CARB052
~~0.16565549 56.69866 CARB053~~
0.17539994 52.81996 CARB054
~~0.18514438 49.36766 CARB055~~
0.19488882 46.27703 CARB056
~~0.20463326 43.49566 CARB057~~
0.21437770 40.98066 CARB058
~~0.22412214 38.69661 CARB059~~

0.23386658	36.61401	CARB060
0.24361102	34.70812	CARB061
0.25335546	32.95802	CARB062
0.26309990	31.34594	CARB063
0.27284434	29.85668	CARB064
0.28258878	28.47718	CARB065
0.29233322	27.19615	CARB066
0.30207767	26.00380	CARB067
0.31182210	24.89159	CARB068
0.32156654	23.85206	CARB069
0.33131099	22.87865	CARB070
0.34105543	21.96558	CARB071
0.36054431	20.30073	CARB072
0.38003319	18.82295	CARB073
0.39952207	17.50485	CARB074
0.41901095	16.32434	CARB075
0.43849983	15.26336	CARB076
0.45798872	14.30697	CARB077
0.47747760	13.44263	CARB078
0.49696648	12.65965	CARB079
0.51645536	11.94882	CARB080
0.53594424	11.30205	CARB081
0.55543312	10.71221	CARB082
0.57492200	10.17298	CARB083
0.59441088	9.67875	CARB084
0.61389977	9.22450	CARB085
0.63338865	8.80585	CARB086
0.65287753	8.41888	CARB087
0.67236641	8.06019	CARB088
0.69185529	7.72680	CARB089
0.71134418	7.41611	CARB090
0.73083305	7.12586	CARB091
0.76981082	6.59905	CARB092
0.80878858	6.13350	CARB093
0.84776634	5.71933	CARB094
0.88674410	5.34890	CARB095
0.92572187	5.01618	CARB096
0.96469963	4.71632	CARB097
1.00367738	4.44539	CARB098
1.04265516	4.20011	CARB099
1.08163291	3.97776	CARB100
1.12061067	3.77602	CARB101
1.15958844	3.59290	CARB102
1.19856620	3.42669	CARB103
1.23754397	3.27591	CARB104
1.27652173	3.13927	CARB105
1.31549948	3.01563	CARB106
1.35447726	2.90398	CARB107
1.39345501	2.80343	CARB108
1.43243277	2.71320	CARB109
1.47141054	2.63258	CARB110
1.51038830	2.56093	CARB111
1.54936607	2.49770	CARB112
1.58834383	2.44234	CARB113

```
1.62732159          2.39439                                                                   CARB114
1.66629936          2.35340                                                                   CARB115
1.70527712          2.31896                                                                   CARB116
  1         0.24007288E-02           0.47315914E-02                                           CARB117
  1         0.58914080E-05           0.23393882E-04                                           CARB118
  1         0.14387012E-07           0.11453320E-06                                           CARB119
  1         0.35090853E-10           0.55937833E-09                                           CARB120
  1         0.85547318E-13           0.27293534E-11                                           CARB121
  1         0.20850362E-15           0.13310806E-13                                           CARB122
  1         0.50811343E-18           0.64897713E-16                                           CARB123
  1         0.12381412E-20           0.31635869E-18                                           CARB124
  1         0.30168568E-23           0.15419860E-20                                           CARB125
  1         0.73505814E-26           0.75153000E-23                                           CARB126
  1         0.17909189E-28           0.36625782E-25                                           CARB127
  1         0.43633560E-31           0.17848781E-27                                           CARB128
  1         0.10630605E-33           0.86979240E-30                                           CARB129
NTEGRATE                                                                                      CARB130
 20    1 CARBON 1                                                                             CARB131
            3.8                              0.02                                             CARB132
```

```
      THIS RUN  3000C  CARBON  AVG=2.393 (1S)2 (2S)1 (2P)3  5/20/64   3000C001
ENTIAL FOR CARBON DETERMINED BY  THE MATTHEISS VERSION OF H-F-S SCF   3000C002
IMA                                                                   3000C003
5  0.00243611  13  2.392807  1.459393                                 3000C004
0  40  60  80                                                         3000C005
.00243611     4911.16571                                              3000C006
.00487222     2448.08942                                              3000C007
.00730833     1626.98192                                              3000C008
.00974444     1216.37170                                              3000C009
.01218055      969.96447                                              3000C010
.01461666      805.66179                                              3000C011
.01705277      688.27858                                              3000C012
.01948888      600.22211                                              3000C013
.02192499      531.71860                                              3000C014
.02436110      476.90369                                              3000C015
.02679721      432.04540                                              3000C016
.02923332      394.65575                                              3000C017
.03166944      363.01220                                              3000C018
.03410555      335.88430                                              3000C019
.03654166      312.36971                                              3000C020
.03897776      291.79159                                              3000C021
.04141387      273.63235                                              3000C022
.04384998      257.48941                                              3000C023
.04628610      243.04486                                              3000C024
.04872221      230.04438                                              3000C025
.05359443      207.58939                                              3000C026
.05846665      188.87945                                              3000C027
.06333887      173.05232                                              3000C028
.06821109      159.49190                                              3000C029
.07308331      147.74617                                              3000C030
.07795553      137.47598                                              3000C031
.08282775      128.42179                                              3000C032
.08769997      120.38168                                              3000C033
.09257219      113.19606                                              3000C034
.09744441      106.73723                                              3000C035
.10231663      100.90172                                              3000C036
.10718885       95.60478                                              3000C037
.11206107       90.77639                                              3000C038
.11693329       86.35811                                              3000C039
.12180551       82.30084                                              3000C040
.12667773       78.56299                                              3000C041
.13154995       75.10907                                              3000C042
.13642217       71.90869                                              3000C043
.14129439       68.93559                                              3000C044
.14616662       66.16701                                              3000C045
.15591105       61.16658                                              3000C046
.16565549       56.77600                                              3000C047
.17539994       52.89303                                              3000C048
.18514438       49.43684                                              3000C049
.19488882       46.34274                                              3000C050
.20463326       43.55831                                              3000C051
.21437770       41.04068                                              3000C052
.22412214       38.75442                                              3000C053
```

.23386658	36.67004	3000C054
.24361102	34.76278	3000C055
.25335546	33.01173	3000C056
.26309990	31.39909	3000C057
.27284434	29.90966	3000C058
.28258878	28.53034	3000C059
.29233322	27.24984	3000C060
.30207767	26.05834	3000C061
.31182210	24.94728	3000C062
.32156654	23.90917	3000C063
.33131099	22.93743	3000C064
.34105543	22.02624	3000C065
.36054431	20.36565	3000C066
.38003319	18.89261	3000C067
.39952207	17.57945	3000C068
.41901095	16.40379	3000C069
.43849983	15.34734	3000C070
.45798872	14.39490	3000C071
.47747760	13.53375	3000C072
.49696648	12.75307	3000C073
.51645536	12.04356	3000C074
.53594424	11.39716	3000C075
.55543312	10.80682	3000C076
.57492200	10.26633	3000C077
.59441088	9.77024	3000C078
.61389977	9.31370	3000C079
.63338865	8.89248	3000C080
.65287753	8.50283	3000C081
.67236641	8.14147	3000C082
.69185529	7.80551	3000C083
.71134418	7.49242	3000C084
.73083305	7.19998	3000C085
.76981082	6.66959	3000C086
.80878858	6.20149	3000C087
.84776634	5.78575	3000C088
.88674410	5.41456	3000C089
.92572187	5.08173	3000C090
.96469963	4.78228	3000C091
.00367738	4.51213	3000C092
.04265516	4.26790	3000C093
.08163291	4.04678	3000C094
.12061067	3.84636	3000C095
.15958844	3.66461	3000C096
.19856620	3.49977	3000C097
.23754397	3.35034	3000C098
.27652173	3.21497	3000C099
.31549948	3.09251	3000C100
.35447726	2.98195	3000C101
.39345501	2.88237	3000C102
.43243277	2.79298	3000C103
.47141054	2.71307	3000C104
.51038830	2.64199	3000C105
.54936607	2.57918	3000C106
.58834383	2.52411	3000C107

```
.62732159       2.47629                                                   3000C108
.66629936       2.43530                                                   3000C109
.70527712       2.40073                                                   3000C110
1        0.24007282E-02        0.47315869E-02                             3000C111
1        0.58914085E-05        0.23393890E-04                             3000C112
1        0.14387015E-07        0.11453329E-06                             3000C113
1        0.35090861E-10        0.55937890E-09                             3000C114
1        0.85547341E-13        0.27293565E-11                             3000C115
1        0.20850368E-15        0.13310822E-13                             3000C116
1        0.50811359E-18        0.64897797E-16                             3000C117
1        0.12381416E-20        0.31635912E-18                             3000C118
1        0.30168578E-23        0.15419881E-20                             3000C119
1        0.73505838E-26        0.75153103E-23                             3000C120
1        0.17909196E-28        0.36625835E-25                             3000C121
1        0.43633576E-31        0.17848806E-27                             3000C122
1        0.10630609E-33        0.86979368E-30                             3000C123
EGRATE                                                                    3000C124
13000 CARBON2393                                                          3000C125
     -1.0                   0.1                                           3000C126
```

REFERENCES

1. J. C. Slater, Phys. Rev. 51, 846(1937).
2. J. H. Wood, Phys. Rev. 126, 517(1962).
3. J. C. Slater, Quantum Theory of Molecules and Solids, Volume 1, McGraw Hill Book Co., Inc., 1963, Chapter 8.
4. J. C. Slater, Quarterly Progress Report No. 26, Solid-State and Molecular Theory Group, M. I. T., October 15, 1962.
5. J. C. Slater, Quarterly Progress Report No. 47, Solid-State and Molecular Theory Group, M. I. T., January 15, 1963.
6. J. H. Wood, Augmented Plane Wave Program Manual, Solid-State and Molecular Theory Group, M. I. T., Unpublished.
7. E. R. Keown, Quarterly Progress Report No. 51, Solid-State and Molecular Theory Group, M. I. T., January 15, 1964.
8. F. Bassani and M. Yoshime, Phys. Rev. 130, 20(1963).
9. P. M. Scop, Ph. D. Thesis, M. I. T., 1964.
10. F. Herman and S. Skillman, Atomic Structure Calculations, Prentice-Hall, Inc., 1963.
11. L. F. Mattheiss, Quarterly Progress Report No. 48, Solid-State and Molecular Theory Group, M. I. T., April 15, 1963.
12. P. O. Lowdin, Advances in Physics 5, 1(1956).
13. E. R. Keown and J. H. Wood, Quarterly Progress Report No. 53, Solid-State and Molecular Theory Group, M. I. T., July 15, 1964.

SPACE TECHNOLOGY PROJECT # 7

COSMIC RAY MUONS

COSMIC RAY MUONS

Project Investigators

Dr. Nelson M. Duller, Principal Investigator, Associate Professor of Physics

Mr. K. W. Bull, Graduate Research Assistant

Mr. W. G. Cantrell, Graduate Research Assistant

Mr. D. L. Edens, Graduate Research Assistant

Mr. A. V. Jelinek, Graduate Research Assistant

Mr. J. R. Sharber, Graduate Research Assistant

Mr. E. L. Walker, Graduate Research Assistant

Mr. J. D. Winningham, Graduate Research Assistant

I. Review of the Work of the Past Period

Work has continued on the various systems involved in the large detectors of muons. Only test data on energetic muons have been recorded. Progress on the projects is described in the following items:

A. The testing of various experimental models of large spark chambers has now been essentially completed except for the wire chambers. Work is now in progress on one of the medium-sized chambers which will be used in the experiments. It consists of a rectangular aluminum frame lined with plate glass on five sides and a heavy O-ringed aluminum plate on the sixth side. The spark chamber electrodes are not yet mounted but will be vertical for display of the near horizontal particle tracks in the experiments. The over-all dimensions of the chamber are 3 ft. x 3 ft. x 2 ft. The telescope elements and triggering system for this chamber will be very similar to those described in a previous progress report. Two large polished slabs of scintillating plastic are now being prepared for coupling to photomultiplier tubes for the two telescope elements.

B. With the objective of developing very large spark chambers with only slight sacrifice of spatial resolution, considerable effort has been expended on various wire configurations as the electrodes in the experimental spark chambers. It is expected that reduced mechanical problems and expense associated with simple wire configurations will justify this work when chambers of total area greater than 50 $ft.^2$ are attempted. So far moderate success has been attained with the straightforward winding of either piano wire or polished tungsten on lucite frames. (See figure 1)

C. Another project which has been initiated during the past period to facilitate the use of very large chambers is the development of large wire proportional counters (sometimes acting also as Geiger counters). It is hoped that these can be used either as the sole telescope elements in the very large chambers or in redundant circuitry to help reduce ambiguity in multiple-particle

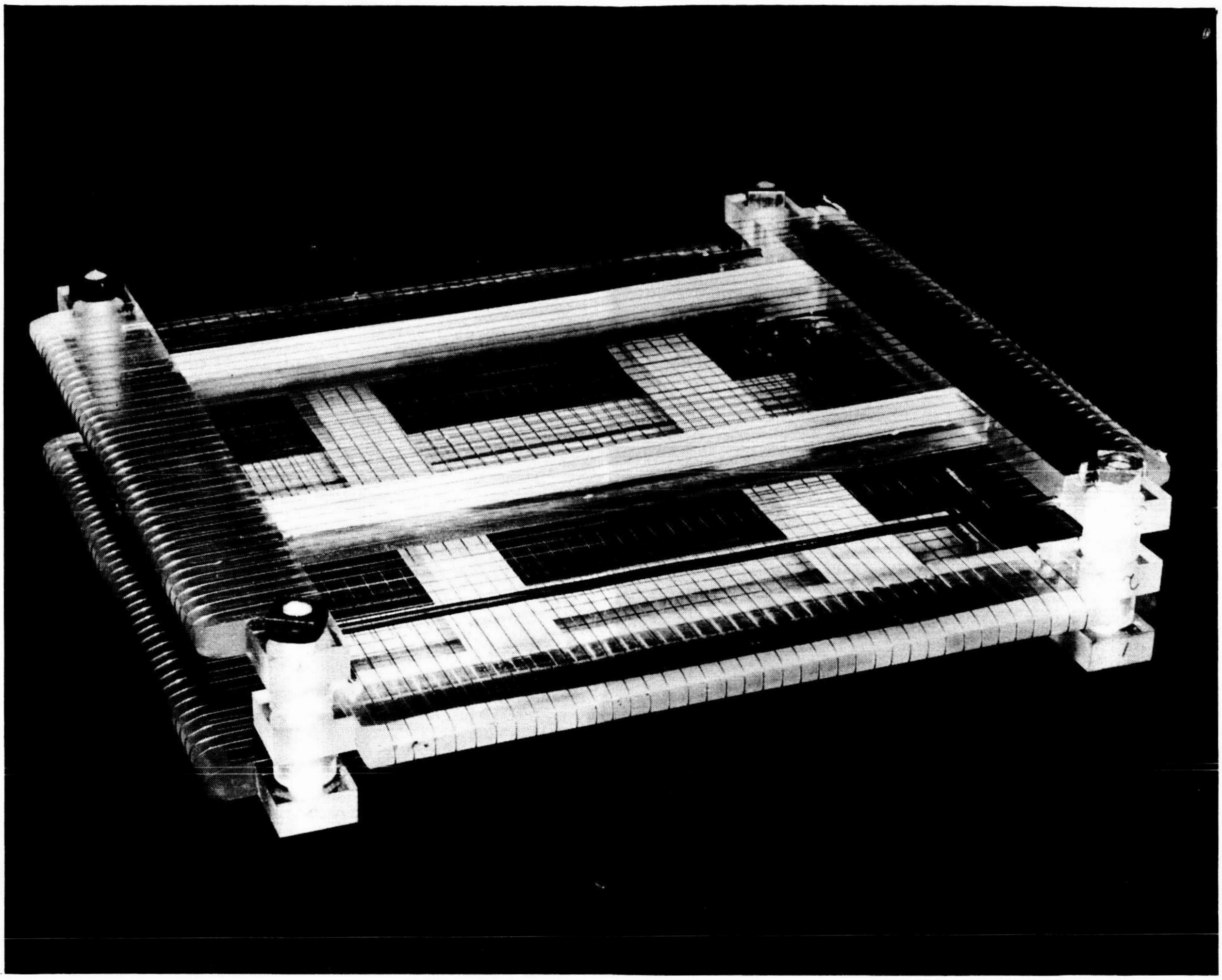

Figure 1. An example of simple wire frames as electrodes for a spark chamber.

events in the chamber. So far only moderate success has been realized with these counters. The structure of the parallel wire electrodes is similar to that of the wire elements shown in Figure 1 but with much closer spacing. These counters will be continually flushed (argon, CO_2 and ethyl alcohol vapor) instead of evacuated and filled.

D. The transistorized hodoscope system has progressed considerably during the past period. A complete set of thirty-six channels with the control and master circuits will soon be tested. Representative individual cards and cards in place in a typical rack are shown in Figures 2 and 3 . Final details of the entire system will be given in the report of the next period.

E. A new site for most of the experiments to be carried out in this project during the next two or three years has recently been made available by the Space Technology Division of Texas A&M University. This is a large ground-level room in the Aerospace Windtunnel Laboratory near Easterwood Airport just west of the main campus. Airconditioning is now being installed and it is planned that the installation of general facilities and laboratory equipment will begin during the first half of July.

F. A contributed paper on the theoretical interpretation of muon intensities at high energies, supported in part by

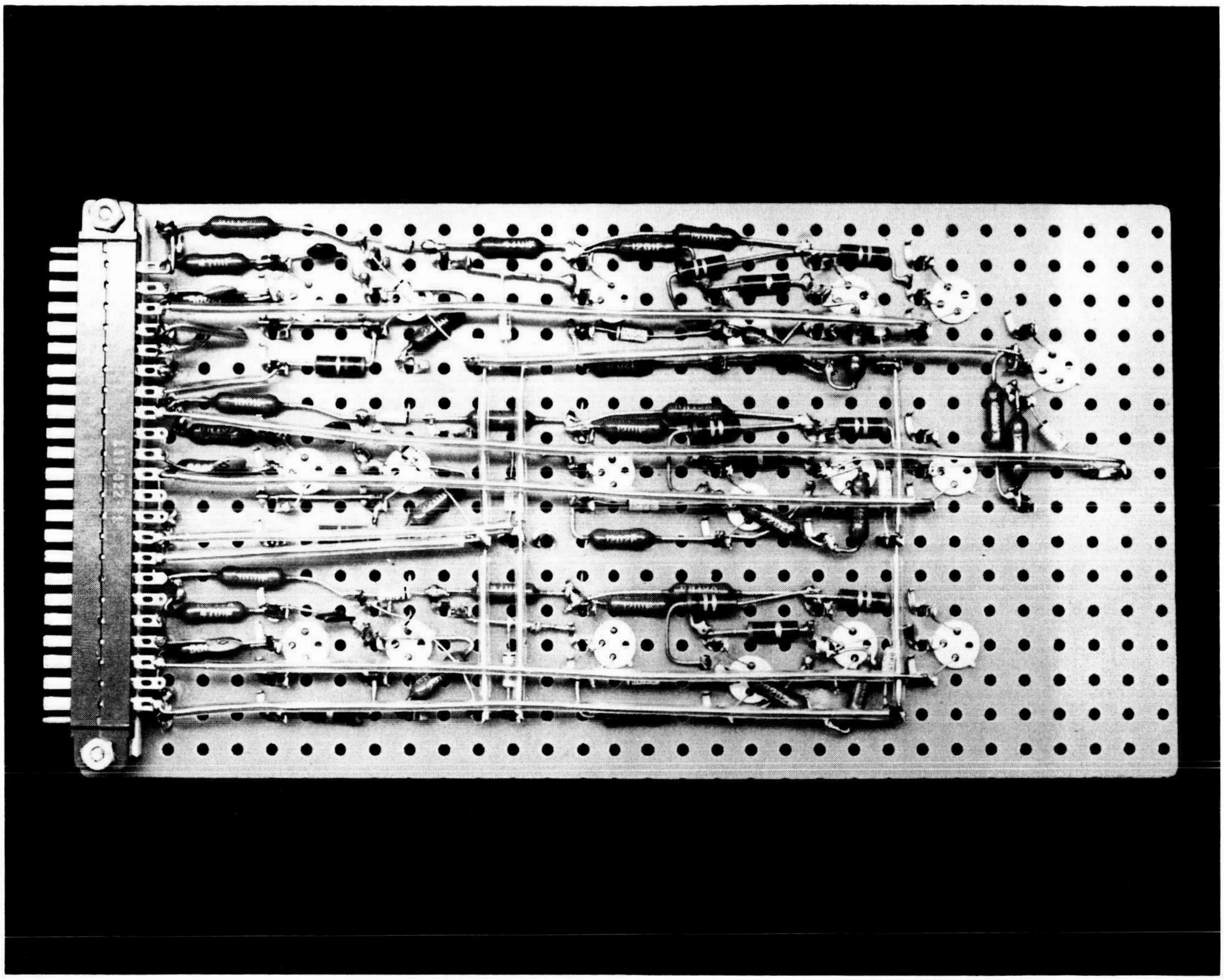

Figure 2. A typical plug-in card in the transistorized hodoscope.

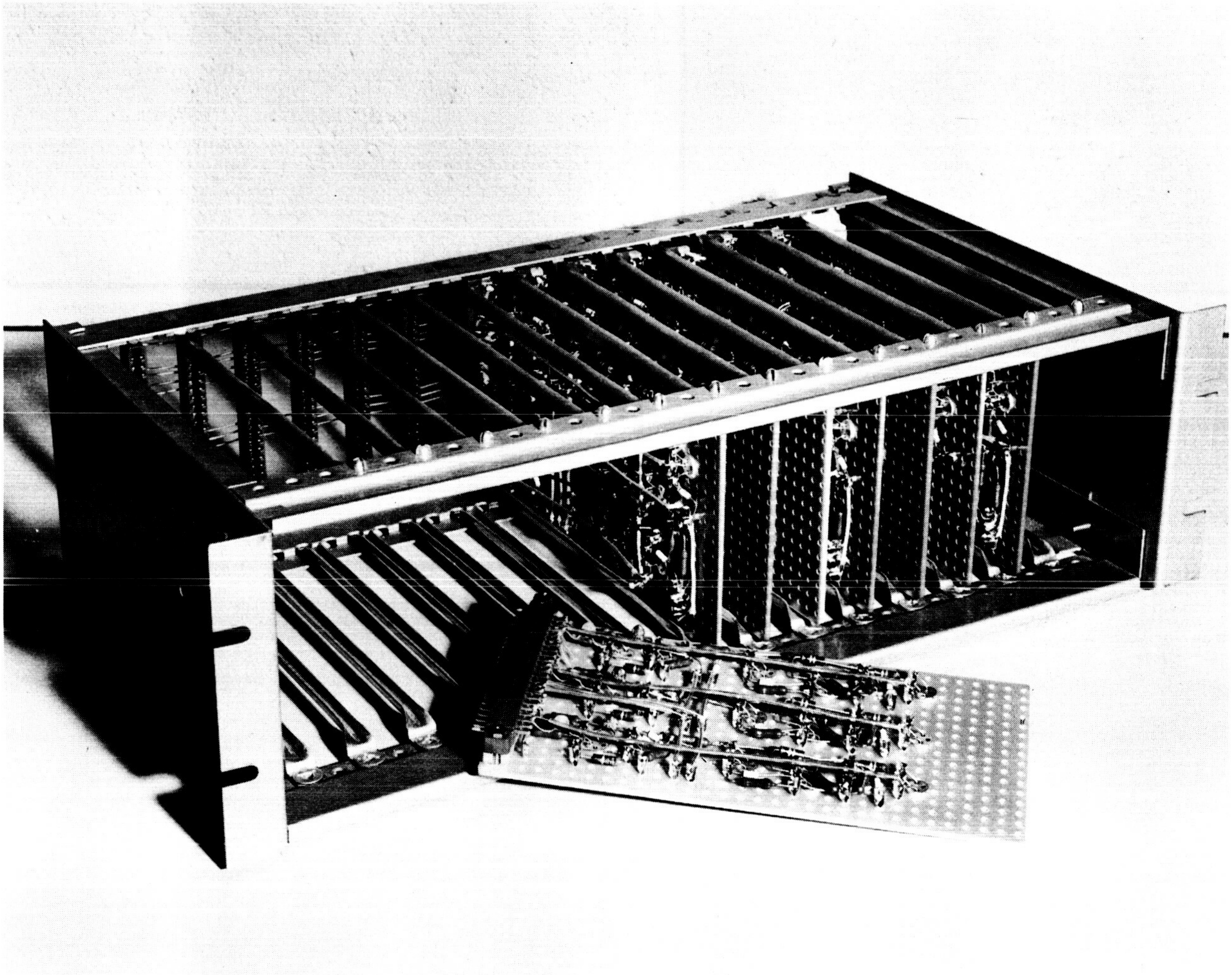

Figure 3. A plug-in card rack for the hodoscope.

this project grant, was given at the Tucson meeting of the American Physical Society, February 27, 1964: High-Energy Pions and Muons in the Atmosphere, R. R. Kasten and N. M. Duller, Bulletin of the American Physical Society 9, 141 (1964).

II. Work Planned for the Next Period

During the latter half of 1964 the new laboratory will be occupied and actual experiments on low-energy and high-energy muons started. Work on the large spark chambers, large proportional counters, the telescope systems, and the hodoscope system will continue. It is planned to begin assembly of large stacks of absorbers on the ground outside the building for energy discrimination during the early part of the next period.

SPACE TECHNOLOGY PROJECT NO. 8

SPACE STRUCTURES

SPACE STRUCTURES

This project is concerned with two areas of research:

1. Behavior of Isotropic and Anisotropic Shells
2. Impact Attenuation of Spacecraft

The study of the structurally anisotropic shell has been broken up into four parts, three of which are analytical in nature and one of which is experimental. The analytical portions are in a form such that each succeeding part introduces a more generalized form of anisotropy. Thus each succeeding portion is applicable to a more general class of problems than the preceeding portions.

The main advantage of such a stepwise procedure is that a check is readily effected in the resulting shell equations. Since each analytical portion deals with a more generalized form of anisotropy than the preceeding section, then by the same token the equations of the succeeding section must degenerate to those of the preceeding sections.

The four phases of the study are summarized as follows.

a) Development of a general set of thin shell equations for an orthotropic material. This form of anisotropy will account for many of the plastics being used in shell construction.

b) Development of a general set of equations for a material exhibiting plane anisotropy. This form of anisotropy can account for plywood type construction and filament wound shells. It can also be applied to multi-ribbed shells if the ribs are spaced sufficiently close together.

c) Development of a general set of shell equations exhibiting plane anisotropy whereby the elastic oonstants do not exhibit diagonal symmetry. It is hoped that this form of anisotropy can account for most of the structurally anisotropic materials encountered.

d) Limited testing of the various structurally anisotropic materials when applied to differnet shell configurations. In this way the degree of compliance between theory and test will be determined.

To date, Part (a) has been completed and is included in this report. Part (b) is being worked on by Mr. H. J. Sweet who is planning to use the results for his Ph.D. dessertation. Part (c) has been worked on.

A detailed progress report covering the impact attenuation study is presented in this report and includes final reports on the studies of the impact attenuation characteristics of collapsable tubes, crushable honeycomb, and conformable legs.

The portion of the project dealing with frangible tubes is still in progress.

ISOTROPIC AND ANISOTROPIC SHELL RESEARCH

PROGRESS REPORT # 1

Project Investigator:

Dr. Thomas J. Kozik, Associate Professor of Mechanical Engineering and Associate Research Engineer

I. Introduction

The necessity of designing structures which yield the greatest strength to weight ratio has resulted in the increased use of materials with anisotropic elastic properties. The anisotropy encountered may be a property of the material as would be the case of some of the plastics, or it might be of constructional type such as sandwich plate.

One type of anisotropy frequently encountered is orthotropy. This type of anisotropy is characterized by having three mutually perpendicular planes of elastic symmetry. In the application of orthotropic materials to shells, these three planes usually have a special configuration relative to the shell surface. That is, two of the three normals to the three planes of elastic symmetry are tangent to the principal curvalinear coordinate lines of the shell middle surface.

The present paper is concerned with the analysis of thin elastic shells composed of an orthotropic material of the type described in the preceding paragraph. A set of three partial differential equations predicting the behavior of such shells is developed and presented in terms of the three components of the shell middle surface displacement.

The analysis differs considerably from that usually employed in the development of shell equations. In the more traditional approach the equilibrium conditions on an element are expressed in terms of stress resultants and then, utilizing the compatibility equations, the resultant shell equations are derived. These equations are six first order partial differential equations expressed in terms of the stress resultants. The present work formulates the equilibrium conditions on an element in terms of the middle surface displacement components. By means of a series of integrations over the shell thickness, a final set of three partial differential equations in the three unknown displacement components result.

The method of analysis employed has two significant advantages over the more traditional approaches. First, simplification of the equations in regard to inisgnficant terms is more readily effected since there are only three variables to consider. The second advantage is by far the most important. That is, a set of shell displacement equations cannot be readily derived from a set of shell equations stated in terms of stress resultants.

This fact is not limited to orthotropic materials but manifests itself for isotropic ones as well. A resultant set of shell equations is given by Novozhilov [1][1] for an isotropic body.

---

1 Numbers in brackets refer to references at end of paper.

V. Z. Vlasov [2] also gives a set of shell equations for an isotropic body but his equations are derived and presented in terms of middle surface displacments. If the middle surface displacement-stress resultant relations are substituted into the stress resultant shell equations and this result compared to the equations given by Vlasov, it will be found that the two sets of shell equations are not identical.

In reducing the stress-resultant equations to those involving middle surface displacements or in deriving directly the middle surface displacement equations, a total of three equations result. Each of the equations corresponds to a force summation in one of three mutually perpendicular directions. One of the equations, say the third, is the equation which represents the force summation in a direction perpendicular to the shell middle surface and hence is the significant equation in the degenerate case of a flat plate in that it leads to the familiar plate equation. The discrepancy in the two sets of shell equations mentioned in the preceding paragraph lies in the tangentical displacement terms of the first two of the displacement equations. The third equation and the normal displacement terms of the two sets of equations check each other exactly. It might be noted that discrepancies in the tangential displacements are such that they disappear whenever the Lame' surface parameters are constant. Thus the discrepancies would disappear for a circular cylindrical shell.

The Formalation of the equilibrium equations in terms of the middle surface displacements and their consequent use to derive the resulting shell equations is attributable to V. Z. Vlasov. In many respects, the derivation presented in this paper parallels that of Vlasov's. However, there is one main point of departure between the two derivations and that is in regard to displacement μ_γ, measured normal to the shell. Vlasov's derivation considers this normal displacement to be a constant through the shell thickness and equal to the corresponding middle surface displacement whereas the present work shows that this displacement must be considered a variable through the shell thickness and in fact its explicit form is derived.

Abundant experimental evidence indicates that the plane stress solution to the thin plate problem is the correct one. Since thin shells are generalizations of thin plates, it might logically be expected that correct shell solutions should also be based on an equivalent plane stress conditions. When shell equations are developed in terms of stress resultants, two simplifications are normally made. One, which is in the nature of an assumption, is that the normal stresses in a direction perpendicular to the surface of a shell are small in comparison to the other stresses and may be neglected. The second, which is in the nature of an approximation, is that the normal strains in a direction perpendicular to the shell surface are similarly small and may be neglected. That the two simplifications are incompatible is readily discernable when one realizes that in the case of a flat plate the first would be the condition of plane stress while the other would be the condition of plane strain. So long as only stress resultants are being considered this contradiction is of little consequence in that the error involved is normally smaller than that due to the Kirchoff hypothesis.

Such is not the case when shell displacement equations are being considered. The coefficients in the resulting set of displacement equations, which are functions of the elastic constants, are very much affected by the choice of approximations. If the length change of a segment normal to the shell surface is neglected, the resulting set of equations, when degenerated to that of a flat plate, will yield the plane strain solution for the plate. In a similar manner, if the noraal stress in the direction perpendicular to the shell is neglected, the corresponding flat plate solution will be the plane stress one. If both assumptions are utilized, the resulting corresponding flat plate solution will be the plane strain condition.

As has been mentioned, the present analysis for orthotropic materials differs in approach from that of Vlasov's for an isotropic material in the consideration of the normal displacement. Remarkably enough, the equations given by Vlasov are correct though his solution is based on a plane strain premise. Though Vlasov claims to use the Lame' elastic constants, his definitions for them are not correct. But the definitions he does use do correct his result such that he arrives at the correct thin shell equations for an equivalent plane stress condition.

The applicability of the nondeformable normal and hence the Kirchoff hypothesis to orthotropic materials is an open question. As pointed out by Ambartsumian in his review of anisotropic shell theory [3], the Kirchoff hypothesis prevents any consideration of the effects of those elastic properties dependent upon a direction normal to the shell. This effect manifests itself in the present derivation in that the resultant displacement equations are independent of the elastic constants associated with the direction of the normal to the shell. In his book [4], Ambartsumian states that the error involved in the use of the Kirchoff hypothesis for anisotropic materials leads to an error which decreases with decrease in the relative thickness, ($k\delta$), and also decreases with a decrease in the degree of anisotropy (or orthotropy) as measured by the ratio of the elastic constants. However he also points out that the limits of applicability of the Kirchoff hypothesis are almost impossible to state for any particular problem except by test data correlation with theory.

That the Kirchoff hypothesis is sufficiently accurate for a large number of anisotropic and hence orthotropic shell structures is evidenced by its applications. Thus the problem of anisotropic laminated shells, which makes up the major portion of Ambartsumian's book, is predicated on the validity of the Kirchoff hypothesis.

II. Theoretical Development

A. Assumptions:

Linear elastic shell theory presupposes a great many assumptions. However the majority of them are so frequently encountered that unless stated to the contrary, they are assumed to be in force. So far as the present orthotropic development is concerned, there are only two assumptions which need be stated less the results be misrepresented.

a) It is assumed that the Kirchoff hypothesis of a non-deformable normal to the shell middle surface is valid. However this assumption will not preclude the extension or contraction of a line element of the shell which is oriented in a direction perpendicular to the shell surface.

b) It is also assumed that the curvature change and the torsion of the shell middle surface expressions may be simplified so as to neglect the tangential displacement terms. This assumption limits the shell analysis in one of two ways. It either restricts the shells to those of the shallow type or restricts the stress condition to be one in which the bending stresses are of the same order of magnitude as in the plane stresses.

The above two assumptions will be used extensively in the simplifications of the shell equations. Since the Kirchoff hypothesis introduces an error of magnitude ($k\delta$) in comparison with unity into shell theory, any term whose order of magnitude in comparison with unity can be shown to be this value will be discarded.

B. Nomenclature:

α, β, γ = Principal curvalinear coordinates of the shell middle surface. γ is the distance measured normal to the surface.

A, B = Lamé surface parameters which are also the coefficients of the first quadratic form of the surface.

k_1, k_2 = Principal curvatures of the surface.

K = Gaussian curvature.

H = Mean curvature and equal to the algebraic mean of the principal curvatures.

L = Mean difference curvature equal to the algebraic mean of the difference of the principal curvatures.

δ = Shell thickness.

K_α, K_β = Principal curvature changes along the α and β coordinate lines respectively.

u, v, w = Middle surface displacement components in the α, β and γ directions respectively.

aij = Elastic constants given by the generalized Hooke's Law.

P_α, P_β, P_γ = Components of the resultant external loading per unit middle surface area in the α, β and γ directions respectively.

C. Preliminaries:

The equations necessary for the subsequent development will be listed in this section. The majority of these equations are well known and their development may be found in any text such as Novozhilovs [1] which deals with thin shell analysis.

A set of principal curvalinear coordinates may be defined for any surface. A set of curvalinear coordinate lines may then be drawn on the surface and this set of lines will have the property of mutual orthogonality. Let the one group be designated as the α coordinate lines and the other as the β coordinate lines. A normal direction, γ, will be designated on the surface such that positive γ is in the direction of the negative curvature of the surface.

The first quadratic form for a surface in principal curvalinear coordinates is given as

$$ds^2 = A^2(d\alpha)^2 + B^2(d\beta)$$

In the above expression, the coefficients A and B are called the Lamé surface parameters. The differential line element along the α and β coordinate lines may then be written as

$$ds_\alpha = Ad\alpha; \; ds_\beta = Bd\beta$$

Since a shell of thickness δ may be thought of as being composed of an infinite number of parallel surfaces, some reference surface must be chosen to describe the shell configuration. This surface will be the middle surface, that is, the surface lying halfway between the top and bottom surface of the shell.

Obviously a set of Lame surface parameters, displacement components or strains may be defined for any of the surfaces comprising the shell. To differentiate these quantities applicable to any surface from the same quantities defined for the middle surface, the following notation will be introduced.

For any surface other than the middle surface, the first quadratic form will be given as

$$ds^2 = (1/h_1)^2(d\alpha)^2 + (1/h_2)^2(d\beta)^2$$

where α and β still are the principal curvalinear coordinates of the middle surface. The quantities h_1 and h_2 are related to A and B as follows

$$h_1 = \frac{1}{A(1+k_1\gamma)} \; ; \; h_2 = \frac{1}{B(1+k_2\gamma)} \qquad (1)$$

The middle surface displacement components will be designated as u, v and w where u is the displacement in the direction tangent to an α coordinate line, v in the direction tangent to the β coordinate line and w in the direction of γ, or normal to the middle surface. For any other surface, the correspondnng displacement components will be designated as u_α, u_β and u_γ. The relation between the two sets of tangential displacement components is found as a consequence of the Kirchoff hypothesis.

$$\begin{aligned} u_\alpha &= (1+k_1\gamma)u - \frac{1}{A}\frac{\partial w}{\partial \alpha}\gamma \\ u_\beta &= (1+k_2\gamma)v - \frac{1}{B}\frac{\partial w}{\partial \beta}\gamma \end{aligned} \qquad (2)$$

The strains associated with a point in the shell will be designated by the usual notation adopted in elasticity theory. However, one exception will be made. Whereas the shear strain will use the conventional double subscript notation, the normal strains will use only a single subscript.

The relation between the strains and the displacements at a point within the shell is given as

$$
\begin{aligned}
e_\alpha &= \frac{\partial\mu_\alpha}{\partial_\alpha} + h_1h_2 \frac{\partial h_1}{\partial_\beta}^{-1}\mu_\beta + h_1\frac{\partial h_1}{\partial_\gamma}^{-1}\mu_\gamma \\
e_\beta &= h_2 \frac{\partial\mu_\beta}{\partial_\beta} + h_1h_2 \frac{\partial h_2}{\partial_\alpha}^{-1}\mu_2 + h_2 \frac{\partial h_2}{\partial_\gamma}^{-1}\mu_\gamma \qquad (3) \\
e_\gamma &= \frac{\partial\mu_\gamma}{\partial_\gamma} \\
e_{\alpha\beta} &= \frac{h_1}{h_2}\frac{\partial}{\partial_\alpha}(h_2\mu_\beta) + \frac{h_2}{h_1}\frac{\partial}{\partial_\beta}(h_1\mu_\alpha)
\end{aligned}
$$

For points lying on the middle surface, the strains will be designated as e_1, e_2, e_3, and e_{12}. These strains, with the exception of $_3$, are given as

$$
\begin{aligned}
e_1 &= \frac{1}{A}\frac{\partial\mu}{\partial_\alpha} + \frac{1}{AB}\frac{\partial A}{\partial_\beta} v + k_1 w \\
e_2 &= \frac{1}{B}\frac{\partial v}{\partial_\beta} + \frac{1}{AB}\frac{\partial B}{\partial_\alpha}\mu + k_2 w \qquad (4) \\
e_{12} &= \frac{A}{B}\frac{\partial}{\partial_\beta}\left(\frac{\mu}{A}\right) + \frac{B}{A}\frac{\partial}{\partial_\alpha}\left(\frac{v}{B}\right)
\end{aligned}
$$

The conditions of Codazzi and Gauss must necessarily be sastified by the middle surface. These Codazzi conditions are

$$\frac{\partial}{\partial_\alpha}(k_2 B) = k_1 \frac{\partial B}{\partial_\alpha};\ \frac{\partial}{\partial_\beta}(k_1 A) = k_2 \frac{\partial A}{\partial_\beta}$$

and the condition of Gauss is given as

$$\frac{\partial}{\partial_\alpha}\left(\frac{1}{A}\frac{\partial B}{\partial_\alpha}\right) + \frac{\partial}{\partial_\beta}\left(\frac{1}{B}\frac{\partial A}{\partial_\beta}\right) = -KAB$$

where K is the Gaussian curvature of the surface.

D. Equilibrium Equations:

Figure 1 shows a differential element of the shell located at a distance γ from the shell middle surface. A general stress condition is assumed to exist on the element and in addition to the stresses, the body forces per unit volume, p_α, p_β and p_γ are in evidence.

Summing forces in the direction of the tangents to the α, β and γ coordinate lines, the following three equations must be satisfied if a state of equilibrium exists.

$$\frac{\partial}{\partial_\alpha}\left(\frac{\sigma_\alpha}{h_2}\right) - \frac{\partial h_2^{-1}}{\partial_\alpha}\sigma_\beta + h_1 \frac{\partial}{\partial_\beta}\left(\frac{\sigma_{\alpha\beta}}{h_1^2}\right) + h_1 \frac{\partial}{\partial_\gamma}\left(\frac{\sigma_{\alpha\gamma}}{h_1^2 h_2}\right) + \frac{p_\alpha}{h_1 h_2} = 0$$

$$\frac{\partial}{\partial\beta}\left(\frac{\sigma_\beta}{h_1}\right) - \frac{\partial h_1^{-1}}{\partial_\beta}\sigma_\alpha + h_2 \frac{\partial}{\partial_\alpha}\left(\frac{\sigma_{\alpha\beta}}{h_2^2}\right) + h_2 \frac{\partial}{\partial_\gamma}\left(\frac{\sigma_{\beta\gamma}}{h_1 h_2^2}\right) + \frac{p_\beta}{h_1 h_2} = 0 \qquad (5)$$

$$-\frac{1}{h_2}\frac{\partial h_1^{-1}}{\partial\gamma}\sigma_\alpha - \frac{1}{h_1}\frac{\partial h_2^{-1}}{\partial\gamma}\sigma_\beta + \frac{\partial}{\partial_\alpha}\left(\frac{\sigma_{\alpha\gamma}}{h_2}\right) + \frac{\partial}{\partial_\beta}\left(\frac{\sigma_{\beta\gamma}}{h_1}\right) + \frac{\partial}{\partial\gamma}\left(\frac{\sigma_\gamma}{h_1 h_2}\right) +$$

$$\frac{p_\gamma}{h_1 h_2} = 0$$

E. Stress Strain Relations

For an orthotropic material whose three planes of elastic symmetry have normals coinciding with tangents to the curvalinear

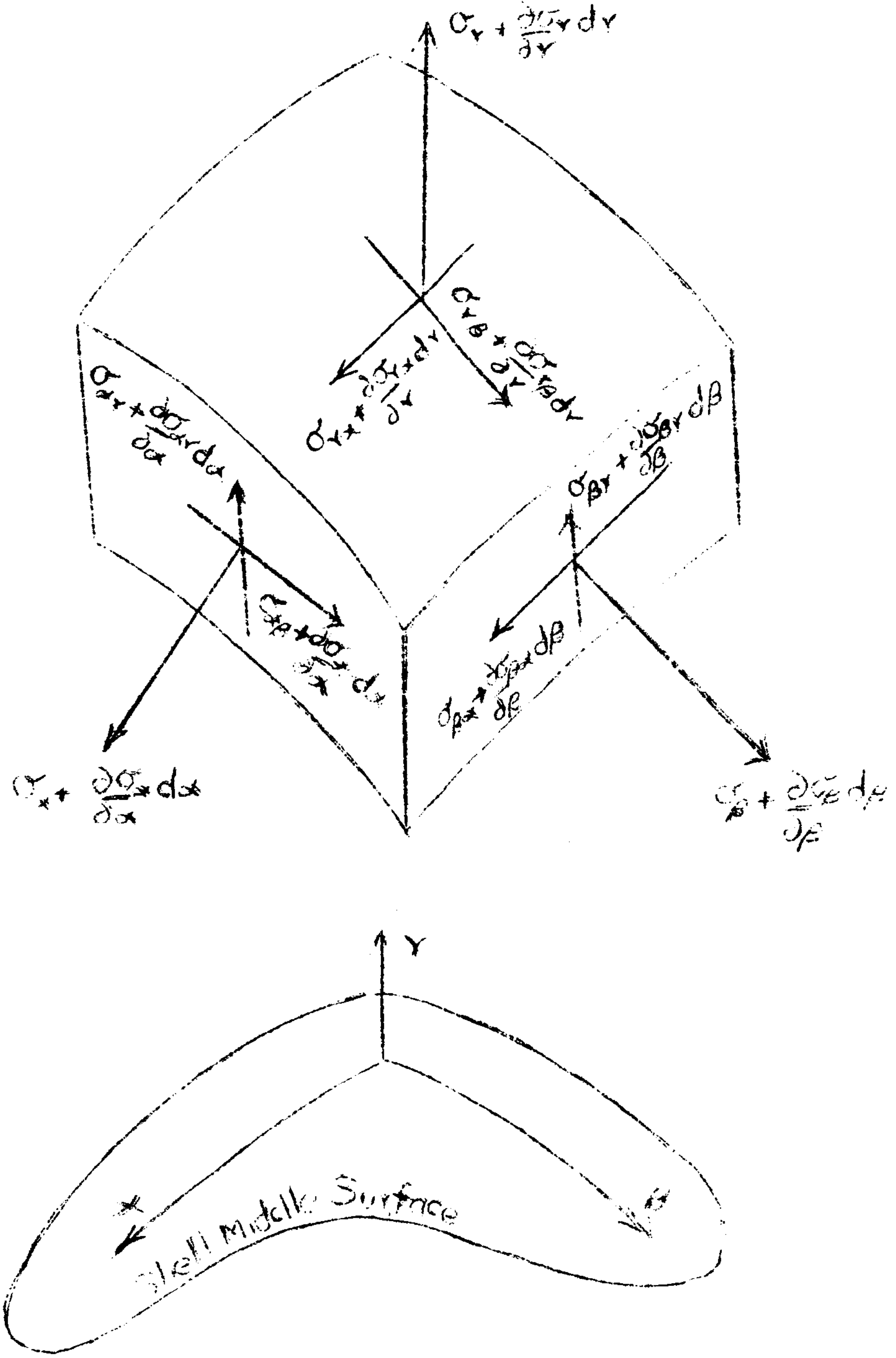

FIG. 1

coordinate lines, the generalized Hookes' Law for anl point in the shell may be written as

$$e_\alpha = a_{11}\,\sigma_\alpha + a_{12}\,\sigma_\beta + a_{13}\,\sigma_\gamma$$

$$e_\beta = a_{21}\,\sigma_\alpha + a_{22}\,\sigma_\beta + a_{23}\,\sigma_\gamma$$

$$e_\gamma = a_{31}\,\sigma_\alpha + a_{32}\,\sigma_\beta + a_{33}\,\sigma_\gamma$$

$$e_{\beta\gamma} = a_{44}\,\sigma_{\beta\gamma}$$

$$e_{\alpha\gamma} = a_{55}\,\sigma_{\alpha\gamma}$$

$$e_{\alpha\beta} = a_{66}\,\sigma_{\alpha\beta}$$

The quantities "aij" are the elastic constants of the material and possess the symmetric property that

$$a_{ij} = a_{ji}$$

An alternate and temporarily more convenient form of expressing the stress strain relations will now be introduced. Define the quantities λ_α, λ_β, μ_α, μ_β and $\mu_{\alpha\beta}$ in terms of the elastic constants as

$$\lambda_\alpha = \frac{-\,a_{12}}{(a_{11}a_{22}-a_{12}^2) + (a_{11}a_{23}-a_{12}a_{13})}$$

$$\lambda_\beta = \frac{-\,a_{12}}{(a_{11}a_{22}-a_{12}^2) + (a_{22}a_{13}-a_{12}a_{23})}$$

$$2\mu_\alpha = \frac{a_{12} + a_{22} + a_{23}}{(a_{11}a_{22}-a_{12}^2) + (a_{11}a_{23}-a_{12}a_{13})} \qquad (6)$$

$$2\mu_\beta = \frac{a_{11} + a_{12} + a_{13}}{(a_{11}a_{22}-a_{12}^2) + (a_{22}a_{13}-a_{12}a_{23})}$$

$$\mu_{\alpha\beta} = \frac{1}{a_{66}}$$

Note that these constants become the Lame' elastic constants in the case of an isotropic body.

The stress strain relations may now be written as the following.

$$\begin{aligned}
\sigma_\alpha &= (\lambda_\alpha + 2\mu_\alpha)\Delta - 2\mu_\alpha\ (e_\beta + e_\gamma) \\
\sigma_\beta &= (\lambda_\beta = 2\mu_\beta)\Delta - 2\mu_\beta\ (e_\alpha + e_\gamma) \qquad (7) \\
\sigma_{\alpha\beta} &= \mu_{\alpha\beta}\ e_{\alpha\beta}
\end{aligned}$$

In the above expressions, Δ is the volume dilatation and in terms of the normal strains is defined as

$$\Delta = e_\alpha + e_\beta + e_\gamma \qquad (8)$$

F. Displacement Equilibrium Equations:

The set of equilibrium equations (5) will be transformed into displacement equations. To do this, the stress strain relations given by (7) will first transform the equations into a set of strain equations and then the strain displacement relations given by (3) will yield the desired displacement equations.

The quantity x, defined as the normal rotation is introduced into these equations. It is given by the expression

$$2x = h_1 h_2 \left[\frac{\partial}{\partial_\alpha}\left(\frac{u_\beta}{h_2}\right) - \frac{\partial}{\partial_\beta}\left(\frac{u_\alpha}{h_1}\right) \right] \qquad (9)$$

Physically, this quantity represents the rotation of an element lying in a tangent plane to some surface of the shell.

The displacement equilibrium equations are then given as the following three.

$$(\lambda_\alpha + 2\mu_\alpha) \frac{1}{h_2} \frac{\partial \Delta}{\partial_\alpha} - \frac{2\mu_{\alpha\beta}}{h_1} \frac{\partial x}{\partial_\beta} + 2\mu_\alpha \; KABu_\alpha - 2\mu_\alpha \frac{\partial}{\partial_\gamma}\left(\frac{1}{h_2} \frac{\partial u_\gamma}{\partial_\alpha}\right)$$

$$+ h_1 \frac{\partial}{\partial\gamma}\left(\frac{\sigma_{\alpha\gamma}}{h_1{}^2 h_2}\right) + \frac{p_\alpha}{h_1 h_2} + \left[(\lambda_\alpha + 2\mu_\alpha) - (\lambda_\beta + 2\mu_\beta) \right] \Delta \frac{\partial h_2{}^{-1}}{\partial_\alpha}$$

$$- 2(\mu_\alpha - \mu_\beta) \frac{\partial}{\partial\gamma}\left(u_\gamma \frac{\partial h_2{}^{-1}}{\partial_\alpha} \right) -2 \; (\mu_\alpha - \mu_{\alpha\beta}) \frac{\partial^2 u_\beta}{\partial\alpha\partial\beta} \qquad (10)$$

$$+2 \; (\mu_\beta - \mu_{\alpha\beta}) \; h_1 h_2 \frac{\partial h_2{}^{-1}}{\partial_\alpha} \frac{\partial h_1{}^{-1}}{\partial_\beta} u_\beta - 2 \; (\mu_\alpha - \mu_\beta) \; h_1 \frac{\partial h_2{}^{-1}}{\partial_\alpha} \frac{\partial u_\alpha}{\partial_\alpha}$$

$$+ 2 \; (\mu_\alpha - \mu_{\alpha\beta}) \frac{\partial}{\partial\beta}\left(h_2 \frac{\partial h_1{}^{-1}}{\partial_\beta} \right) u_\alpha = 0$$

$$\frac{(\lambda_\beta + 2\mu_\beta)}{h_1} \frac{\partial \Delta}{\partial_\beta} + \frac{2\mu_{\alpha\beta}}{h_2} \frac{\partial x}{\partial_\alpha} + 2\mu_\beta \; ABKu_\beta - 2\mu_\beta \frac{\partial}{\partial_\gamma}\left(\frac{1}{h_1} \frac{\partial u_\gamma}{\partial_\beta}\right)$$

$$+ h_2 \frac{\partial}{\partial\gamma}\left(\frac{\sigma_{\beta\gamma}}{h_2{}^2 h_1}\right) + \frac{p_\beta}{h_1 h_2} + \left[(\lambda_\beta + 2\mu_\beta) - (\lambda_\alpha + 2\mu_\alpha) \right] \Delta \frac{\partial h_1{}^{-1}}{\partial_\beta}$$

$$- 2 \; (\mu_\beta - \mu_\alpha) \frac{\partial}{\partial\gamma}\left(u_\gamma \frac{\partial h_1{}^{-1}}{\partial_\beta} \right) - 2 \; (\mu_\beta - \mu_{\alpha\beta}) \frac{\partial^2 u_\alpha}{\partial\alpha\partial\beta} \qquad (11)$$

$$+ 2 \; (\mu_\beta - \mu_{\alpha\beta}) \; h_1 h_2 \frac{\partial h_2{}^{-1}}{\partial_\alpha} \frac{\partial h_1{}^{-1}}{\partial_\beta} u_\alpha - 2(\mu_\beta - \mu_\alpha) h_2 \frac{\partial h_1{}^{-1}}{\partial_\beta} \frac{\partial u_\beta}{\partial_\beta}$$

$$+ 2 \; (\mu_\beta - \mu_{\alpha\beta}) \frac{\partial}{\partial_\alpha}\left(h_1 \frac{\partial h_2{}^{-1}}{\partial\alpha} \right) u_\beta = 0$$

$$- 2 \left[\frac{(\lambda_\alpha + 2\mu_\alpha) + (\lambda_\beta + 2\mu_\beta)}{2} \right] (H + K\gamma) \; AB_\Delta + 2\mu_\alpha \frac{\partial}{\partial_\alpha} (Bk_2 u_\alpha)$$

$$+ 2\mu_\beta \frac{\partial}{\partial_\beta} (Ak_1 u_\beta) + 4 \frac{(\mu_\alpha + \mu_\beta)}{2} ABK \; u_\gamma + 4 \frac{(\mu_\alpha + \mu_\beta)}{2} AB(H + K_\gamma) \frac{\partial u_\gamma}{\partial_\gamma}$$

$$+\frac{\partial}{\partial\alpha}\left(\frac{\sigma_{\alpha\gamma}}{h_2}\right)+\frac{\partial}{\partial\beta}\left(\frac{\sigma_{\beta\gamma}}{h_1}\right)+\frac{\partial}{\partial\gamma}\left(\frac{\sigma_\gamma}{h_1h_2}\right)+\frac{p_\gamma}{h_1h_2}-\Big[(\lambda_\alpha+2\mu_\alpha)-$$

$$(\lambda_\beta+2\mu_\beta)\Big]ABL\Delta-2(\mu_\alpha-\mu_\beta)Bk_2\frac{\partial u_\alpha}{\partial\alpha}-2(\mu_\beta-\mu_\alpha)Ak_1\frac{\partial u_\beta}{\partial\alpha} \tag{12}$$

$$+2(\mu_\alpha-\mu_\beta)ABL\frac{\partial u_\gamma}{\partial\gamma}=0$$

G. Middle Surface Displacement Equations:

In first order theory, the normal strains can be shown to be linear functions of γ, the distance from the shell middle surface.[3] As a consequence, the volume dilatation Δ, which is a sum of the normal strains, will also be a linear function of γ and may be written as

$$\Delta = \Delta_o + \Delta_1\,\gamma \tag{13}$$

The normal rotation 2x is of the same order of magnitude as the shear strain, $e_{\alpha\beta}$, and since this strain is a linear function of γ, then the rotation may be written as

$$x = x_o + x_1\,\gamma \tag{14}$$

The equilibrium equations, (10), (11), (12) are in terms of the displacement components, the transverse shear stresses, the normal stress σ_γ and the body forces p_α, p_β and p_γ. Substitution of (2) for u_α and u_β and (13) and (14) for Δ and x in the equilibrium equations will transform these quantities into functions of the middle surface displacement components

---

[3] Though this is true for e_α, e_β and $e_{\alpha\beta}$, it has as yet not been shown to be true for e_γ. However, the subsequent development for e_γ will justify this statement.

and the variable γ. Series expansion and truncation at order two will ultimately cause these quantities in the equilibrium equations to become quadratic polynomials in the variable γ. The equilibrium equations can then be written as follows.

$$\Big\{ (\lambda_\alpha + 2\mu_\alpha) B \frac{\partial \Delta_o}{\partial \alpha} - 2\mu_{\alpha\beta} A \frac{\partial x_o}{\partial \beta} + 2\mu_\alpha ABKu + \Big[(\lambda_\alpha + 2\mu_\alpha) -$$

$$(\lambda_\beta + 2\mu_\beta) \Big] \frac{\partial \beta}{\partial \alpha} \Delta_o + 2(\mu_\alpha - \mu_{\alpha\beta}) \frac{\partial}{\partial \beta} \left(\frac{1}{B} \frac{\partial A}{\partial \beta} \right) u -$$

$$2(\mu_\alpha - \mu_\beta) \frac{1}{A} \frac{\partial B}{\partial \alpha} \frac{\partial u}{\partial \alpha} - 2(\mu_\alpha - \mu_{\alpha\beta}) \frac{\partial^2 v}{\partial \alpha \partial \beta} + 2(\mu_\beta - \mu_{\alpha\beta}) \frac{1}{AB} \frac{\partial A}{\partial \beta} \frac{\partial B}{\partial \alpha} v \Big\} +$$

$$\Big\{ (\lambda_\alpha + 2\mu_\alpha) Bk_2 \frac{\partial \Delta_o}{\partial \alpha} + (\lambda_\alpha + 2\mu_\alpha) B \frac{\partial \Delta_1}{\partial \alpha} - 2\mu_{\alpha\beta} Ak_1 \frac{\partial x_o}{\partial \beta} -$$

$$2\mu_{\alpha\beta} A \frac{\partial x_1}{\partial \beta} + 2\mu_\alpha ABK k_1 u - 2\mu_\alpha BK \frac{\partial w}{\partial \alpha} + \Big[(\lambda_\alpha + 2\mu_\alpha) -$$

$$(\lambda_\beta + 2\mu_\beta) \Big] k_1 \frac{\partial B}{\partial \alpha} \Delta_o + \Big[(\lambda_\alpha + 2\mu_\alpha) - (\lambda_\beta + 2\mu_\beta) \Big] \frac{\partial B}{\partial \alpha} \Delta_1$$

$$+ 2(\mu_\alpha - \mu_{\alpha\beta}) k_1 \frac{\partial}{\partial \beta} \left(\frac{1}{B} \frac{\partial A}{\partial \beta} \right) u - 2(\mu_\alpha - \mu_{\alpha\beta}) \frac{1}{A} \frac{\partial}{\partial \beta} \left(\frac{1}{B} \frac{\partial A}{\partial \beta} \right) \frac{\partial w}{\partial \alpha}$$

$$- 2(\mu_\alpha - \mu_\beta) \frac{1}{A} \frac{\partial \beta}{\partial \alpha} \frac{\partial (k_1 u)}{\partial \alpha} + 2(\mu_\alpha - \mu_\beta) \frac{1}{A} \frac{\partial B}{\partial \alpha} \frac{\partial}{\partial \alpha} \left(\frac{1}{A} \frac{\partial w}{\partial \alpha} \right)$$

$$- 2(\mu_\alpha - \mu_{\alpha\beta}) \frac{\partial^2 (k_2 v)}{\partial \alpha \partial \beta} + 2(\mu_\alpha - \mu_{\alpha\beta}) \frac{\partial^2}{\partial \alpha \partial \beta} \left(\frac{1}{B} \frac{\partial w}{\partial \beta} \right) \qquad (15)$$

$$+ 2(\mu_\beta - \mu_{\alpha\beta}) \frac{k_2}{AB} \frac{\partial A}{\partial \beta} \frac{\partial B}{\partial \alpha} v - 2(\mu_\beta - \mu_{\alpha\beta}) \frac{1}{AB^2} \frac{\partial A}{\partial \beta} \frac{\partial B}{\partial \alpha} \frac{\partial w}{\partial \beta} \Big\} \gamma$$

$$+ \Big\{ (\lambda_\alpha + 2\mu_\alpha) Bk_2 \frac{\partial \Delta_1}{\partial \alpha} - 2\mu_{\alpha\beta} Ak_1 \frac{\partial x_1}{\partial \beta} + \Big[(\lambda_\alpha + 2\mu_\alpha) -$$

$$(\lambda_\beta+2\mu_\beta)k_1 \frac{\partial B}{\partial\alpha}\Delta_1\Big\}\gamma^2 - 2\mu_\alpha \frac{\partial}{\partial\gamma}\left(\frac{1}{h_2}\frac{\partial u_\gamma}{\partial\alpha}\right) - 2(\mu_\alpha-\mu_\beta)\frac{\partial}{\partial\gamma}\left(u_\gamma \frac{\partial h_2^{-1}}{\partial\alpha}\right)$$

$$+ h_1 \frac{\partial}{\partial\gamma}\left(\frac{\sigma_{\alpha\gamma}}{h_1^2 h_2}\right) + \frac{p_\alpha}{h_1h_2} = 0$$

$$\Big\{(\lambda_\beta + 2\mu_\beta)A\frac{\partial\Delta_o}{\partial\beta} + 2\mu_{\alpha\beta} B \frac{\partial xo}{\partial\alpha} + 2\mu_\beta ABKv + \Big[(\lambda_\beta + 2\mu_\beta) -$$

$$(\lambda_\alpha + 2\mu_\alpha)\Big]\frac{\partial A}{\partial\beta}\Delta_o + 2(\mu_\beta - \mu_{\alpha\beta})\frac{\partial}{\partial\alpha}\left(\frac{1}{A}\frac{\partial B}{\partial\alpha}\right)v - 2(\mu_\beta-\mu_\alpha)\frac{1}{B}\frac{\partial A}{\partial\beta}\frac{\partial v}{\partial\beta} -$$

$$2(\mu_\beta - \mu_{\alpha\beta})\frac{\partial^2 u}{\partial\alpha\partial\beta} + 2(\mu_\alpha-\mu_{\alpha\beta})\frac{1}{AB}\frac{\partial B}{\partial\alpha}\frac{\partial A}{\partial\beta}u\Big\} + \Big\{(\lambda_\beta + 2\mu_\beta)Ak_1\frac{\partial\Delta_o}{\partial\beta} +$$

$$(\lambda_\beta + 2\mu_\beta)A\frac{\partial\Delta_1}{\partial\beta} + 2\mu_{\alpha\beta} Bk_2\frac{\partial xo}{\partial\alpha} + 2\mu_{\alpha\beta} B\frac{\partial x_1}{\partial\alpha} + 2\mu_\beta ABKk_2v -$$

$$2\mu_\beta AK\frac{\partial w}{\partial\beta} + \Big[(\lambda_\beta + 2\mu_\beta)-(\lambda_\alpha + 2\mu_\alpha)\Big]k_2\frac{\partial A}{\partial\beta}\Delta_o + \Big[(\lambda_\beta + 2\mu_\beta) -$$

$$(\lambda_\alpha + 2\mu_\alpha)\Big]\frac{\partial A}{\partial\beta}\Delta_1 + 2(\mu_\beta - \mu_{\alpha\beta})k_2\frac{\partial}{\partial\alpha}\left(\frac{1}{A}\frac{\partial B}{\partial\alpha}\right)v -$$

$$2(\mu_\beta - \mu_{\alpha\beta})\frac{1}{B}\frac{\partial}{\partial\alpha}\left(\frac{1}{A}\frac{\partial B}{\partial\alpha}\right)\frac{\partial w}{\partial\beta} - 2(\mu_\beta-\mu_\alpha)\frac{1}{B}\frac{\partial A}{\partial\beta}\frac{\partial}{\partial\beta}(k_2v) +$$

$$2(\mu_\beta - \mu_\alpha)\frac{1}{B}\frac{\partial A}{\partial\beta}\frac{\partial}{\partial\beta}\quad\frac{1}{B}\frac{\partial w}{\partial\beta} - 2(\mu_\alpha - \mu_{\alpha\beta})\frac{\partial^2(k_1u)}{\partial\alpha\partial\beta} +$$

$$2(\mu_\beta - \mu_{\alpha\beta})\frac{\partial^2}{\partial\alpha\partial\beta}\quad\frac{1}{A}\frac{\partial w}{\partial\alpha} + 2(\mu_\alpha - \mu_{\alpha\beta})\frac{k_1}{AB}\frac{\partial A}{\partial\beta}\frac{\partial B}{\partial\alpha}u - \qquad (16)$$

$$2(\mu_\alpha - \mu_{\alpha\beta})\frac{1}{A^2B}\frac{\partial A}{\partial\beta}\frac{\partial B}{\partial\alpha}\frac{\partial w}{\partial\alpha}\Big\}\gamma + \Big\{(\lambda_\beta + 2\mu_\beta)Ak_1\frac{\partial\Delta_1}{\partial\beta} +$$

$$2\mu_{\alpha\beta} Bk_2\frac{\partial x_1}{\partial\alpha} + \Big[(\lambda_\alpha + 2\mu_\alpha)-(\lambda_\beta + 2\mu_\beta)\Big]k_2\frac{\partial A}{\partial\beta}\Delta_1\Big\}\gamma^2$$

$$- 2\mu_\beta\frac{\partial}{\partial\gamma}\left(\frac{1}{h_1}\frac{\partial u_\gamma}{\partial\beta}\right) - 2(\mu_\beta-\mu_\alpha)\frac{\partial}{\partial\gamma}\left(u_\gamma\frac{\partial h_1^{-1}}{\partial\beta}\right) + h_2\frac{\partial}{\partial\gamma}\left(\frac{\sigma_{\beta\gamma}}{h_1h_2^2}\right) + \frac{p_\beta}{h_1h_2} = 0$$

$$\left\{ -2\frac{\left[(\lambda_\alpha + 2\mu_\alpha) + (\lambda_\beta + 2\mu_\beta)\right]}{2} HAB\Delta_o + 2\mu_\alpha \frac{\partial}{\partial\alpha}(k_2Bu) + \right.$$

$$2\mu_\beta \frac{\partial}{\partial\beta}(k_1Av) - \left[(\lambda_\alpha + \mu_\alpha)-(\lambda_\beta + 2\mu_\beta)\right] LAB\Delta_o - 2(\mu_\alpha-\mu_\beta)k_2B \frac{\partial u}{\partial\alpha} -$$

$$\left. 2(\mu_\beta-\mu_\alpha)\, k_1A \frac{\partial v}{\partial\beta}\right\} + \left\{ -2 \frac{\left[(\lambda_\alpha + 2\mu_\alpha)+(\lambda_\beta + 2\mu_\beta)\right]}{2} KAB\Delta_o - \right.$$

$$2\frac{\left[(\lambda_\alpha + 2\mu_\alpha)+(\lambda_\beta + 2\mu_\beta)\right]}{2} HAB\Delta_1 + 2\mu_\alpha \frac{\partial}{\partial\alpha}(KBu) -$$

$$2\mu_\alpha \frac{\partial}{\partial\alpha}\left(\frac{B}{A} k_2 \frac{\partial w}{\partial\alpha}\right) + 2\mu_\beta \frac{\partial}{\partial\beta}(KAv) - 2\mu_\beta \frac{\partial}{\partial\beta}\left(k_1 \frac{A}{B}\frac{\partial w}{\partial\beta}\right) - \qquad (17)$$

$$\left[(\lambda_\alpha + 2\mu_\alpha)-(\lambda_\beta + 2\mu_\beta)\right] LAB\Delta_1 - 2(\mu_\alpha-\mu_\beta)\, k_2\, B \frac{\partial}{\partial\alpha}(k_1u) +$$

$$2(\mu_\alpha-\mu_\beta)\, k_2\, B \frac{\partial}{\partial\alpha}\left(\frac{1}{A}\frac{\partial w}{\partial\alpha}\right) - 2(\mu_\beta-\mu_\alpha)\, k_1\, A \frac{\partial}{\partial\beta}(k_2v) +$$

$$\left. 2(\mu_\beta-\mu_\alpha)\, k_1\, A \frac{\partial}{\partial\beta}\left(\frac{1}{B}\frac{\partial w}{\partial\beta}\right)\right\}\gamma + \left\{-2\frac{\left[(\lambda_\alpha+2\mu_\alpha)+(\lambda_\beta+2\mu_\beta)\right]}{2}KAB\Delta_1\right\}\gamma^2$$

$$+ 4\frac{(\mu_\alpha + \mu_\beta)}{2} KABu_\gamma + 4\frac{(\mu_\alpha + \mu_\beta)}{2} HAB \frac{\partial u_\gamma}{\partial\gamma} + 4\frac{(\mu_\alpha+\mu_\beta)}{2}KAB\left(\frac{\partial u_\gamma}{\partial\gamma}\right)\gamma$$

$$+ 2(\mu_\alpha - \mu_\beta)\, LAB \frac{\partial u_\gamma}{\partial\gamma} + \frac{\partial}{\partial\alpha}\left(\frac{\sigma_{\alpha\gamma}}{h_2}\right) + \frac{\partial}{\partial\beta}\left(\frac{\sigma_{\beta\gamma}}{h_1}\right) + \frac{\partial}{\partial\gamma}\left(\frac{\sigma_\gamma}{h_1h_2}\right) +$$

$$\frac{p_\gamma}{h_1h_2} = 0$$

H. Integration of the Equilibrium Equations:

Though equations (13), (14) and (15) are written in terms of displacements they still represent the resultant force components in the α, β and γ directions on a differential element of a shell. If now the equations are integrated with respect to γ over the shell thickens δ, the result will be a set of equilibrium equations representing the resultant force components on a differential shell element of finite thickness δ. Further if equations (15) and (16) are multiplied by γ, the expressions will within first order theory represent the moment of the resultant force components about the middle surface tangents to the α and β coordinate lines. Integration of the two moment expressions will then represent the resultant moment on an element of shell of finite thickness δ about the middle surface tangents to the curvalinear coordinate lines.

As previously stated, the Kirchoff hypothesis introduces an error of $(k\delta)$ into basic shell theory. Thus terms which are of order $(k\delta)$ in comparison to unity may be neglected without introducing any additional errors greater than that arising from the Kirchoff premise. In integrating the displacement equilibrium equations, a number of displacement terms can be neglected since it can be shown that their order will be of $(k\delta)$ in comparison to some other terms.

Integrating equations (15), (16) and (17) with respect to γ over the shell thickness δ and then dividing by this quantity leads to the following three equations, simplified in accordance with the statements made in the preceding paragraph.

$$\Big\{(\lambda_\alpha + 2\mu_\alpha)\, B \frac{\partial \Delta_o}{\partial \alpha} - 2\mu_{\alpha\beta}\, A \frac{\partial x_o}{\partial \beta} + 2\mu_\alpha\, ABKu + \Big[(\lambda_\alpha + 2\mu_\alpha) -$$

$$(\lambda_\beta + 2\mu_\beta)\Big] \frac{\partial B_{\Delta_o}}{\partial \alpha} + 2(\mu_\alpha - \mu_{\alpha\beta}) \frac{\partial}{\partial \beta}\left(\frac{1}{B}\frac{\partial A}{\partial \beta}\right) u - 2(\mu_\alpha - \mu_\beta)\frac{1}{A}\frac{\partial_\beta}{\partial \alpha}\frac{\partial u}{\partial \alpha} -$$

$$2(\mu_\alpha - \mu_{\alpha\beta}) \frac{\partial^2 v}{\partial\alpha\partial\beta} + 2(\mu_\beta - \mu_{\alpha\beta}) \frac{1}{AB} \frac{\partial A}{\partial\beta} \frac{\partial B v}{\partial\alpha}\Big\} + \Big\{(\lambda_\alpha + 2\mu_\alpha)Bk_2 \frac{\partial\Delta_1}{\partial\alpha} -$$

$$2\mu_{\alpha\beta}\, Ak_1 \frac{\partial x_1}{\partial\beta} + \Big[(\lambda_\alpha + 2\mu_\alpha) - (\lambda_\beta + 2\mu_\beta)\Big] k_1 \frac{\partial B}{\partial\alpha} \Delta_1\Big\} \frac{\delta^2}{12} - \qquad (18)$$

$$\frac{2\mu_\alpha}{\delta}\int_{-\frac{\delta}{2}}^{\frac{\delta}{2}} \frac{\partial}{}\Big(\frac{1}{h_2}\frac{\partial u_\gamma}{\partial\alpha}\Big) d\gamma - \frac{2(\mu_\alpha - \mu_\beta)}{\delta}\int_{-\frac{\delta}{2}}^{\frac{\delta}{2}} \frac{\partial}{\partial\gamma}\Big(u_\gamma \frac{\partial h_2^{-1}}{\partial\alpha}\Big) d\gamma +$$

$$\frac{ABk_1}{\delta} Q_\alpha + \frac{AB}{\delta} P_\alpha = 0$$

$$\Big\{(\lambda_\beta + 2\mu_\beta)A \frac{\partial\Delta_o}{\partial\beta} + 2\mu_{\alpha\beta}\, B \frac{\partial x_o}{\partial\alpha} + 2\mu_\beta\, ABKv + \Big[(\lambda_\beta + 2\mu_\beta) -$$

$$(\lambda_\alpha + 2\mu_\alpha)\Big] \frac{\partial A}{\partial\beta}\Delta_o + 2(\mu_\beta - \mu_{\alpha\beta}) \frac{\partial}{\partial\alpha}\Big(\frac{1}{A}\frac{\partial B}{\partial\alpha}\Big) v - 2(\mu_\beta - \mu_\alpha)\frac{1}{B}\frac{\partial A}{\partial\beta}\frac{\partial v}{\partial\beta} -$$

$$2(\mu_\beta - \mu_{\alpha\beta}) \frac{\partial^2 u}{\partial\alpha\partial\beta} + 2(\mu_\alpha - \mu_{\alpha\beta}) \frac{1}{AB} \frac{\partial A}{\partial\beta} \frac{\partial B}{\partial\alpha} u\Big\} + \Big\{(\lambda_\beta + 2\mu_\beta)Ak_1 \frac{\partial\Delta_1}{\partial\beta} +$$

$$2\mu_{\alpha\beta}\, Bk_2 \frac{\partial x_1}{\partial\alpha} + \Big[(\lambda_\beta + 2\mu_\beta) - (\lambda_\alpha + 2\mu_\alpha)\Big] k_2 \frac{\partial A}{\partial\beta} \Delta_1 \Big\} \frac{\delta^2}{12} -$$

$$\frac{2\mu_\beta}{\delta}\int_{-\frac{\delta}{2}}^{\frac{\delta}{2}} \frac{\partial}{\partial\gamma}\Big(\frac{1}{h_1}\frac{\partial u_\gamma}{\partial\beta}\Big) d\gamma - \frac{2(\mu_\beta - \mu_\alpha)}{\delta}\int_{-\frac{\delta}{2}}^{\frac{\delta}{2}} \frac{\partial}{\partial\gamma}\Big(u_\gamma \frac{\partial h_1^{-1}}{\partial\beta}\Big) d\gamma + \qquad (19)$$

$$\frac{ABk_2}{\delta} Q_\beta + \frac{ABP_\beta}{\delta} = 0$$

$$\Big\{-2\Big[\frac{(\lambda_\alpha + 2\mu_\alpha) + (\lambda_\beta + 2\mu_\beta)}{2}\Big] HAB\Delta_o - 2\mu_\alpha \frac{\partial}{\partial\alpha}(k_2 Bu) + 2\mu_\beta \frac{\partial}{\partial\beta}(k_1 Av)$$

$$-\Big[(\lambda_\alpha + 2\mu_\alpha) - (\lambda_\beta + 2\mu_\beta)\Big] LAB\Delta_o - 2(\mu_\alpha - \mu_\beta)k_2 B \frac{\partial u}{\partial\alpha} - 2(\mu_\beta - \mu_\alpha)k_1 A \frac{\partial v}{\partial\beta}\Big\}$$

$$+\Big\{-\Big[\frac{(\lambda_\alpha + 2\mu_\alpha) + (\lambda_\beta + 2\mu_\beta)}{2}\Big] KAB\Delta_1\Big\} \frac{\delta^2}{6} + 4\frac{(\mu_\alpha + \mu_\beta)}{2}\frac{KAB}{\delta}\int_{-\frac{\delta}{2}}^{\frac{\delta}{2}} u_\gamma d\gamma \qquad (20)$$

$$+ 4\frac{(\mu_\alpha + \mu_\beta)}{2}\frac{HAB}{\delta}\int_{-\frac{\delta}{2}}^{\frac{\delta}{2}} \frac{\partial u_\gamma}{\partial\gamma} d\gamma + 4\frac{(\mu_\alpha + \mu_\beta)}{2}\frac{KAB}{\delta}\int_{-\frac{\delta}{2}}^{\frac{\delta}{2}} \gamma \frac{\partial u_\gamma}{\partial\gamma} d\gamma$$

$$+ 2(\mu_\alpha - \mu_\beta)\frac{LAB}{\delta}\int_{-\frac{\delta}{2}}^{\frac{\delta}{2}} \frac{\partial u_\gamma}{\partial\gamma}\, d\gamma + \frac{\partial}{\partial\alpha}\left(\frac{BQ_\alpha}{\delta}\right) + \frac{\partial}{\partial\beta}\left(\frac{AQ_\beta}{\delta}\right) + \frac{ABP_\gamma}{\delta} = 0$$

Multiplying equations (15) and (16) by γ and integrating over the shell thickness, the following two equations result.

$$\Big\{(\lambda_\alpha + 2\mu_\alpha)Bk_2 \frac{\partial\Delta_o}{\partial\alpha} + (\lambda_\alpha + 2\mu_\alpha)B \frac{\partial\Delta_1}{\partial\alpha} - 2\mu_{\alpha\beta} Ak_1 \frac{\partial x_o}{\partial\beta} - 2\mu_{\alpha\beta} A \frac{\partial x_1}{\partial\beta}$$

$$+ 2\mu_\alpha ABKk_1 u - 2\mu_\alpha BK \frac{\partial w}{\partial\alpha} + \left[(\lambda_\alpha + 2\mu_\alpha) - (\lambda_\beta + 2\mu_\beta)\right]k_1 \frac{\partial B}{\partial\alpha}\Delta_o$$

$$+ \left[(\lambda_\alpha + 2\mu_\alpha) - (\lambda_\beta + 2\mu_\beta)\right] \frac{\partial B}{\partial\alpha}\Delta_1 + 2(\mu_\alpha - \mu_{\alpha\beta})k_1 \frac{\partial}{\partial\beta}\left(\frac{1}{B}\frac{\partial A}{\partial\beta}\right) u \tag{21}$$

$$- 2(\mu_\alpha - \mu_{\alpha\beta})\frac{1}{A}\frac{\partial}{\partial\beta}\left(\frac{1}{B}\frac{\partial A}{\partial\beta}\right)\frac{\partial w}{\partial\alpha} - 2(\mu_\alpha - \mu_\beta)\frac{1}{A}\frac{\partial B}{\partial\alpha}\frac{\partial(k_1 u)}{\partial\alpha}$$

$$+ 2(\mu_\alpha - \mu_\beta)\frac{1}{A}\frac{\partial B}{\partial\alpha}\frac{\partial}{\partial\alpha}\left(\frac{1}{A}\frac{\partial w}{\partial\alpha}\right) - 2(\mu_\alpha - \mu_{\alpha\beta})\frac{\partial^2 k_2 v}{\partial\alpha\partial\beta}$$

$$+ 2(\mu_\alpha - \mu_{\alpha\beta})\frac{\partial^2}{\partial\alpha\partial\beta}\left(\frac{1}{B}\frac{\partial w}{\partial\beta}\right) + 2(\mu_\beta - \mu_{\alpha\beta})\frac{k_2}{AB}\frac{\partial A}{\partial\beta}\frac{\partial B}{\partial\alpha} v$$

$$- 2(\mu_\beta - \mu_{\alpha\beta})\frac{1}{AB^2}\frac{\partial A}{\partial\beta}\frac{\partial B}{\partial\alpha}\frac{\partial w}{\partial\beta}\Big\}\frac{\delta^2}{12} - \frac{2\mu_\alpha}{\delta}\int_{-\frac{\delta}{2}}^{\frac{\delta}{2}} \gamma\frac{\partial}{\partial\gamma}\left(\frac{1}{h_2}\frac{\partial u_\gamma}{\partial\alpha}\right) d\gamma$$

$$- 2\,\frac{(\mu_\alpha - \mu_\beta)}{\delta}\int_{-\frac{\delta}{2}}^{\frac{\delta}{2}} \gamma\frac{\partial}{\partial}\left(u_\gamma \frac{\partial h_2^{-1}}{\partial\alpha}\right) d\gamma - \frac{AB}{\delta} Q_\alpha = 0$$

$$\Big\{(\lambda_\beta + 2\mu_\beta)Ak_1 \frac{\partial\Delta_o}{\partial\beta} + (\lambda_\beta + 2\mu_\beta)A \frac{\partial\Delta_1}{\partial\beta} + 2\mu_{\alpha\beta} Bk_2 \frac{\partial x_o}{\partial\alpha} + 2\mu_{\alpha\beta} B\frac{\partial x_1}{\partial\alpha}$$

$$+ 2\mu_\beta ABKk_2 v - 2\mu_\beta AK \frac{\partial w}{\partial\beta} + \left[(\lambda_\beta + 2\mu_\beta) - (\lambda_\alpha + 2\mu_\alpha)\right]k_2 \frac{\partial A}{\partial\beta}\Delta_o +$$

$$+ \left[(\lambda_\beta + 2\mu_\beta) - (\lambda_\alpha + 2\mu_\alpha)\right]\frac{\partial A}{\partial\beta}\Delta_1 + 2(\mu_\beta - \mu_{\alpha\beta})k_2 \frac{\partial}{\partial\alpha}\left(\frac{1}{A}\frac{\partial B}{\partial\alpha}\right) v$$

$$- 2(\mu_\beta - \mu_{\alpha\beta})\frac{1}{B}\frac{\partial}{\partial\alpha}\left(\frac{1}{A}\frac{\partial B}{\partial\alpha}\right)\frac{\partial w}{\partial\beta} - 2(\mu_\beta - \mu_\alpha)\frac{1}{B}\frac{\partial A}{\partial\beta}\frac{\partial}{\partial\beta}(k_2 v)$$

$$+ 2(\mu_\beta - \mu_\alpha)\frac{1}{B}\frac{\partial A}{\partial\beta}\frac{\partial}{\partial\beta}\left(\frac{1}{B}\frac{\partial w}{\partial\beta}\right) - 2(\mu_\beta - \mu_{\alpha\beta})\frac{\partial^2}{\partial\alpha\partial\beta}(k_1 u) +$$

$$2(\mu_\beta - \mu_{\alpha\beta})\frac{\partial^2}{\partial\alpha\partial\beta}\left(\frac{1}{A}\frac{\partial w}{\partial\alpha}\right) + 2(\mu_\alpha - \mu_{\alpha\beta})\frac{k_1}{AB}\frac{\partial A}{\partial\beta}\frac{\partial B}{\partial\alpha} u -$$

$$2(\mu_\alpha - \mu_{\alpha\beta})\frac{1}{A^2 B}\frac{\partial A}{\partial\beta}\frac{\partial B}{\partial\alpha}\frac{\partial w}{\partial\alpha}\Bigg\}\frac{\delta^2}{12} - \frac{2\mu_\beta}{\delta}\int_{-\frac{\delta}{2}}^{\frac{\delta}{2}}\gamma\frac{\partial}{\partial\gamma}\left(\frac{1}{h_1}\frac{\partial u_\gamma}{\partial\beta}\right)d\gamma -$$

$$\frac{2(\mu_\beta - \mu_\alpha)}{\delta}\int_{-\frac{\delta}{2}}^{\frac{\delta}{2}}\gamma\frac{\partial}{\partial\gamma}\left(u_\gamma\frac{\partial h_1^{-1}}{\partial\beta}\right)d\gamma - \frac{AB}{\delta}Q_\beta = 0$$

In the above expressions, Q_α, Q_β, P_α, P_β, P_γ are defined as

$$Q_\alpha = \frac{1}{B}\int_{-\frac{\delta}{2}}^{\frac{\delta}{2}}\frac{\sigma_{\alpha\gamma}}{h_2}d\gamma \tag{23}$$

$$Q_\beta = \frac{1}{A}\int_{-\frac{\delta}{2}}^{\frac{\delta}{2}}\frac{\sigma_{\beta\gamma}}{h_1}d\gamma \tag{24}$$

$$P_\alpha = \frac{1}{AB}\left\{\frac{\sigma_{\alpha\gamma}}{h_1 h_2}\Bigg|_{-\frac{\delta}{2}}^{\frac{\delta}{2}} + \int_{-\frac{\delta}{2}}^{\frac{\delta}{2}}\frac{p_\alpha}{h_1 h_2}d\gamma\right\}$$

$$P_\beta = \frac{1}{AB}\left\{\frac{\sigma_{\beta\gamma}}{h_1 h_2}\Bigg|_{-\frac{\delta}{2}}^{\frac{\delta}{2}} + \int_{-\frac{\delta}{2}}^{\frac{\delta}{2}}\frac{p_\beta}{h_1 h_2}d\gamma\right\} \tag{25}$$

$$P_\gamma = \frac{1}{AB}\left\{\frac{\sigma_\gamma}{h_1 h_2}\Bigg|_{-\frac{\delta}{2}}^{\frac{\delta}{2}} + \int_{-\frac{\delta}{2}}^{\frac{\delta}{2}}\frac{p_\gamma}{h_1 h_2}d\gamma\right\}$$

The quantities Q_α and Q_β are the familiar transverse shear stress resultants while P_α, P_β and P_γ are the components of the external loading per unit surface area of the shell middle surface.

The five integrated equilibrium equations, (18)-(22), basically contain five unknowns, the three components of the middle surface displacement, u,v,w and the stress resultants Q_α and Q_β. It is true that as matters stand these are an additional number of unknowns namely the dilatation components Δ_o and Δ_1, the rotation components x_o and x_1, and the normal displacement u_γ. However as will be shown in the suceeding sections, these quantities can all be expressed in terms of u,v and w. Thus basically, equations (18)-(22) reduce to a system of five equations in five unknowns. Following the procedure usually adopted in deriving shell equations, the transverse shear stress resultants ultimately will be eliminated and the final result will be a set of three independent equations in the three unknown middle surface displacement components.

I. Rotation Components x_o and x_1:

Equating the two definitions for the normal rotation as given in (9) and (14)

$$x_o + x_1\gamma = \frac{h_1h_2}{2}\left[\frac{\partial}{\partial\alpha}\left(\frac{u_\beta}{h_2}\right) - \frac{\partial}{\partial\beta}\left(\frac{u_\alpha}{h_1}\right)\right]$$

Substituting for h_1, h_2 u_α and u_β their expressions involving the variable γ, truncating the resulting series and comparing coefficients, the result becomes

$$x_o = \frac{1}{2AB}\left[\frac{\partial}{\partial_\alpha}(Bv)-\frac{\partial}{\partial_\beta}(Au)\right] \qquad (26)$$

$$x_1 = \frac{-L}{2}\left[\frac{A}{B}\frac{\partial}{\partial_\beta}\left(\frac{u}{A}\right)+\frac{B}{A}\frac{\partial}{\partial_\alpha}\left(\frac{v}{B}\right)\right] \qquad (27)$$

J. Normal Displacement u_γ:

From the generalized Hookes' Law for an orthotropic material subjected to a plane stress condition ($\sigma_\gamma = o$), the normal strain e_γ is given as

$$e_\gamma = \frac{(a_{22}a_{13} - a_{12}a_{23})}{(a_{11}a_{22} - a_{12}^2)}\, e_\alpha + \frac{(a_{11}a_{23} - a_{12}a_{13})}{(a_{11}a_{22} - a_{12}^2)}\, e_\beta$$

or more conveniently,

$$e_\gamma = G_\alpha\, e_\alpha + G_\beta\, e_\beta$$

Now the volume dilatation Δ has been defined as

$$\Delta = e_\alpha + e_\beta + e_\gamma$$

so that e_γ can also be written in terms of the dilatation as

$$e_\gamma = \frac{G_\alpha}{(1+G_\alpha)}\,\Delta + \frac{(G_\beta - G_\alpha)}{(1+G_\alpha)}\, e_\beta$$

or

$$e_\gamma = \frac{G_\beta}{(1+G_\beta)}\,\Delta + \frac{(G_\alpha - C_\beta)}{(1+G_\beta)}\, e_\alpha$$

To insure symmetry of e_γ, with respect to α and β the above two expressions in terms of the dilatation will be added. Thus in symmetrical form, e_γ becomes

$$e_\gamma = \frac{1}{2}\left[\frac{C_\alpha}{(1+C_\alpha)}+\frac{C_\beta}{(1+G_\beta)}\right]\Delta + \frac{1}{2}\left[\frac{(C_\alpha - C_\beta)}{(1+C_\beta)}\, e_\alpha + \frac{(C_\beta - C_\alpha)}{(1+C_\alpha)}\, e_\beta\right]$$

Define the auxilliary constants η_α and η_β as

$$\eta_\alpha = \frac{C_\alpha}{(1+C_\alpha)} \quad ; \quad \eta_\beta = \frac{C_\beta}{(1+C_\beta)}$$

the terms of these new constants, e_γ becomes

$$e_\gamma = \frac{(\eta_\alpha + \eta_\beta)\Delta}{2} + \frac{(\eta_\alpha - \eta_\beta)e_\alpha}{2(1-\eta_\alpha)} + \frac{(\eta_\beta - \eta_\alpha)}{2(1-\eta_\beta)} e_\beta$$

Substituting for the strains their expressions given by (3) and then for the cosresponding displacements, the relations given by (2), the dilatation by (13) and expanding the necessary terms to form polynomials in γ, a differential equation for the solution of u_γ results. The polynomials in γ are truncated so as to exclude powers of γ higher than three. This equation is given as

$$(1 + 2H\gamma + K\gamma^2)\frac{\partial u_\gamma}{\partial \gamma} + \left\{ \frac{-1}{2}\left[\frac{(\eta_\alpha-\eta_\beta)k_1}{(1-\eta_\alpha)} + \frac{(\eta_\beta-\eta_\alpha)k_2}{(1-\eta_\beta)}\right] + \left[\frac{(\eta_\alpha-\eta_\beta)K}{(1-\eta_\alpha)} + \frac{(\eta_\beta - \eta_\alpha)K}{(1-\eta_\beta)}\right]\gamma \right\} u_\gamma = F_o + F_1\gamma + F_2\gamma^2 + F_3\gamma^3 \qquad (28)$$

where

$$F_o = \frac{(\eta_\alpha + \eta_\beta)AB\Delta_o}{2} + \frac{(\eta_\beta-\eta_\alpha)A}{2(1-\eta_\beta)}\frac{\partial v}{\partial \beta} + \frac{(\eta_\alpha - \eta_\beta)}{2(1-\eta_\alpha)} B \frac{\partial u}{\partial \alpha}$$

$$+ \frac{(\eta_\beta - \eta_\alpha)}{2(1-\eta_\beta)}\frac{\partial B}{\partial \alpha} u + \frac{(\eta_\alpha - \eta_\beta)}{2(1-\eta_\alpha)}\frac{\partial A}{\partial \beta} v$$

$$F_1 = (\eta_\alpha + \eta_\beta)\, ABH\Delta_o + \frac{(\eta_\alpha + \eta_\beta)AB\Delta_1}{2} + \frac{(\eta_\beta - \eta_\alpha)A}{2(1-\eta_\beta)}\frac{\partial}{\partial \beta}(k_2 v)$$

$$+ \frac{(\eta_\alpha - \eta_\beta)B}{2(1-\eta_\alpha)}\frac{\partial}{\partial \alpha}(k_1 u) - \frac{(\eta_\beta - \eta_\alpha)}{2(1-\eta_\beta)} A \frac{\partial}{\partial \beta}\left(\frac{1}{B}\frac{\partial w}{\partial \beta}\right)$$

$$-\frac{(\eta_\alpha - \eta_\beta)B}{2(1-\eta_\alpha)}\frac{\partial}{\partial\alpha}\left(\frac{1}{A}\frac{\partial w}{\partial\alpha}\right) + \frac{(\eta_\beta - \eta_\alpha)Ak_1}{2(1-\eta_\beta)}\frac{\partial v}{\partial\beta} + \frac{(\eta_\alpha-\eta_\beta)Bk_2}{2(1-\eta_\alpha)}\frac{\partial u}{\partial\alpha}$$

$$+\frac{(\eta_\beta - \eta_\alpha)\partial B}{(1-\eta_\beta)\,\partial\alpha}k_1 u + \frac{(\eta_\alpha-\eta_\beta)\partial A}{(1-\eta_\alpha)\,\partial\beta}k_2 v - \frac{(\eta_\beta - \eta_\alpha)}{2(1-\eta_\beta)}\frac{1}{A}\frac{\partial B}{\partial\alpha}\frac{\partial w}{\partial\alpha}$$

$$-\frac{(\eta_\alpha - \eta_\beta)}{2(1-\eta_\alpha)}\frac{1}{B}\frac{\partial A}{\partial\beta}\frac{\partial w}{\partial\beta}$$

$$F_2 = \frac{(\eta_\alpha + \eta_\beta)K\Delta_o}{2} + (\eta_\alpha + \eta_\beta)ABH\Delta_1 + \frac{(\eta_\beta-\eta_\alpha)Ak_1}{2(1-\eta_\beta)}\frac{\partial(k_2 v)}{\partial\beta}$$

$$+\frac{(\eta_\alpha - \eta_\beta)Bk_1}{2(1-\eta_\alpha)}\frac{\partial(k_1 u)}{\partial\alpha} - \frac{(\eta_\beta-\eta_\alpha)Ak_1}{2(1-\eta_\beta)}\frac{\partial}{\partial\beta}\left(\frac{1}{B}\frac{\partial w}{\partial\beta}\right)$$

$$-\frac{(\eta_\alpha-\eta_\beta)Bk_2}{2(1-\eta_\alpha)}\frac{\partial}{\partial\alpha}\left(\frac{1}{A}\frac{\partial w}{\partial\alpha}\right) + \frac{(\eta_\beta-\eta_\alpha)}{2(1-\eta_\beta)}\frac{\partial B}{\partial\alpha}k_1^2 u + \frac{(\eta_\alpha-\eta_\beta)}{2(1-\eta_\alpha)}\frac{\partial A}{\partial\beta}k_2^2 v$$

$$-\frac{(\eta_\beta - \eta_\alpha)}{2(1-\eta_\beta)}\frac{1}{A}\frac{\partial B}{\partial\alpha}k_1\frac{\partial w}{\partial\alpha} - \frac{(\eta_\alpha - \eta_\beta)}{2(1-\eta_\alpha)}\frac{1}{B}\frac{\partial A}{\partial\beta}k_2\frac{\partial w}{\partial\beta}$$

$$F_3 = \frac{(\eta_\alpha + \eta_\beta)}{2}ABK\Delta_1$$

The solution to equation (28) can be obtained in a straight forward manner. The only boundary condition is that the displacement u_γ at the shell middle surface ($\gamma = 0$) be equal to w. Letting D represent the constant of integration

$$u_\gamma = De^{\rho(\gamma)} + e^{\rho(\gamma)}\int \frac{(F_o + F_1\gamma + F_2\gamma^2 + F_3\gamma^3)e^{-\rho(\gamma)}}{(1 + 2H\gamma + K\gamma^2)}d\gamma \qquad (29)$$

where

$$\rho(\gamma) = \int \frac{\frac{1}{2}\left[\frac{(\eta_\alpha-\eta_\beta)k_1}{(1-\eta_\alpha)} + \frac{(\eta_\beta-\eta_\alpha)k_2}{(1-\eta_\beta)}\right] - \left[\frac{(\eta_\alpha-\eta_\beta)K}{(1-\eta_\alpha)} + \frac{(\eta_\beta-\eta_\alpha)K}{(1-\eta_\beta)}\right]\gamma}{(1 + 2H\gamma + K\gamma^2)}d\gamma$$

A polynomial form of solution in the variable γ is desired and as such, though equation (27) does represent a solution for u_γ, this solution is not a satisfactory one. To transform (27) into a polynomial form, the integrand of $\rho(\gamma)$ is expanded into a power series in γ by means of a series expansion of the denominator. Upon integration, $\rho(\gamma)$ still remains a power series. The expenentials which have power series exponents, are themselves expanded into power series form by means of the Maclaurin series. Since a power series raised to an exponent still remains a power series the net result is that (29) becomes a power series in the variable γ. As might be expected, the resulting expression contains many terms. However, utilizing the simplification permitted by the Kirchoff hypothesis, namely terms of order $(k\delta)$ in comparison to unity may be neglected, the resulting expression for u_γ simplifies considerably in the number of terms contained as well as in the highest power of γ retained. Thus

$$u_\gamma = w + \left\{ \frac{(\eta_\beta - \eta_\alpha)k_2 w}{2(1-\eta_\beta)} + \frac{(\eta_\alpha - \eta_\beta)k_1 w}{2(1-\eta_\alpha)} + \frac{(\eta_\alpha + \eta_\beta)\Delta_o}{2} \right. \tag{30}$$

$$+ \frac{(\eta_\beta - \eta_\alpha)}{2(1-\eta_\beta)}\frac{1}{B}\frac{\partial v}{\partial \beta} + \frac{(\eta_\alpha - \eta_\beta)}{2(1-\eta_\alpha)}\frac{1}{A}\frac{\partial u}{\partial \alpha} + \frac{(\eta_\beta - \eta_\alpha)}{2(1-\eta_\beta)}\frac{1}{AB}\frac{\partial B}{\partial \alpha} u$$

$$\left. + \frac{(\eta_\alpha - \eta_\beta)}{2(1-\eta_\alpha)}\frac{1}{AB}\frac{\partial A}{\partial \beta} v \right\}\gamma + \left\{ \frac{(\eta_\beta + \eta_\beta)\Delta_1}{2} - \frac{(\eta_\beta - \eta_\alpha)}{2(1-\eta_\beta)}\frac{1}{B}\frac{\partial}{\partial \beta}\left(\frac{1}{B}\frac{\partial w}{\partial \beta}\right) \right.$$

$$- \frac{(\eta_\alpha - \eta_\beta)}{2(1-\eta_\alpha)}\frac{1}{A}\frac{\partial}{\partial \alpha}\left(\frac{1}{A}\frac{\partial w}{\partial \alpha}\right) - \frac{(\eta_\beta - \eta_\alpha)}{2(1-\eta_\beta)}\frac{1}{A^2 B}\frac{\partial B}{\partial \alpha}\frac{\partial w}{\partial \alpha}$$

$$\left. - \frac{(\eta_\alpha - \eta_\beta)}{2(1-\eta_\alpha)}\frac{1}{AB^2}\frac{\partial A}{\partial \beta}\frac{\partial w}{\partial \beta} \right\}\frac{\gamma^2}{2}$$

Unlike the tangential displacements u_α and u_β, which vary linearly with the distance from the shell middle surface, it is seen that the normal displacement is a quadratic function of that distance. However it should also be noted that the normal strain e_γ, which is obtained by differentiating the normal displacement u_γ, will be a linear function of γ and hence in accord with the results found for e_α and e_β, both of which are linear on the variable γ.

Equation (30), contains many terms which are inconvenient to handle for subsequent substitutions. To simplify the handling of this equation, the shell middle surface strain expressions e_1, e_2, e_{12} and the curvature change expressions K_α and K_β will be introduced into this equation. The curvature change expressions as simplified according to the basic assumptions are given as

$$\begin{aligned} K_\alpha &= \frac{-1}{A}\frac{\partial}{\partial\alpha}\left(\frac{1}{A}\frac{\partial w}{\partial\alpha}\right) - \frac{1}{AB^2}\frac{\partial A}{\partial\beta}\frac{\partial w}{\partial\beta} \\ K_\beta &= \frac{-1}{B}\frac{\partial}{\partial\beta}\;\frac{1}{B}\frac{\partial w}{\partial\beta} - \frac{1}{A^2B}\frac{\partial B}{\partial\alpha}\frac{\partial w}{\partial\alpha} \end{aligned} \qquad (31)$$

Thus equation (30) may be put in the following form.

$$u_\gamma = w + \left\{\frac{(\eta_\alpha + \eta_\beta)\Delta_o}{2} + \frac{(\eta_\alpha - \eta_\beta)e_1}{2(1-\eta_\alpha)} + \frac{(\eta_\beta - \eta_\alpha)e_2}{2(1-\eta_\beta)}\right\}\gamma \qquad (32)$$

$$+ \left\{\frac{(\eta_\alpha + \eta_\beta)\Delta_1}{2} + \frac{(\eta_\alpha - \eta_\beta)K_\alpha}{2(1-\eta_\alpha)} + \frac{(\eta_\beta - \eta_\alpha)K_\beta}{2(1-\eta_\beta)}\right\}\frac{\gamma^2}{2}$$

The resultant expression for u_γ has as yet not been formed in that (30) or (32) contain the dilatation components. These component will be evaluated in the following sect on and at that time the final expression for u_γ will be stated.

K. Dilatation Components Δ_o, Δ_1, and Final Form of u_γ

The volume dilatation at any point within the shell is given as the sum of the three normal strains. Thus

$$\Delta = e_\alpha + e_\beta + e_\gamma$$

In first order shell theory, the normal strains e_α and e_β may be expressed in terms of the corresponding values of the normal strains at the shell middle surface and the curvature change expressions.[4] Thus

$$e_\alpha = e_1 + K_\alpha \gamma$$
$$e_\beta = e_2 + K_\beta \gamma$$

Differentiating equation (32) with respect to γ in order to determine the normal strain e_γ and the above relations for e_α and e_β, the expression for the dilation under direct substitution for the strains becomes

$$\Delta = \left\{ \frac{(\eta_\alpha + \eta_\beta)\Delta_o}{2} + \frac{(2-\eta_\alpha-\eta_\beta)e_1}{2(1-\eta_\alpha)} + \frac{(2-\eta_\alpha-\eta_\beta)e_2}{2(1-\eta_\beta)} \right\}$$
$$+ \left\{ \frac{(\eta_\alpha + \eta_\beta)\Delta_1}{2} + \frac{(2-\eta_\alpha-\eta_\beta)K_\alpha}{2(1-\eta_\alpha)} + \frac{(2-\eta_\alpha-\eta_\beta)K_\beta}{2(1-\eta_\beta)} \right\} \gamma$$

However, the dilatation is also written as

$$\Delta = \Delta_o + \Delta_1 \gamma$$

Comparing coefficients and solving for Δ_o and Δ_1

---

[4] It is assumed that the simplified curvature change expressions as given by (31) are being used.

$$\Delta_o = \frac{e_1}{(1-\eta_\alpha)} + \frac{e_2}{(1-\eta_\beta)}$$

$$\Delta_1 = \frac{K_\alpha}{(1-\eta_\alpha)} + \frac{K_\beta}{(1-\eta_\beta)} \tag{33}$$

Substituting (33) into (32), the resulting expression for u_γ becomes (34)

$$u_\gamma = w + \left[\frac{\eta_\alpha}{(1-\eta_\alpha)} e_1 + \frac{\eta_\beta}{(1-\eta_\beta)} e_2\right]\gamma + \left[\frac{\eta_\alpha}{(1-\eta_\alpha)} K_\alpha + \frac{\eta_\beta}{(1-\eta_\beta)} K_\beta\right]\frac{\gamma^2}{2}$$

L. Evaluation of the Transverse Shear Stress Resultants Q_α and Q_β

Having evaluated the expressions for u_γ, Δ_o, Δ_1, x_o and x_1, the integrated equlibrium equations (18)-(22) can now be expressed in terms of the five unknowns, the three components of the middle surface displacement and the two transverse shear stress resultants Q_α and Q_β. Following the procedure previously outlined, equations (21) and (22) are solved for Q_α and Q_β. After some rearranging, the final form for these expressions becomes

$$\begin{aligned}
\frac{12AB}{\delta^3} Q_\alpha = &\left[\frac{(\lambda_\alpha + 2\mu_\alpha)}{(1-\eta_\alpha)} - \frac{2\mu_\alpha\eta_\alpha}{(1-\eta_\alpha)}\right] B\frac{\partial K_\alpha}{\partial\alpha} + \left[\frac{(\lambda_\alpha+2\mu_\alpha)}{(1-\eta_\beta)} - \frac{2\mu_\alpha\eta_\beta}{(1-\eta_\beta)}\right. \\
&\left. -2(\mu_\alpha - \mu_{\alpha\beta})\right] B\frac{\partial K_\beta}{\partial\alpha} + \left[\frac{(\lambda_\alpha+2\mu_\alpha)}{(1-\eta_\alpha)} - \frac{(\lambda_\beta+2\mu_\beta)}{(1-\eta_\beta)} - 2\eta_\alpha\frac{(\mu_\alpha - \mu_\beta)}{(1-\eta_\alpha)}\right. \\
&\left. -2(\mu_\alpha - \mu_\beta) + 2(\mu^\alpha - \mu_{\alpha\beta})\right]\frac{\partial B}{\partial\alpha} K_\alpha + \left[\frac{(\lambda_\alpha+2\mu_\alpha)}{(1-\eta_\beta)} - \frac{(\lambda_\beta + 2\mu_\beta)}{(1-\eta_\beta)}\right. \\
&\left. - 2\eta_\beta\frac{(\mu_\alpha - \mu_\beta)}{(1-\eta_\beta)} - 2(\mu_\alpha - \mu_{\alpha\beta})\right]\frac{\partial B}{\partial\alpha} K_\beta
\end{aligned} \tag{35}$$

$$\frac{12AB}{\delta^3} Q_\beta = \left[\frac{(\lambda_\beta + 2\mu_\beta)}{(1-\eta_\beta)} - \frac{2\mu_\beta\eta_\beta}{(1-\eta_\beta)}\right] A\frac{\partial K_\beta}{\partial\beta} + \left[\frac{(\lambda_\beta + 2\mu_\beta)}{(1-\eta_\alpha)} - \frac{2\mu_\beta\eta_\alpha}{(1-\eta_\alpha)}\right.$$

$$-2(\mu_\beta - \mu_{\alpha\beta})\Big]\, A \frac{\partial K_\alpha}{\partial \beta} + \Big[\frac{(\lambda_\beta + 2\mu_\beta)}{(1-\eta_\beta)} - \frac{(\lambda_\alpha + 2\mu_\alpha)}{(1-\eta_\beta)} - 2\eta_\beta \frac{(\mu_\beta - \mu_\alpha)}{(1-\eta_\beta)}$$

$$-2(\mu_\beta - \mu_\alpha) + 2(\mu_\beta - \mu_{\alpha\beta})\Big] \frac{\partial A}{\partial \beta} K_\beta + \Big[\frac{(\lambda_\beta + 2\mu_\beta)}{(1-\eta_\alpha)} - \frac{(\lambda_\alpha + 2\mu_\alpha)}{(1-\eta_\alpha)} \qquad (36)$$

$$-2\eta_\alpha \frac{(\mu_\beta - \mu_\alpha)}{(1-\eta_\alpha)} - 2(\mu_\beta - \mu_{\alpha\beta})\Big] \frac{\partial A}{\partial \beta} K_\alpha$$

Inspection of the above two equations indicates that elastic constants λ_α, λ_β, μ_α, μ_β, η_α and η_β are becoming cumbersome in their combinations. At this point it becomes advantagous to readopt the elastic constants, a_{ij}, as first defined in the generalized Hookes' Law. Thus equations (35) and (36) may also be written as

$$\frac{12AB\, Q_\alpha}{\delta^3} = \frac{a_{22}}{(a_{11}a_{22}-a_{12}^2)} B \frac{\partial K_\alpha}{\partial \alpha} + \Big[\frac{2}{a_{66}} - \frac{a_{12}}{(a_{11}a_{22}-a_{12}^2)}\Big] B \frac{\partial K_\beta}{\partial \alpha} \qquad (37)$$

$$+ \Big[\frac{(a_{22}+a_{12})}{(a_{11}a_{22}-a_{12}^2)} - \frac{2}{a_{66}}\Big] \frac{\partial B}{\partial \alpha} K_\alpha + \Big[\frac{2}{a_{66}} - \frac{(a_{11}+a_{12})}{(a_{11}a_{22}-a_{12}^2)}\Big] \frac{\partial B}{\partial \alpha} K_\beta$$

$$\frac{12AB\, Q_\beta}{\delta^3} = \frac{a_{11}}{(a_{11}a_{22}-a_{12}^2)} A \frac{\partial K_\beta}{\partial \beta} + \Big[\frac{2}{a_{66}} - \frac{a_{12}}{(a_{11}a_{22}-q_{12}^2)}\Big] A \frac{\partial K_\alpha}{\partial \beta}$$

$$+ \Big[\frac{(a_{11}+a_{12})}{(a_{11}a_{22}-a_{12}^2)} - \frac{2}{a_{66}}\Big] \frac{\partial A}{\partial \beta} K_\beta + \Big[\frac{2}{a_{66}} - \frac{(a_{22}+a_{12})}{(a_{11}a_{22}-a_{12}^2)}\Big] \frac{\partial A}{\partial \beta} K_\alpha \qquad (38)$$

The derivation of (35) and (36) from (21) and (22) necessitates simplifications which are in accord with the assumption that the change of curvature expression can be simplified so as to neglect any of the tangential displacement terms. The tangential displacement terms in (21) and (22) can be shown to be of the same order of magnitude as the tangential displacement terms in the curvature change expressions. Hence if these terms are neglected in the latter, consistency requires that they also be neglected in the former.

M. Resultant Shell Equations

Substituting (37) and (38) into (18), (19) and (20), a set of resultant equilibrium equations are formed in terms of the three middle surface displacement components. The equations have been simplified in their elastic constants so as to contain the more familiar "aij" Since the curvature change K, defined in (31), contains only the normal displacement and appears only in the third of the final expressions and then only when prefixed by the square of the thickness, it was felt that the equations could be simplified in their presentation by the inclusion of this parameter in the resulting equations.

In deriving the final set of equations, a number of terms of the following type appeared

$$\frac{\delta^2}{12}\frac{\partial K}{\partial \alpha}; \quad \frac{\delta^2}{12}\frac{\partial K}{\partial \beta}; \quad \frac{K\delta^2}{12}$$

In part III, section 1 of his book, Vlasov [2] discusses terms of this type in reference to general shell theory. He points out that the contribution of such terms to the displacements is small and their effect decreases with decreasing relative thickness ($k\delta$). The only curvature change terms which are significant in the displacement equations are those dependent on its second derivative. The resulting three displacement equations have been simplified in accord with the above statements.

The three resulting displacement equations follow.

$$\frac{a_{22}}{(a_{11}a_{22}-a_{12}^2)} B \frac{\partial}{\partial\alpha}\left\{\frac{1}{AB}\left[\frac{\partial}{\partial\alpha}(Bu)+\frac{\partial}{\partial\beta}(Av)\right]\right\} + \frac{(a_{22}+a_{12})}{(a_{11}a_{22}-a_{12}^2)} ABKu$$

$$+\frac{1}{a_{66}} A \frac{\partial}{\partial\beta}\left\{\frac{1}{AB}\left[\frac{\partial}{\partial\beta}(Au)-\frac{\partial}{\partial\alpha}(Bv)\right]\right\} + \frac{2a_{22}}{(a_{11}a_{22}-a_{12}^2)} B\frac{\partial}{\partial\alpha}(Hw)$$

$$-\frac{(a_{22}+a_{12})}{(a_{11}a_{22}-a_{12}^2)} Bk_2 \frac{\partial w}{\partial\alpha} + \frac{(a_{22}-a_{11})}{(a_{11}a_{22}-a_{12}^2)}\frac{1}{AB}\left(\frac{\partial B}{\partial\alpha}\right)^2 u \qquad (39)$$

$$+\left[\frac{(a_{22}+a_{12})}{(a_{11}a_{22}-a_{12}^2)}-\frac{2}{a_{66}}\right]\frac{\partial}{\partial\beta}\left(\frac{1}{B}\frac{\partial A}{\partial\beta}\right)u-\left[\frac{(a_{22}-a_{12})}{(a_{11}a_{22}-a_{12}^2)}-\frac{2}{a_{66}}\right]\frac{\partial^2 v}{\partial\alpha\partial\beta}$$

$$+\left[\frac{(a_{22}+a_{12})}{(a_{11}a_{22}-a_{12}^2)}-\frac{2}{a_{66}}\right]\frac{1}{AB}\frac{\partial B}{\partial\alpha}\frac{\partial A}{\partial\beta}v + \frac{(a_{22}+a_{11})}{(a_{11}a_{22}-a_{12}^2)}\frac{1}{B}\frac{\partial B}{\partial\alpha}\frac{\partial v}{\partial\beta}$$

$$+\frac{(a_{22}-a_{11})}{(a_{11}a_{22}-a_{12}^2)} k_2 \frac{\partial B}{\partial\alpha} w + \frac{AB}{\delta} P_\alpha = 0$$

$$\frac{a_{11}}{(a_{11}a_{22}-a_{12}^2)} A \frac{\partial}{\partial\beta}\left\{\frac{1}{AB}\left[\frac{\partial}{\partial\beta}(Av)+\frac{\partial}{\partial\beta}(Bu)\right]\right\} + \frac{(a_{11}+a_{12})}{(a_{11}a_{22}-a_{12}^2)} ABKv$$

$$+\frac{1}{a_{66}} B \frac{\partial}{\partial\alpha}\left\{\frac{1}{AB}\left[\frac{\partial}{\partial\alpha}(Bv)-\frac{\partial}{\partial\beta}(Au)\right]\right\} + \frac{2a_{11}}{(a_{11}a_{22}-a_{12}^2)} A\frac{\partial}{\partial\beta}(Hw)$$

$$-\frac{(a_{11}+a_{12})}{(a_{11}a_{22}-a_{12}^2)} Ak_1 \frac{\partial w}{\partial\beta} + \frac{(a_{11}-a_{22})}{(a_{11}a_{22}-a_{12}^2)}\frac{1}{AB}\left(\frac{\partial A}{\partial\beta}\right)^2 v \qquad (40)$$

$$+\left[\frac{(a_{11}+a_{12})}{(a_{11}a_{22}-a_{12}^2)}-\frac{2}{a_{66}}\right]\frac{\partial}{\partial\alpha}\left(\frac{1}{A}\frac{\partial B}{\partial\alpha}\right)v-\left[\frac{(a_{11}+a_{12})}{(a_{11}a_{22}-a_{12}^2)}-\frac{2}{a_{66}}\right]\frac{\partial^2 u}{\partial\alpha\partial\beta}$$

$$
+ \left[\frac{(a_{11}+a_{12})}{(a_{11}a_{22}-a_{12}^2)} - \frac{2}{a_{66}}\right] \frac{1}{AB}\frac{\partial A}{\partial \beta}\frac{\partial B}{\partial \alpha} u + \frac{(a_{11}-a_{22})}{(a_{11}a_{22}-a_{12}^2)} \frac{1}{A}\frac{\partial A}{\partial \beta}\frac{\partial u}{\partial \alpha}
$$

$$
+ \frac{(a_{11}-a_{22})}{(a_{11}a_{22}-a_{12}^2)} k_1 \frac{\partial A}{\partial \beta} w + \frac{AB}{\delta} P_\beta = 0
$$

$$
(a_{11}+a_{12}) \frac{\partial}{\partial \alpha}(Bk_2u) + (a_{22}+a_{12}) \frac{\partial}{\partial \beta}(Ak_1v) - 2H\left[a_{11}\frac{\partial}{\partial \alpha}(Bu)\right.
$$

$$
\left. + a_{22}\frac{\partial}{\partial \beta}(Av)\right] + (a_{11}-a_{12}) k_1 B \frac{\partial u}{\partial \alpha} + 2AB\left\{ \left[\frac{(a_{11}+a_{22})+a_{12}}{2}\right]K\right.
$$

$$
\left. - \frac{2(a_{11} + a_{22})}{2} H^2 \right\} w - \frac{(a_{11}-a_{22})}{2} k_2^2 ABw - \frac{(a_{22}-a_{11})k_1^2 ABw}{2}
$$

$$
+ \frac{\delta^2}{12}\left\{ a_{22}\frac{\partial}{\partial \alpha}\left(\frac{B}{A}\frac{\partial \nabla^2_e w}{\partial \alpha}\right) + a_{11}\frac{\partial}{\partial \beta}\left(\frac{A}{B}\frac{\partial}{\partial \beta}\nabla^2_e w\right)\right. \tag{41}
$$

$$
+ \left[\frac{2}{a_{66}}(a_{11}a_{22}-a_{12}^2) - (a_{22}+a_{12})\right] \frac{\partial}{\partial \alpha}\left(\frac{B}{A}\frac{\partial K_\beta}{\partial \alpha}\right) + \left[\frac{2}{a_{66}}(a_{11}a_{22}-a_{12}^2)\right.
$$

$$
\left. \left. - (a_{11}+a_{12})\right] \frac{\partial}{\partial \beta}\left(\frac{A}{B}\frac{\partial K_\alpha}{\partial \beta}\right)\right\} + \frac{AB}{\delta}(a_{11}a_{22}-a_{12}^2) P_\gamma = 0
$$

In the above equation, the elliptical operator ∇^2_e is defined as

$$
\nabla^2_e = \frac{1}{AB}\left[\frac{\partial}{\partial \alpha}\left(\frac{B}{A}\frac{\partial}{\partial \alpha}\right) + \frac{\partial}{\partial \beta}\left(\frac{A}{B}\frac{\partial}{\partial \beta}\right)\right]
$$

REFERENCES

1. Novozhilov, V. V., The Theory of Thin Shells, Groningen, The Netherlands: P. Noordhoff Ltd. (1959)
2. Vlosov, V. Z., General Theory of Shells and its Application in Engineering, (in Russian), Moscow-Leningrad: Government Bureau of Technical and Theoretical Literature. (1949)
3. Ambartsumian, S. A., "Contributions to the Theory of Anisotropic Layered Shells", Applied Mechanics Reviews, Vol. 15, No. 4 (April 1962)
4. Ambartsumian, S. A., Theory of Anisotropic Shells (in Russian) 1st ed., Moscow: Government Bureau of Physics and Mathematics Literature Distribution (1961)

IMPACT ATTENUATION RESEARCH

Project Investigators

Mr. H. E. Whitmore, Head
Space Technology Division

Dr. Charles H. Samson, Jr., Professor
Departments of Aerospace & Civil Engineering

Mr. C. A. Rodenberger, Associate Professor
Department of Aerospace Engineering

Mr. H. J. Sweet, Assistant Professor
Department of Aerospace Engineering

Mr. H. C. Kavanaugh, Instructor
Department of Aerospace Engineering

Captain (USAF) W. J. Bland, Candidate for
M.S. in Aerospace Engineering

Mr. A. J. Chaput,
NASA Doctoral Trainee

Captain (USAF) L. B. Harding, Candidate for
M.S. in Aerospace Engineering

Captain (USAF) A. F. Herrmann, Candidate for
M.S. in Aerospace Engineering

I. Introduction

This report covers the work accomplished from January through July 1964. The following work has been accomplished:

1. A drop-test facility has been constructed and the necessary instrumentation has been installed.
2. Projects have been completed involving experiments for impact attenuation by the following methods:
    a. Tube buckling
    b. Collapsible legs
    c. Honeycomb compression

3. Reports on the results of these three projects have been written and are included in this progress report.

4. The investigation of impact attenuation by means of frangible tubes is being continued.

II. Drop-test Facility

The test rig that was described in the previous progress report was completed and used for a number of dynamic tests. It performed satisfactorily as a dynamic crushing device, but the vibrations in the rig due to its flexibility resulted in excessive "noise" in the accelerometer output, making the traces unusable. To remedy this, a more compact device was constructed and used for the majority of the tests. This change improved the quality of t e traces significantly, but problems were still encountered because of shock waves traveling up and down the center post with a frequency of about 5,000 c.p.s. It is expected that this problem will be eliminated by taking the future traces on a ecording oscillograph with galvanometers that are incapable of recording frequencies above 1,000 c.p.s.

III. Frangible Tubes

In Progress Report #2 an equation was developed to predict the initial peak fragmentation force in the frangible tube energy absorption process. Good correlation was found between predicted and actual valves of the initial force for ten tube and die geometries. However, the values of the mechanical properties used in the equations were handbook values which are for a 95% confidence limit application, giving mechanical properties much lower than those generally encountered in practice. Therefore, laboratory experiments were devised to yield actual values of the per cent circumfrential elongation, and the sum of the yield and ultimate stress for 2024-T3 aluminum tubing. Substitution of the experimentally obtained valves into the prediction equation previously derived, resulted in unsatisfactory correlation with test data.

It was felt that the inadequacy of the first equation resulted from two erroneous initial assumptions, the first being the shape of the deflected end of the tube and the second , the method for predicting the point of zero deflection.

A second analysis was performed, taking the above corrections into account. While the second equation checks quite well with a few experimental results, not enough data are yet availble to confirm conclusive correlation.

In addition to the new analytical approach, considerable laboratory experimentation has been performed since the previous report. The experimentation includes the determination of the coefficient of friction, between the tube and die properties of the tube, and static experimental investigation of the frangible tube process. The experimental and analytical investigation is progressing such that a final report on frangible tubes investigated at this institution will appear in the next published progress report.

IV. Tube Buckling

Tube buckling processes were studied by Captain A. F. Herrmann, who performed static and dynamic tests on various tubes to determine the relationships between the respective forces exerted by the tube. A report of his results is given in Enclosure 1.

The most important conclusions that can be drawn from his work are:

1) For aluminum and presumably for other materials that do not generate excessive heat when deformed at the rates investigated here, the dynamic buckling behavior of the tubes duplicates the static behavior with respect to forces developed and modes of failure. This would make it possible to base a design on static results and use dynamic tests as a final check. This does not apply to materials that generate a great deal of heat during deformation because the resulting high termperatures alter the mechanical properites of the material.

2) Tubes of the type studied have a severe limitation because of the characteristic high ratio of maximum force to average force. This problem could probably be lessened by filling the tube with a gas or a crushable solid. This appears to be the most promising direction for continued research on this system.

V. Collapsible Legs

Static and dynamic tests were performed on various configurations of aluminum legs by Captain L.B. Harding. A report of his results is given in Enclosure 2.

Here again, the most important results would appear to be the verification of the fact that at least for the material and loading rates investigated, the dynamic behavior can be accurately predicted, with data obtained from static tests.

VI. Honeycomb

Static and dynamic tests were perfomred on aluminum honeycomb specimens by Captain W. J. Bland. A report of his results is given in Enclosure 3.

Captain Bland demonstrated the feasibility of using a variable geometry loading head to vary the crushing forces exerted by a given piece of honeycomb material.

AN EXPERIMENTAL INVESTIGATION OF THE ENERGY-ABSORPTION CHARACTERISTICS OF METAL TUBES LOADED IN COMPRESSION *

by

ARMIN F. HERRMANN, JR.

Aerospace Engineering Department and Space Technology Division

Texas A&M University

* The material presented here was extracted from a thesis having the above title which was submitted by the author in partial fulfillment of the requirements for the degree of Master of Science in Aerospace Engineering at Texas A&M University.

Enclosure 1

LIST OF SYMBOLS

a	Acceleration
A	Cross-sectional area of type
d	Drop height
D	Diameter of tube
F	Force
g	Acceleration due to gravity
g_c	Gravitational constant
G	a/g
ℓ	Length of specimen
m	Mass
s	Deformation Stroke
s_i	Oscilloscope lead distance
t	Wall-thickness of specimen
t_i	Oscilloscope trigger lead time
t_s	Time of deformation stroke
v_i	Impact velocity
w	Density of material
W	Weight of specimen
W_d	Weight of drop carriage
PE	Potential energy
KE	Kinetic energy

I. Introduction

This investigation is concerned with the energy-absorption characteristics inherent in axially compressed metal tubes.

Certain metal tubes, when loaded axially in compression, will buckle plastically. There is a capability for absorbing an amount of energy equal to the product of the average force in the tube multiplied by the deformation undergone by the tube.

In 1956, an investigation was conducted at the University of Texas into the use of fluid-filled metal cylinders as energy absorbers on impact. This report was prepared for the Quartermaster Research and Development Command and was directed toward minimizing the cost per unit energy absorbed with little consideration given the weight of the mechanisms involved.

It is recommended, in the report just cited, that additional experimental research be done on empty tubes with different ratios of diameter to wall-thickness. The literature investigated does not contain theoretical methods of determining forces involved in plastic buckling that agree with empirical results.

II. Objectives

This investigation was designed to utilize static and dynamic compression loadings on various metal tubes to find the most desirable configuration, using as a criterion the maximum ratio of the average resisting force through the stroke in plastic buckling to the weight of the specimen.

In addition, a method was sought by which to predict dynamic behavior by applying the results of static tests to equations describing the principle of the conservation of energy.

III. Experimental Procedures

Static Testing Procedures

Nine tube configurations were tested statically. They were:

Material	Outer Diameter	Wall Thickness
3003-H14 Aluminum	2"	0.035"
	2"	.049"
	2"	.065"
6061-T6 Aluminum	2"	.049"
	2"	.058"
	2"	.065"
Abco alloy brass	2"	.032"
	2"	.065"
1015 Mechanical steel	2"	.028"

These materials were selected because of their commercial availability and because they provide a representative range of strength and diameter to wall-thickness ratios.

All tubing was cut into 9-inch lengths and was sanded and squared on the ends.

The static tests were performed on a Baldwin Universal Testing Machine. Compression loading was accomplished at a rate producing less than one-half inch of deformation per minute.

Tubes were set in the machine with the tops inserted into a grove of 2-inches outer diameter in a cast iron pipe flange.

The bottoms rested on a cast iron plate to preclude eccentric loading.

As the tubes were loaded im compression, force readings were recorded at each 0.1 inch deformation. In addition to these incremental readings, maximum and minimum forces were recorded as they occurred. Each plastic fold in the tubes had a maximum and minimum force reading associated with it.

The resisting force inherent in each tube during plastic buckling was then portrayed graphically by a plot of deformed length versus resisting force.

These graphs were then utilized to plot dimensionless curves for each material. These curves portrayed the diameter to wall-thickness ratio versus the ratio of average resisting force-to-specimen weight.

Dynamic Testing Procedures

Eight tube configurations were tested dynamically. They were:

Material	Outer Diameter	Wall Thickness
3003-H14 Aluminum	2"	0.035"
	2"	.049"
	2"	.065"
6061-T6 Aluminum	2"	.049"
	2"	.058"
	2"	.065"
Abco alloy brass	2"	.032"
1015 Mechanical steel	2"	.028"

Specimen preparation was accomplished in the same manner as for the static tests.

Dynamic testing took place on a special drop-test mechanism. It was designed to allow a know weight to free-fall from a known height and to impact on a stationary specimen. An accelerometer mounted on the drop carriage supplied input voltage to an oscilloscope which presented a display of acceleration versus time.

Data from the static tests were used to perform computations in order to predict the desirable drop carriage weight, drop height, stroke time, and range of accelerations. This was necessary to provide a basis of comparison between static and dynamic tests and to provide insurance against exceeding the limitations of the equipment.

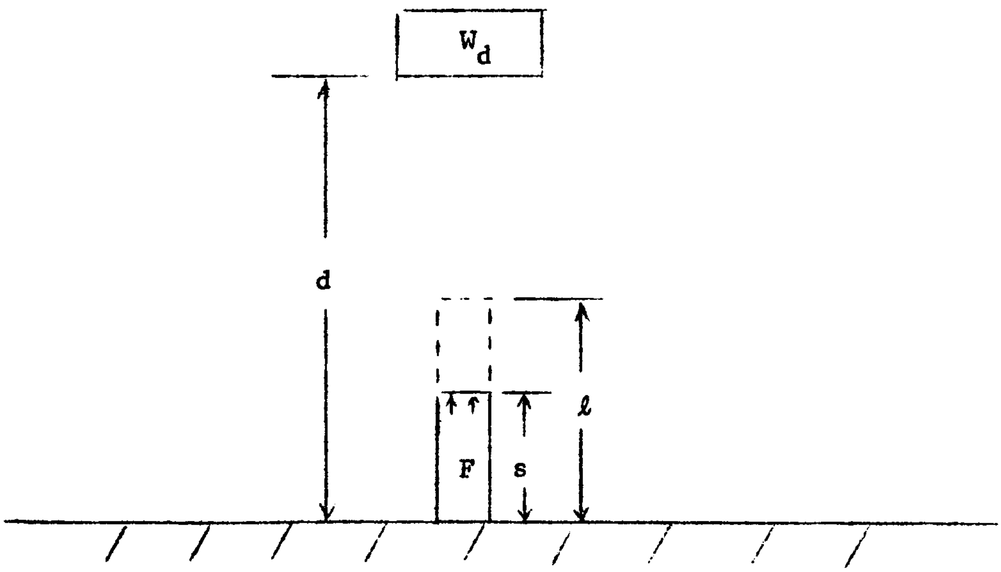

Figure 1. Distances Used in Development of Pre-Drop Data

To determine average acceleration through the stroke:

$$\Sigma F = ma \text{(positive downward)}$$

$$W_d - F\frac{g_c}{g} = \frac{W_d a}{g}$$

$$= W_d G$$

$$G = \frac{W_d - F\left(\frac{g_c}{g}\right)}{W_d}$$

$$G = 1 - \frac{F\left(\frac{g_c}{g}\right)}{W_d}$$

To determine drop height:

$$\Delta \text{ PE} + \text{Work}$$

$$W_d(\ell - s) - W_d d = -Fs\left(\frac{g_c}{g}\right)$$

$$-d = s\left[1 - \frac{F\left(\frac{g_c}{g}\right)}{W_d}\right] - \ell$$

$$d = s\left[\frac{F\left(\frac{g_c}{g}\right)}{W_d} - 1\right] + \ell$$

$$d = -sG + \ell$$

To determine impact velocity:

$$\Delta \text{ PE} = \Delta \text{ KE}$$

$$W_d(d-\ell) = 1/2\,\frac{W_d}{g}\left(v_i^2 - \cancel{v_0^2}\right)$$

$$v_i = \left[2g(d-\ell)\right]^{1/2}$$

To determine stroke time:

$$at_s = v_2 - v_i$$

$$t_s = -\frac{v_i}{a}$$

$$t_s = - \frac{v_i}{gG}$$

To determine trigger lead distance:

$$v = v_i - gt_i$$

$$s_i = vt_i + 1/2\ gt_i^2$$

$$= (v_i - gt_i)\ t_i + 1/2\ gt_i^2$$

$$s_i = t_i\ (v_i - 1/2\ gt_i)$$

An average force resisting plastic buckling for each tube configuration was approximated by estimating a mean force through the stroke from the graphs which portrayed the static results. All tests were programmed for a desired deformation stroke of 5 inches.

The oscilloscope trace was triggered ahead of impact to provide a reference line. The time between trace initiation and impact varied with the time range on the scope required to portray the entire deformation stroke.

Tubes to be crushed were centered on the base plate of the drop mechanism and were not restrained in any way.

IV. Discussion of Results

Static Tests

Static test results are portrayed in the form of representative curves shown in Figures 2 and 3.

The characteristic form of the force versus deformation durves showed a steady increase in resisting force until the first fold or buckle occurred. The force then dropped off as

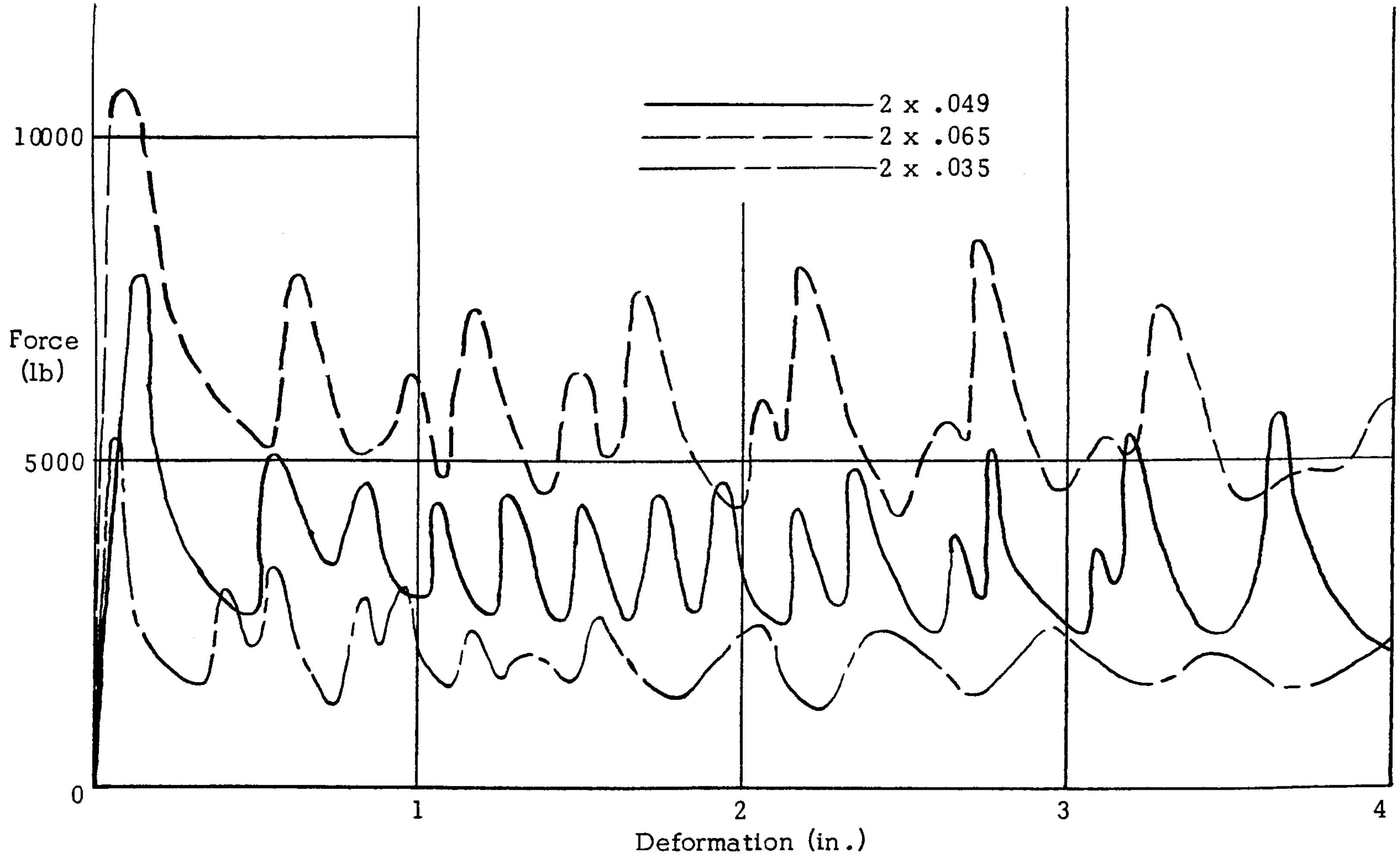

Figure 2. Representative Curves of 3003 H14 Static Tests

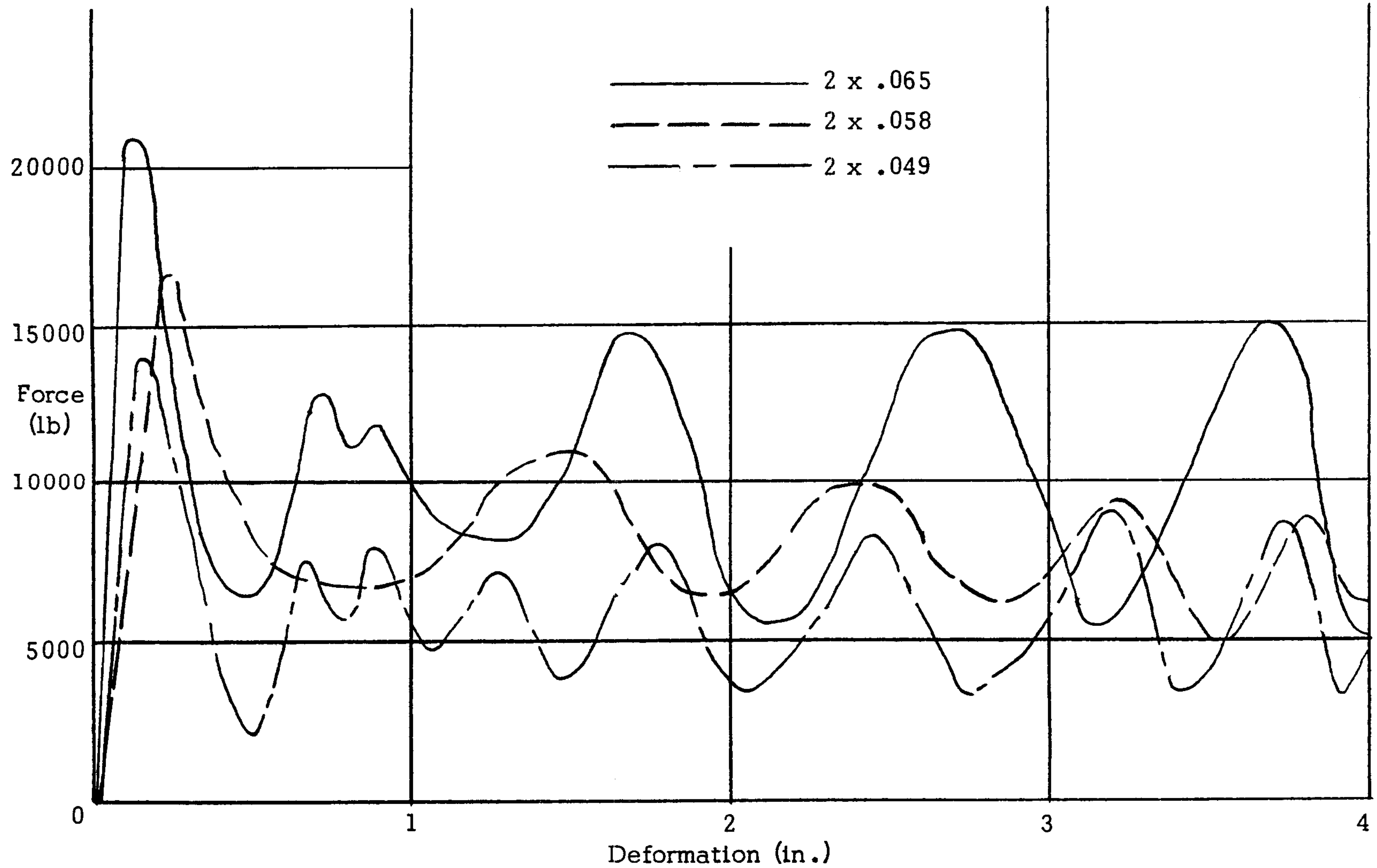

Figure 3. Representative Curves of 6061 T6 Static Tests

deformation took place and started to build again proir to formation of the se ond fold. Peaks and valleys in the curve as each fold took place roughly approximated the shape of a sine curve.

An average resisting force to plastic buckling was extracted from the curves by visually determining the mean value between the peaks and valleys through the stroke. This mean value was normally about one-half the original maximum force.

Dimensionless plots comparing the ratio of diameter to wall-thickness against the ratio of average resisting force to specimen-weight were plotted for each material. They are shown in Figure 4.

These curves indicate that the thicker walled specimens of 6061-T6 aluminum have the best ratio of average resisting force to specimen-weight.

The large initial force prior to buckling and the variation through the stroke are not desirable in an energy-attenuation device.

Tubes could be loaded to the point where the first fold formed before use. This would decrease the magnitude of the initial peak force.

Variation through the stroke could be decreased by some sort of internal pressurization.

<u>Dynamic Tests</u>

The dynamic test program showed that, with one exception, static test results gave accurate predictions of both deformation stroke and average resisting force. Actual results for these

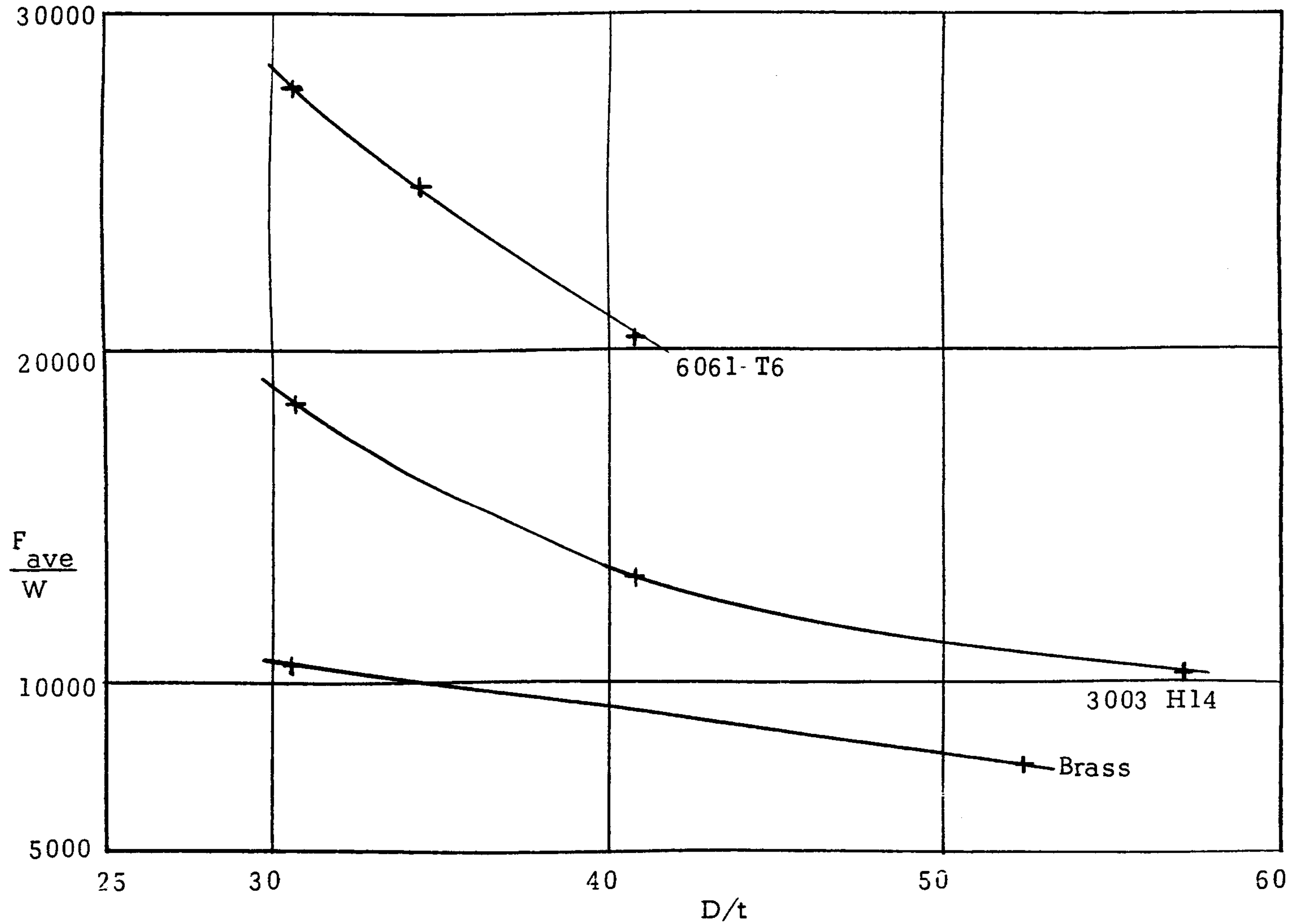

Figure 4. Static Test Results

two parameters were within 10 per cent of predicted values.

Deformation strokes, which were predicted to be 5 inches in all tests, ranged upward to a maximum difference of 7 per cent, indicating that less resisting force was available in the tubes when loaded dynamically.

Average accelerations through the stroke as portrayed on the oscilloscope ranged downward from those predicted to a maximum difference of 10 per cent.

Equipment limitations precluded an appraisal of onset rate and maximum force because of high-frequency noise. It was possible to visually estimate average acceleration through the stroke.

The exception noted above was the steel specimen configuration Deformations were up to 25 per cent shorter than predicted. These tubes, however, wete too hot to touch immediately after testing, indicating the release of a large amount of energy in the form of heat. This heat energy could also account for the differences from predicted values found in other tube configurations.

Table 1 compares predicted and actual G readings and stroke distances.

Table 1

Dynamic Test Results

Specimen		Average G Predicted	Average G Actual	Stroke (in.) Predicted	Stroke (in.) Actual
3003	2 x .035	14.4	13.9	5	5.15
	2 x .049	11.5	10.5	5	5.15
	2 x .065	31.0	28.7	5	5.10
6061	2 x .049	18.6	16.8	5	5.30
	2 x .058	25.8	24.6	5	5.10
	2 x .065	34.7	32.8	5	5.05
Brass	2 x .032	29.8	28.0	5	5.20
Steel	2 x .028	15.0		5	4.30

V. Conclusions

The results of this investigation indicate that an effective, predictable energy-attenuation system can be constructed using metal tubes as the energy absorbers.

For the aluminum alloys investigated here, this system can be designed without the expense and time limitations imposed by a dynamic testing program, since static tests can be used to accurately predict dynamic behavior.

A basic design approach would be to equate the kinetic energy developed by the vehicle at impact to the work done by the tubes. The average force through the deformation stroke is a known quantity. The work done by the tubes is equal to the product of this force multiplied by the length of the stroke.

If structural limitations dictate available deformation stroke length, a combination of tubes can be used to provide the necessary force.

A variable range of available deformation stroke lengths can be used to attenuate energy developed from a compatible range of impact velocities.

The rather large ratio of maximum force to average force that appears to be inherent in collapsable tubes presents a rather severe limitation.

LITERATURE CITED

1. Morgan, Carl W. and Moore, Walter L., Theoretical and Experimental Investigations of Fluid-Filled Metal Cylinders for Use as Energy Absorbers on Impact, University of Texas Structural Mechanics Research Laboratory, Austin, Texas, 1956.

(See the February, 1964 Progress Report for a complete bibliography.)

AN EXPERIMENTAL INVESTIGATION OF THE ENERGY-ATTENUATION CAPABILITIES OF VARIOUS-SHAPED COMPLIABLE METAL STRUCTURES*

by

LYNN B. HARDING

Aerospace Engineering Dept. & Space Technology Division

Texas A&M University

*The material presented here was extracted from a thesis having the above title which was submitted by the author in partial fulfillment of the requirements for the degree of Master of Science in Aerospace Engineering at Texas A&M University.

Enclosure 2

I. Introduction

The National Aeronautics and Space Administration has made limited investigations of structural energy-absorption systems which can be classified as those which derive the deceleration stroke from change of length of impact device and penetration into the impacted medium (1).* Specifically, these systems have involved the use of honeycomb core, compression tubes, spikes, frangible tubes, strain straps, and compliable metal structures under compressive loads.

The investigation of compliable metal structures made by Hoffman (2) in 1961 at the Langley Research Center concluded that load-alleviating compliable metal structures can give major reductions in accelerations encountered during space capsule landings. However, only one shape was investigated at that time.

This report presents the results of experimental investigations of the energy-attenuation capabilities of various-shaped compliable metal structures. The results obtained from statically and dynamically loaded specimens are shown, comparison of the energy-absorption characteristics of the various shapes is made, and the possibility of the existence of a relationship between the static and dynamic energy-attenuation characteristics of the various shapes is studied.

---

*References cited in parentheses are listed numerically under Literature Cited.

II. Theory

Energy-attenuation systems for decelerating spacecraft upon landing must absorb and dissipate the kinetic energy of the vehicle in such a manner that the forces transmitted to the payload do not exceed the limitations of the components of the payload. Ideally, such a system would transmit the impact forces to the payload so that after an initially low onset rate, a uniform rate of force application is maintained until all deceleration forces are eliminated (1). Since force is proportional to acceleration, these ideal conditions can be shown graphically by an acceleration versus time curve similar to the following:

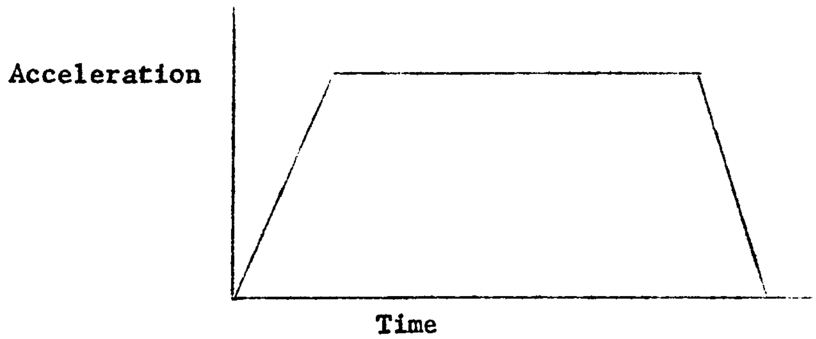

Figure 1. Representative Shape of Ideal Acceleration versus Time Curve.

In addition, other physical and operational considerations dictate that any impact energy-absorbing system incorporated in a spacecraft must be a light-weight, low-volume system with a high degree of predictability and reproducibility.

Thus, one measure of the relative value of energy-absorbing systems is the comparison of their respective energy-absorption efficiencies, which are defined as the ratio of the amount of energy absorbed to the weight of the system.

Another factor to be considered in determination of the relative value of energy-absorbing systems is the ratio of peak acceleration to average acceleration. This ratio should ideally be as close to unity as possible.

One type device for absorbing the kinetic energy of a spacecraft upon impact is a system composed of compliable metal structures, which in effect are collapsible struts which, upon impact, undergo bending and yielding in the plastic range.

Hoffman (2) investigated one shape of such compliable metal structures for alleviating the kinetic energy of spacecraft impact and found, for vertical contact at a velocity of 30 ft/sec on a concrete surface, the maximum acceleration to be 35g. The rebound of this model was slight, which indicated that very little elastic energy was stored in the compliable structures.

Since the use of compliable metal structures as load alleviating devices relies mainly on the energy abosrbed during plastic bending, it is desirable that the structures bend at as many stations as possible along their length (3). Thus, the initial shape of the compliable structure plays a major role in its value as an energy-absorption device and the relative value of any given shape can be expressed by comparison of its energy-absorption efficiency with that of any other shape, coupled with the comparison of their respective acceleration versus time curves.

III. Experimental Procedures

Compliable aluminum structures made of Al 2024-T3 with a thickness of 0.1 inch were constructed in nine different shapes. Specific dimensions of these shapes are shown in Figures 2 through 6, with the given plan-view dimensions being those of the structure prior to pre-test bending. These shapes are identified by the letter designations A through I as shown in Figures 2 through 6. Shapes A through E were also constructed of Al 6061-T6 with a thickness of 0.1 inch.

Pre-test bending was accomplished on each of the shapes to control the location and direction of the bending during the actual tests. Side views of these struts after pre-test bending are shown in Figures 2 and 6.

The struts were mounted on round, 7-inch diameter, base plates made of Al 2024-T3 with a thickness of 0.5 inch. Static test facilities precluded the use of bigger base plates. The struts were secured to the plates with 3/16-inch cadmium plated chrome-moly aircraft bolts. These shapes were mounted in sets of four struts for each test, except in the case of shape B, which was mounted in a set of two struts.

For static tests, the test units were loaded in compression in a Baldwin Universal Testing Machine. This loading resulted in a decrease in the distance between the base plates. The amount of loading at each 0.1-inch of decrease in this distance was recorded; thus, the loading at each 0.1-inch of stroke was determined.

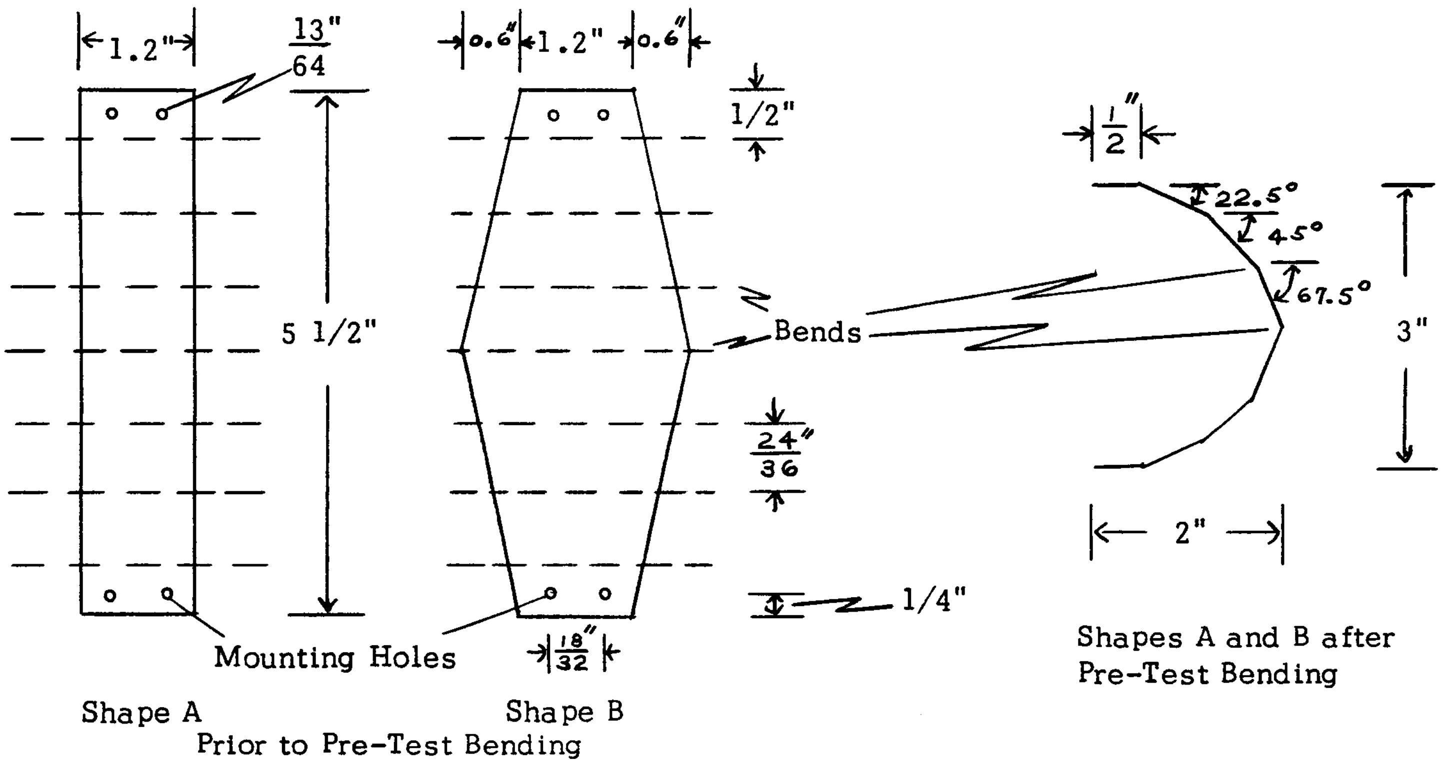

Figure 2. Compliable Structures - Shape A and Shape B (Scale: 1" = 2").

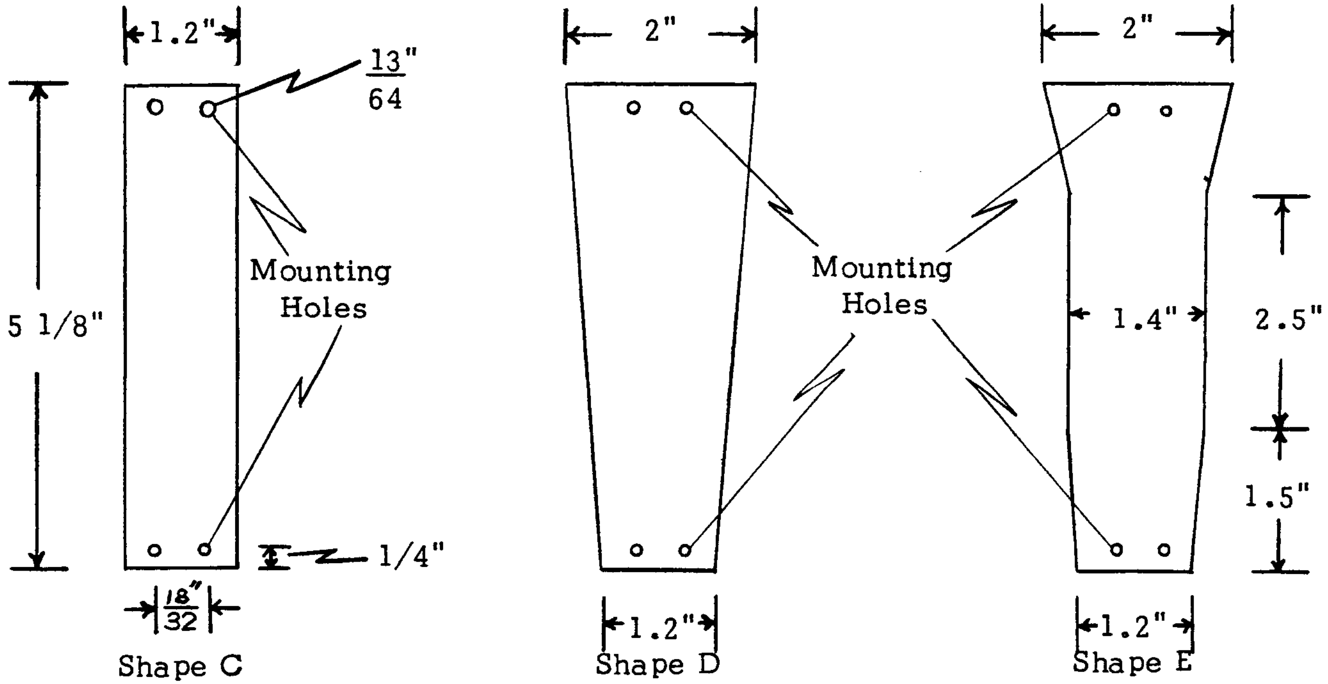

Figure 3. Compliable Structures - Shape C, Shape D, and Shape E Prior to Pre-Test Bending (Scale: 1" = 2").

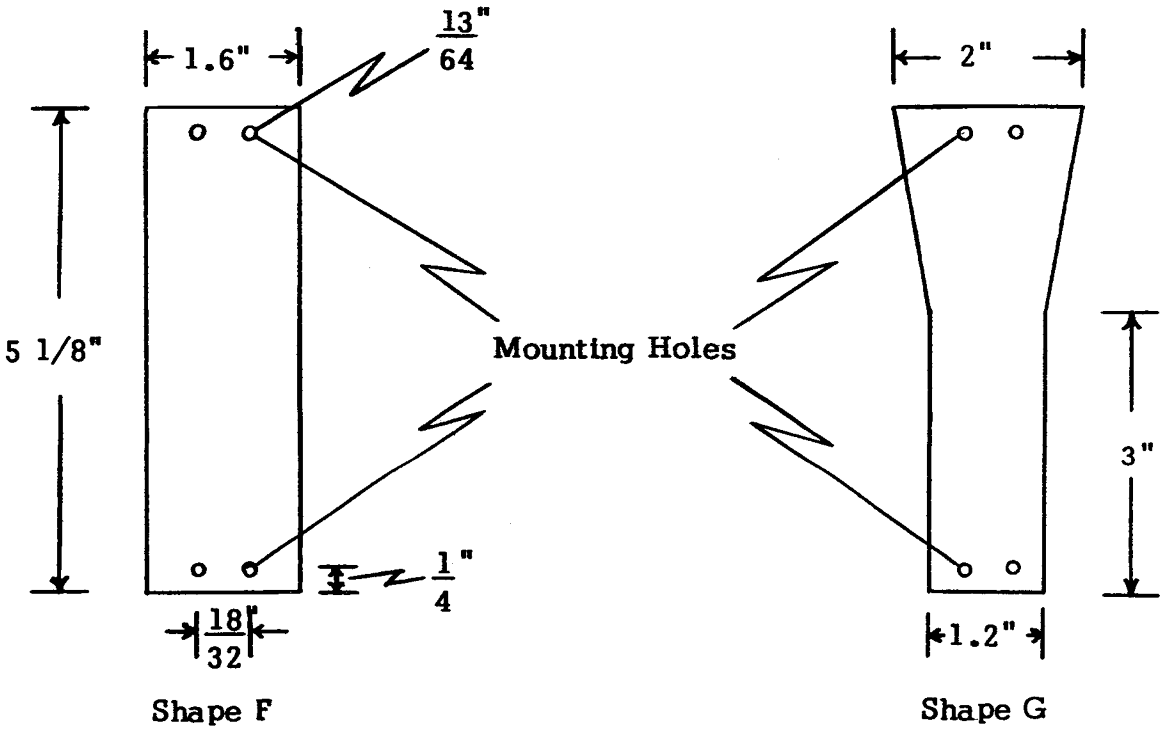

Figure 4. Compliable Structures- Shape F and Shape G Prior to Pre-Test Bending (Scale: 1" = 2").

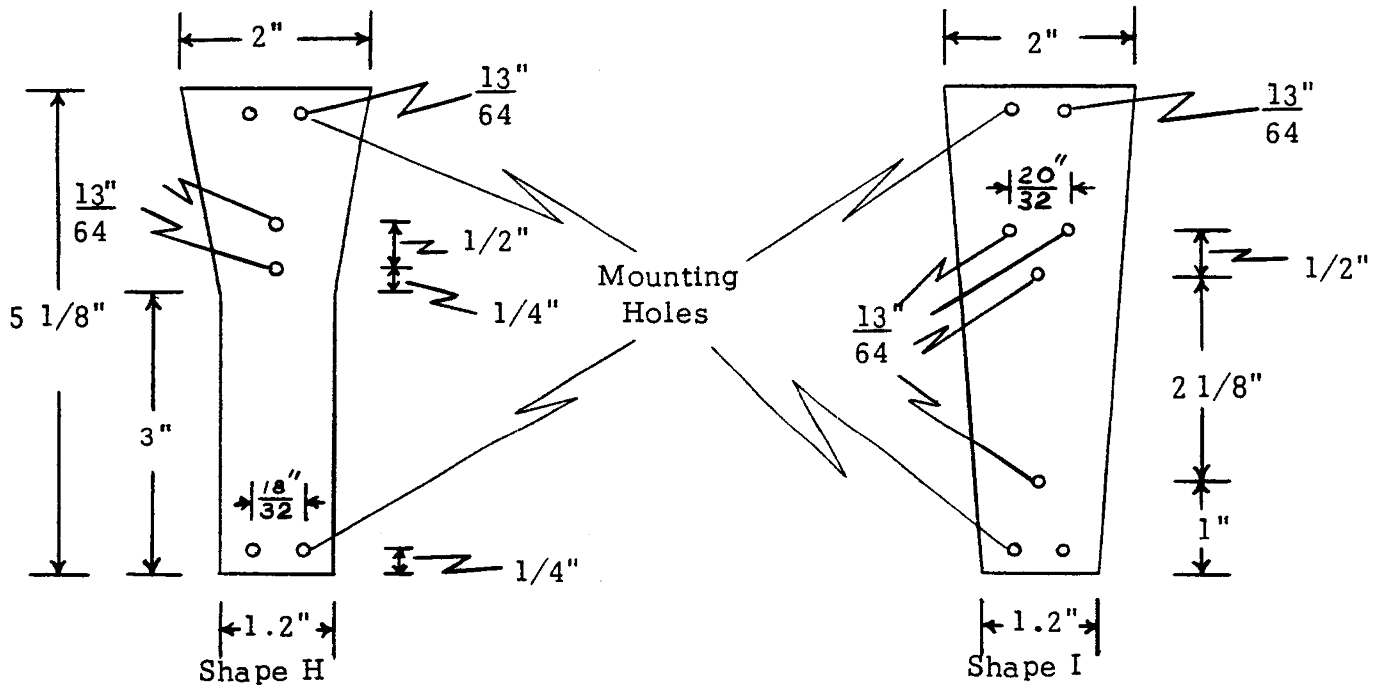

Figure 5. Compliable Structures - Shape H and Shape I Prior to Pre-Test Bending (Scale: 1" = 2").

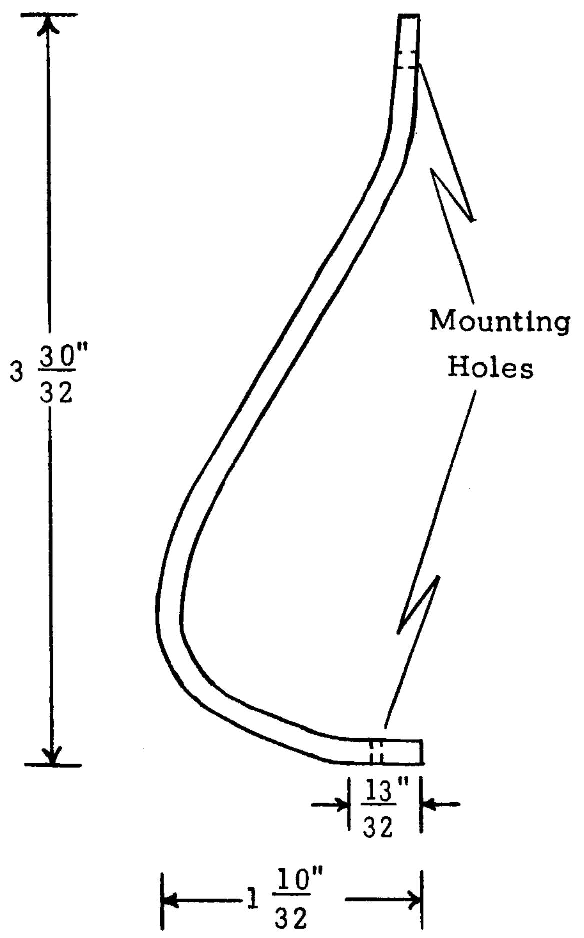

Figure 6. Compliable Structures - Shapes C through I after Pre-Test Bending (Side View, Full Scale).

To determine the energy absorbed by each test unit, the trapezoidal rule was applied to the load-stroke plot for that shape structure. The energy-absorption capacity thus identified was then used to establish conditions to be used during dynamic load tests.

Dynamic tests were conducted using a facility which consisted of a carriage-mounted test mass which was hoisted to a predetermined height and then released so as to impact the test unit with a specific amount of kinetic energy. The carriage, able to accommodate various sizes of test masses, was lifted into drop position by a 4,000-pound capacity electric hoist and electrically released by a 6,000-pound capacity helicopter cargo release. Guide wires were used to control the carriage impact position and to minimize any tumbling tendency of the carriage.

Instrumentation for the dynamic testing consisted of an accelerometer mounted on the test mass and electrically connected to a Tektronix Type 502 Dual-Beam Oscilloscope equipped with a Tektronix C-12 Oscilloscope camera for recording the acceleration pattern through the test stroke.

The dynamic load test conditions were developed in the manner described in Enclosure 1.

Since all the test units demonstrated energy-absorbing capacity through at least 2 inches of stroke during static loading tests, a 2-inch stroke was designated as the desired stroke for all dynamic loading tests. The energy-absorbing capacity of each set of struts as determined during static loading tests, the weight of the test mass to be used, the height of the test unit, and the 2-inch stroke were used to determine the drop height of the carriage for each dynamic test drop. With this drop height known, the predicted acceleration, impact velocity, stroke time, and the trigger lead height above the specimen were computed.

IV. Results and Conclusions

Static loading tests produced the load-stroke relations for each shape tested as shown graphically in Figures 7 through 12. The weight per strut, total energy absorbed, and the corresponding energy-absorption efficiencies obtained from static loading tests for a 2-inch stroke are shown in Table 1.

The load-stroke plots of shapes A and B under static loading were quite similar and were characterized by a low onset rate, a period of relative uniform force, and then a peak force followed by a rapid decrease (Figures 7 and 11). Shapes C through I showed a more rapid onset rate, a short period of uniform force, and then a gradual force decrease (Figures 8 through 10 and Figure 12).

By the standard of energy-absorption efficiencies determined from static loading tests, shapes A and B were inferior to shapes C through I (Table 1) but would be more desirable if a condition of lower onset rate were paramount.

Although shape D absorbed the most total energy during static loading tests (Table 1), the energy-absorption efficiency of Shape I was greater by 4.9 per cent. The load-stroke plots of the two shapes were quite similar and the only difference in the two shapes

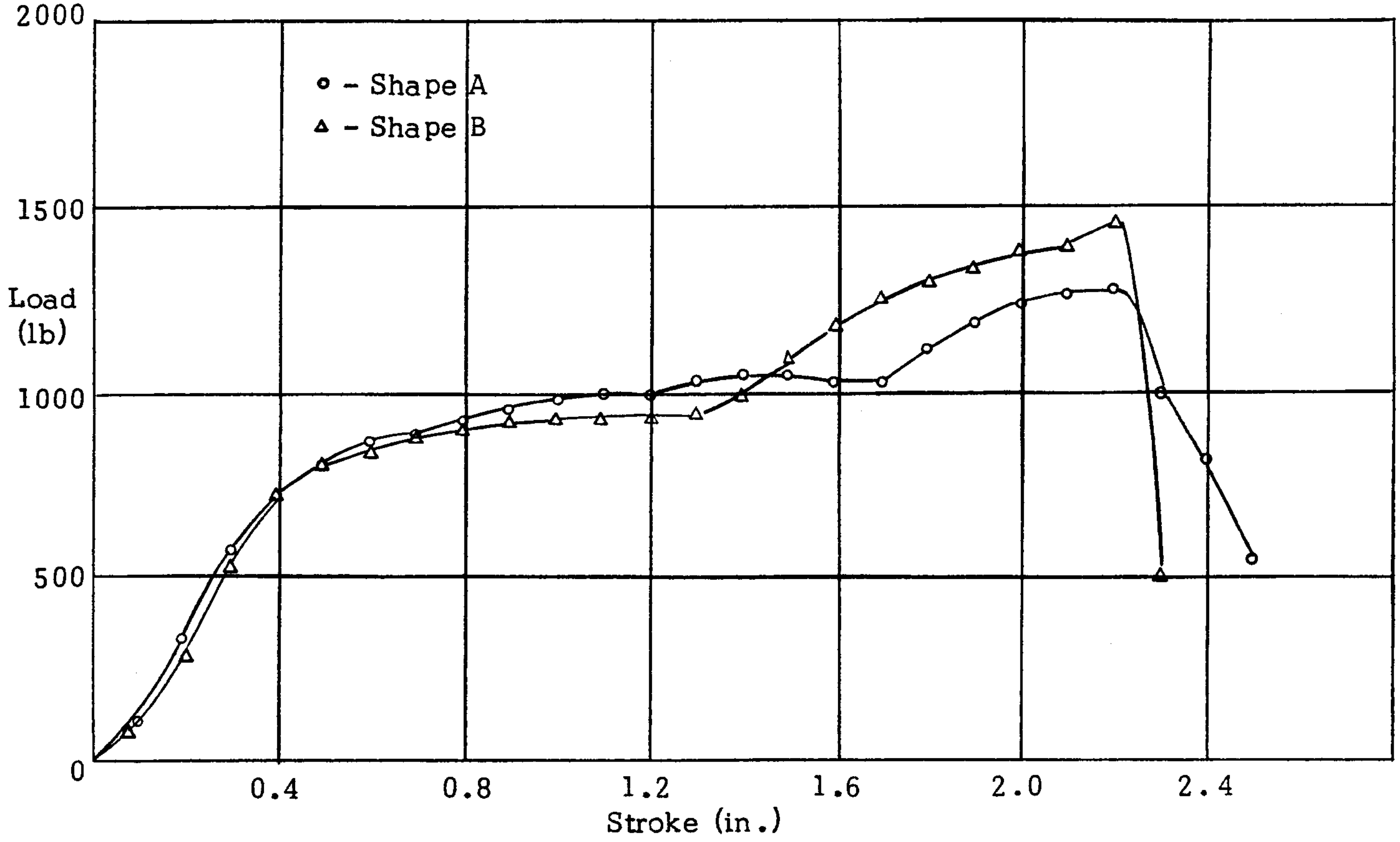

Figure 7. Load-Stroke Plot of Static Loading of Shapes A and B (Al 2024-T3).

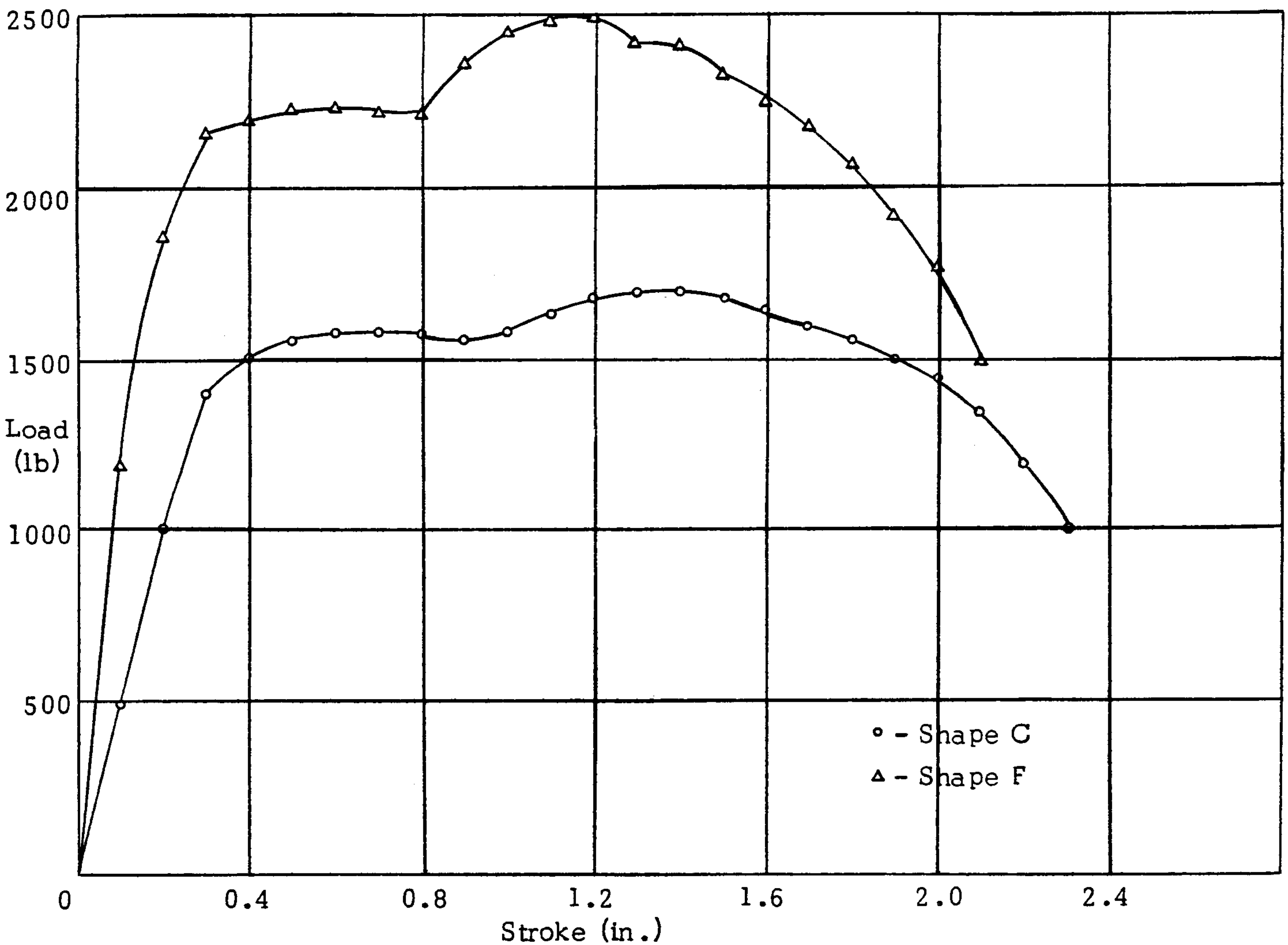

Figure 8. Load-Stroke Plot of Static Loading of Shapes C and F (Al 2024-T3).

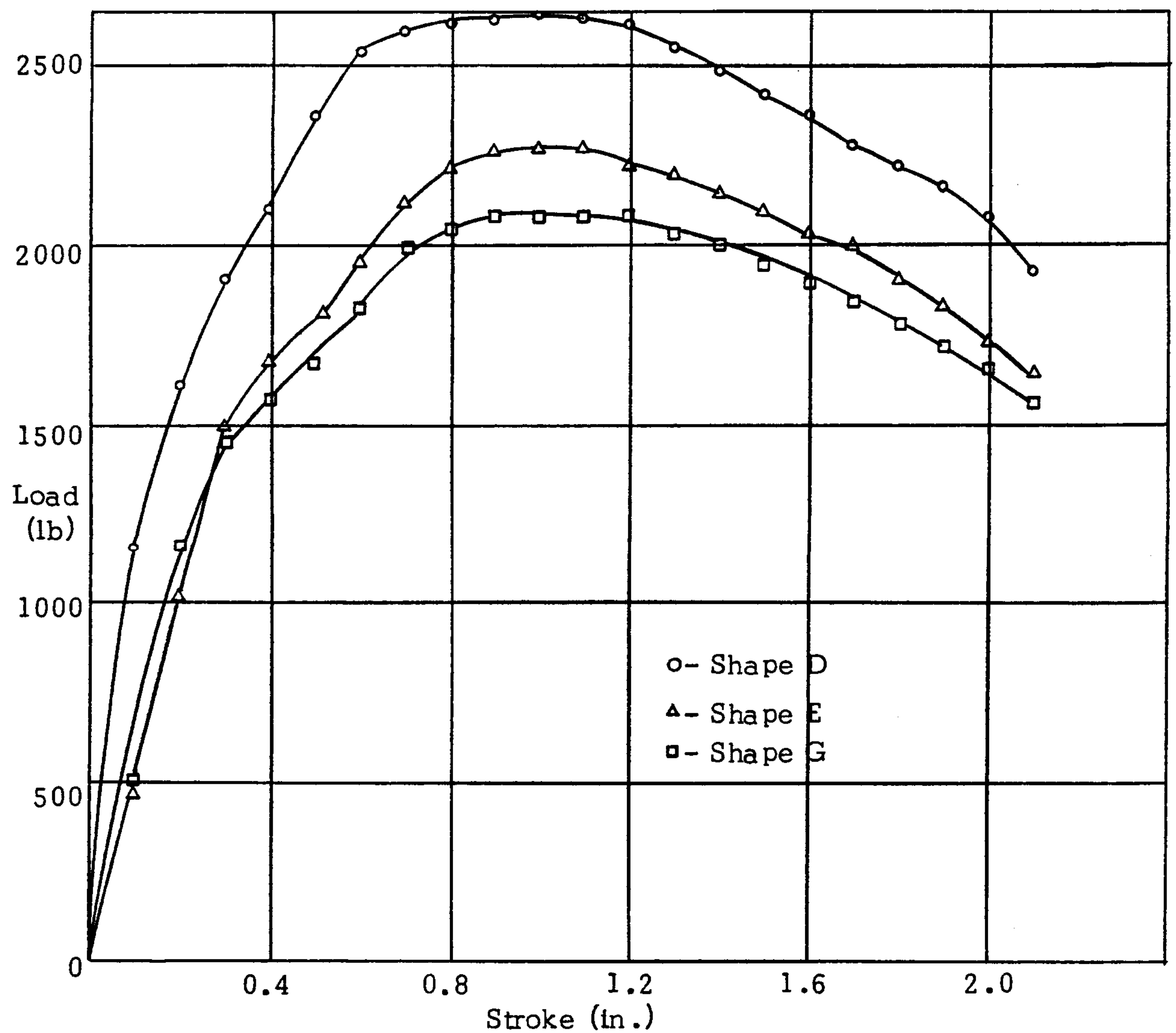

Figure 9. Load-Stroke Plot of Static Loading of Shapes D. E, and G (Al 2024-T3).

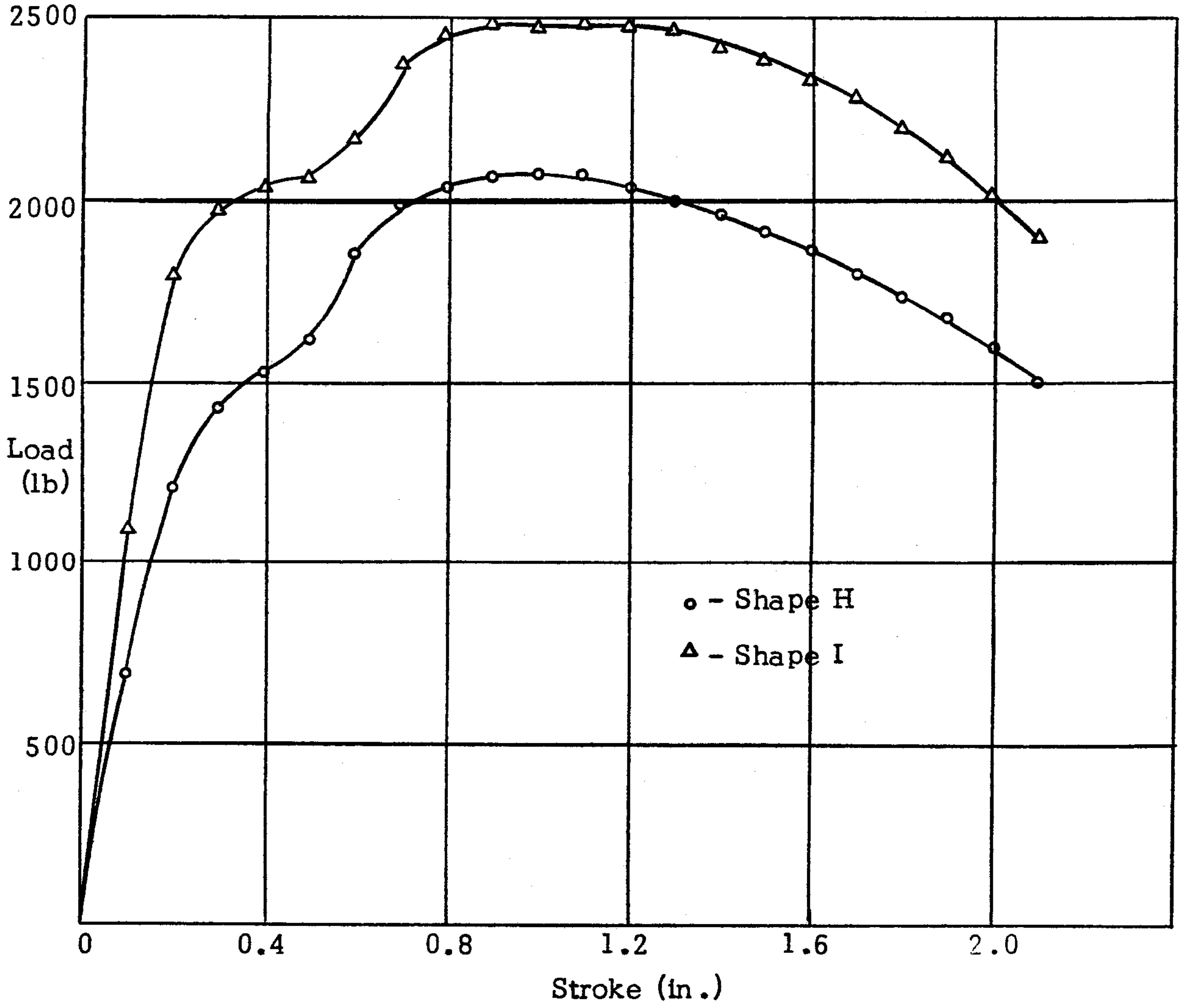

Figure 10. Load-Stroke Plot of Static Loading of Shapes H and I (Al 2024-T3).

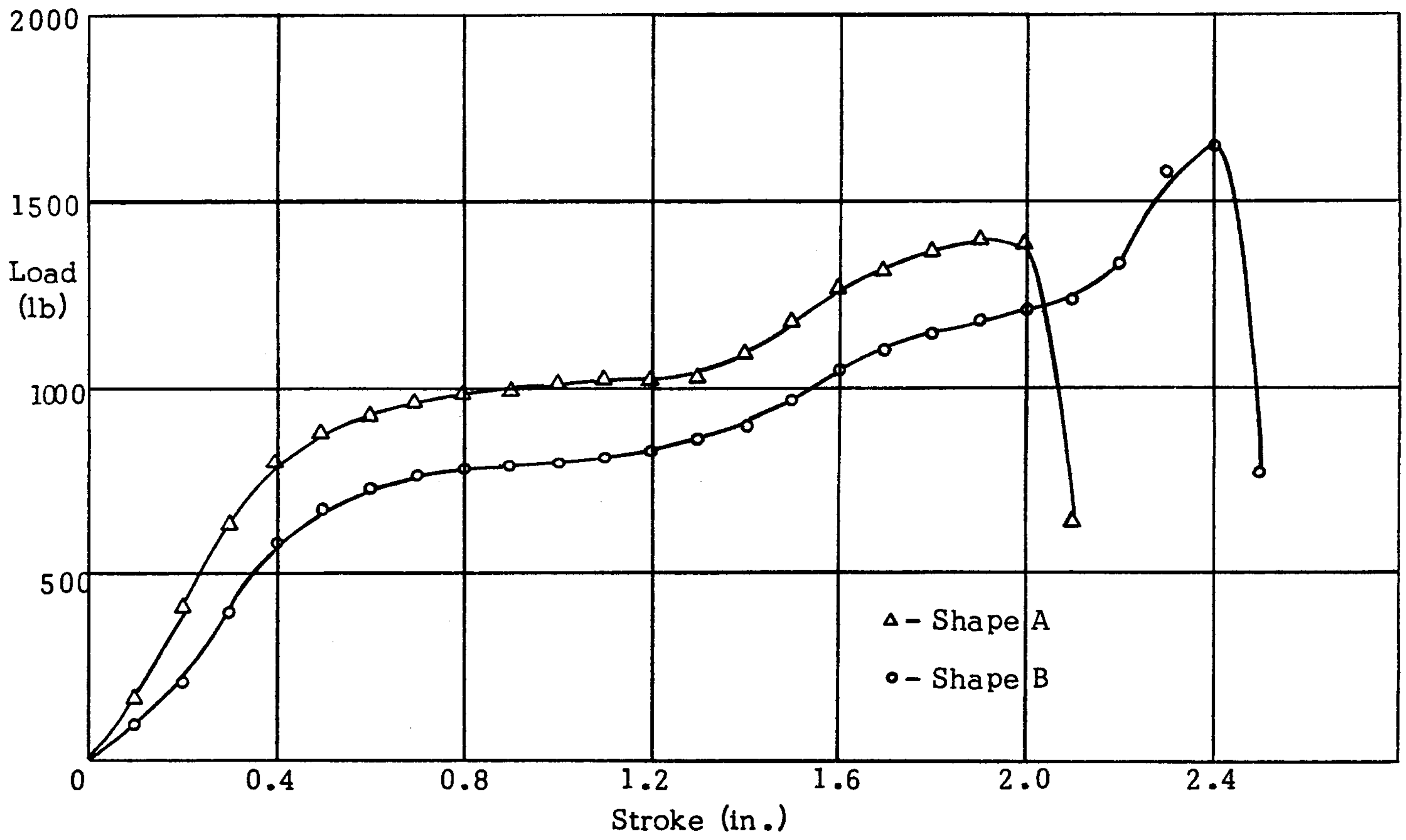

Figure 11. Load-Stroke Plot of Static Loading of Shapes A and B (Al 6061-T6).

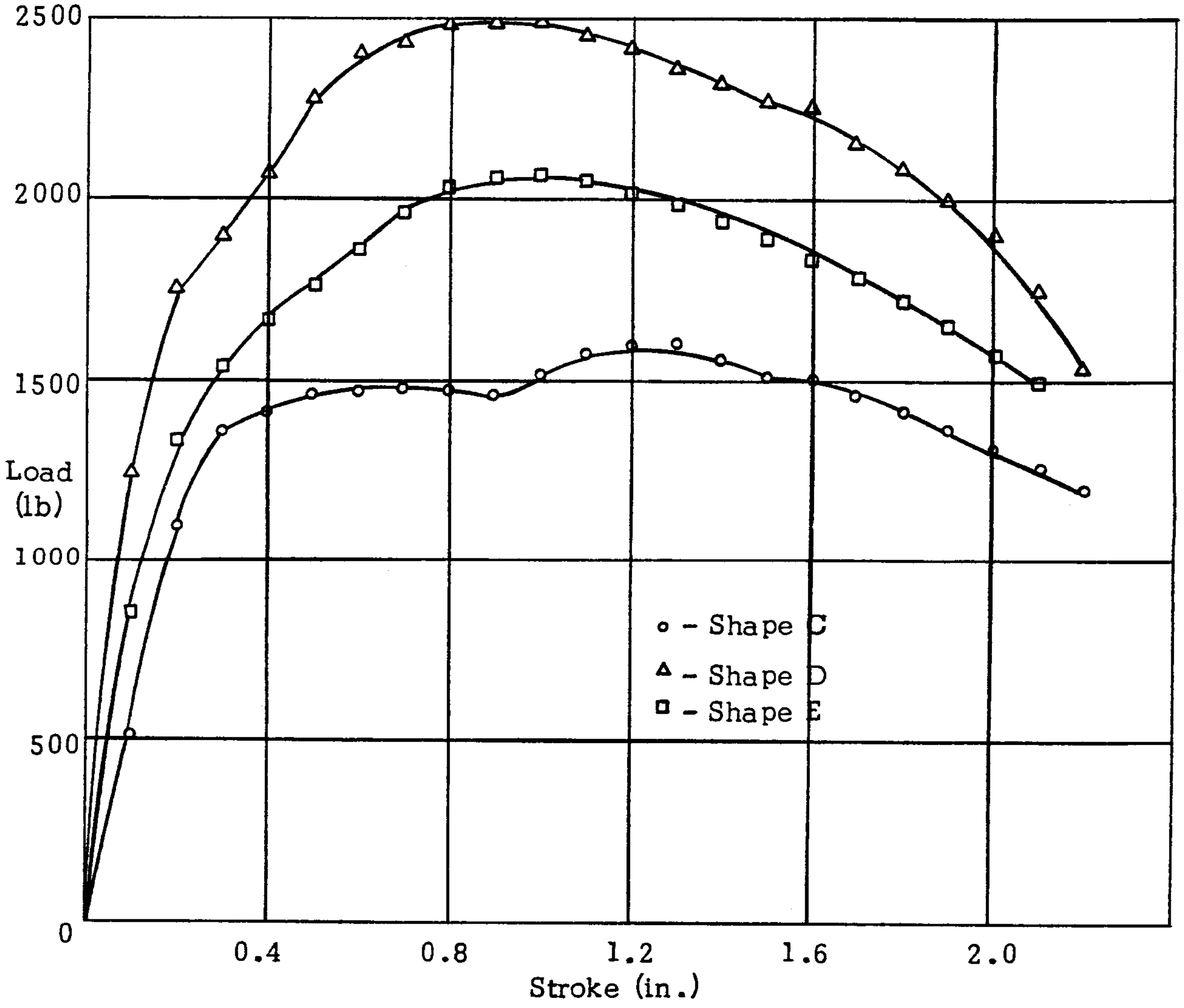

Figure 12. Load-Stroke Plot of Static Loading of Shapes C, D, and E (Al 6061-T6).

Table 1. Experimental Values of Weight per Strut, Total Energy Absorbed, and Energy Absorption Efficiencies Obtained from Static Loading Tests

Shape	Wt. per Strut (lb)	Total Energy Absorbed (in. lb)	Energy Absorption Efficiencies $(\frac{\text{in. lb}}{\text{lb}})$
		(Al 2024-T3)	
A	0.066	1740	6600
B	0.101	1795	8890
C	0.062	2876	11600
D	0.084	4438	13200
E	0.074	3651	12340
F	0.084	4235	12600
G	0.070	3450	12300
H	0.067	3434	12800
I	0.078	4319	13850
		(Al 6061-T6)	
A	0.065	1909	7340
B	0.100	1508	7900
C	0.061	2651	10850
D	0.085	4187	12300
E	0.073	3463	11900

was the perforations located at places in the strut which underwent only a small amount of bending; therefore, it was possible to increase the energy-absorption efficiency while sacrificing only a small amount of total energy absorbed. Shapes G and H demonstrated the same quality, wherein the perforations increased the energy-absorption efficiency by 4.06 per cent.

The dynamic loading tests of the same shape struts were then conducted.

The actual values of peak accelerations could not be calculated because of the effects of the shock wave in the centerpost, which appeared in the photographs at the beginning of the strike. However, estimates of these peaks agreed favorably with predicted peak accelerations.

In all cases the dynamic tests showed a more uniform acceleration through the stroke than was predicted from static tests. Actual stroke distances agreed favorably with those predicted with a maximum difference of 6.5 per cent. Predicted average accelerations agreed with actual accelerations within 9.4 per cent. In general, the actual stroke distances were shorter and the actual average accelerations were greater during dynamic tests than were predicted from static loading tests. Actual values of stroke, average acceleration, and per cent difference of each from predicted are shown in Table 2.

The similarity between predicted and actual conditions suggests that static load testing could be used to advantage in any investigation of the energy-absorbing characteristics of such compliable

Table 2. Experimental Values from Dynamic Tests of Stroke, Average Acceleration, Per Cent Difference from Predicted Stroke, and Per Cent Difference from Predicted Average Acceleration

Shape	Stroke (in.)	Per Cent Difference from Predicted Stroke (%)	Average Acceleration (g)	Per Cent Difference from Predicted Average Acceleration (%)
		(Al 2024-T3)		
A	1.92	-4.0	-7.3	4.6
B	2.0	0	-6.4	7.8
C	1.89	-5.5	-10.1	8.6
D	1.91	-4.5	-16.4	1.82
E	1.93	-3.5	-5.8	2.8
F	1.9	-5.0	-14.4	-6.25
G	1.87	-6.5	-11.2	-9.4
H	1.95	-2.5	-12.3	1.63
I	2.05	2.5	-13.4	-6.1
		(Al 6061-T6)		
A	1.9	-5.0	-6.55	3.05
B	1.96	-2.0	-6.1	6.3
C	1.91	-4.5	-9.8	7.3
D	1.9	-5.0	-15.3	1.31
E	1.95	-2.5	-5.33	2.4

structures. Testing time and cost could be greatly reduced in any such large-scale testing program by selecting for dynamic testing only those structures which demonstrate the best energy-absorbing characteristics during static load tests. Dynamic tests would then be performed on the most promising structures in order to determine actual conditions.

LITERATURE CITED

1. Coppa, A. P., Collapsible Shell Structures for Lunar Landings, Space Sciences Laboratory, General Electric Corp., Philadelphia, Pa., February, 1962.

2. Hoffman, Edward L., Stubbs, Sandy M., and McGehee, John R., Effect of a Load-Alleviating Structure on the Landing Behavior of a Reentry-Capsule Model, National Aeronautics and Space Administration, Washington, D. C., May, 1961.

3. Fisher, Lloyd F., Jr., Landing Energy Dissipation for Manned Reentry Vehicles, National Aeronautics and Space Administration, Washington, D. C., September, 1960.

4. Morgan, Carl W., Moore, Walter L., Theoretical and Experimental Investigations of Fluid-Filled Metal Cylinders for Use as Energy Absorbers on Impact, The University of Texas Structural Mechanics Research Laboratory, Austin, Texas, December, 1956.

(See the February, 1964 Progress Report for a complete bibliography)

AN EXPERIMENTAL INVESTIGATION
OF ALUMINUM HONEYCOMB AS AN ENERGY ABSORBER *

by

WILLIAM J. BLAND

Aerospace Engineering Department and Space Technology Division

Texas A&M University

* The material presented here was extracted from a thesis having the above title which was submitted by the author in partial fulfullment of the requiremnts for the degree of Master of Science in Aerospace Engineering at Texas A&M University.

Enclosure 3

LIST OF SYMBOLS

a	Acceleration
F	Force
g	Acceleration due to gravity
G	a/g
KE	Kinetic energy
m	Mass
s	stroke
V_I	Impact velocity

I. Introduction

In 1954, the Structural Mechanics Research Laboratory of the University of Texas (1)* conducted an investigation of the air-drop energy-absorption problem using paper honeycomb. It was concluded that deformation of higher strength materials, although more costly, would be more suitable for energy absorption. Since weight is always at a premium for space vehicles, a system that exhibits high energy capacity per pound of device is desirable. Aluminum honeycomb has this characteristic when crushed parallel to the cell walls.

Hexel Products, Inc. (2) of Berkeley, California, has found that aluminum honeycomb exhibits a relatively uniform load level during deformation with no appreciable rebound. The material is usuable to within 75 per cent of its depth. A major disadvantage of this type material is the steep slope of the force-displacement curve (see Figures 1-4), which induces high deceleration-onset rate during dynamic deformation. It has been suggested that to reduce high onset rate, one may precrush the material past the yield point to initiate accordion-like folding of the cell walls. Another method is to shape the material in the form of a cone so that a smaller force is required to initiate crushing.

---

*Numbers in parentheses refer to references listed numerically under Literature Cited.

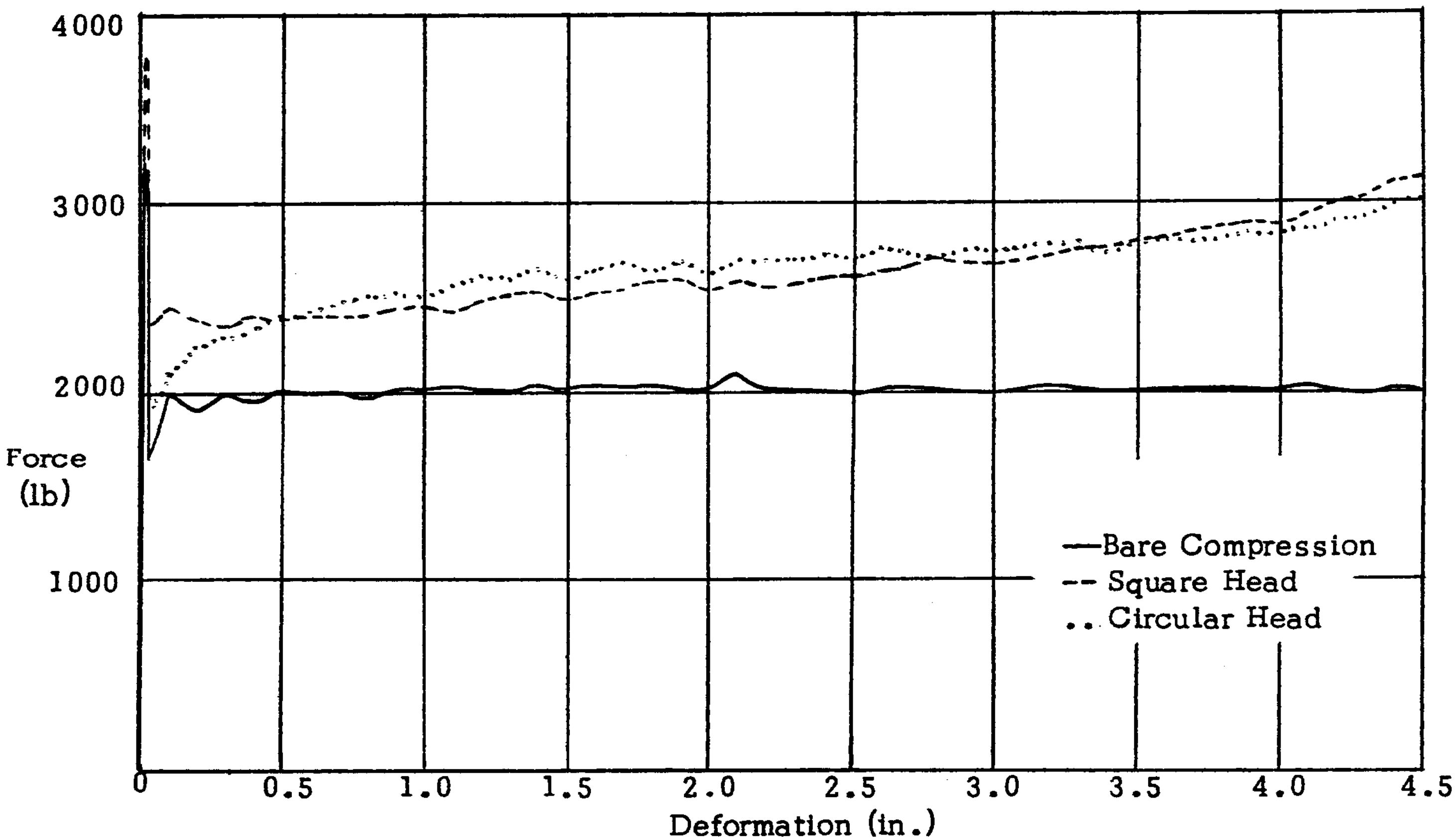

Figure 1. Static Test, 6 in. thickness x 4 in.^{2} Area.

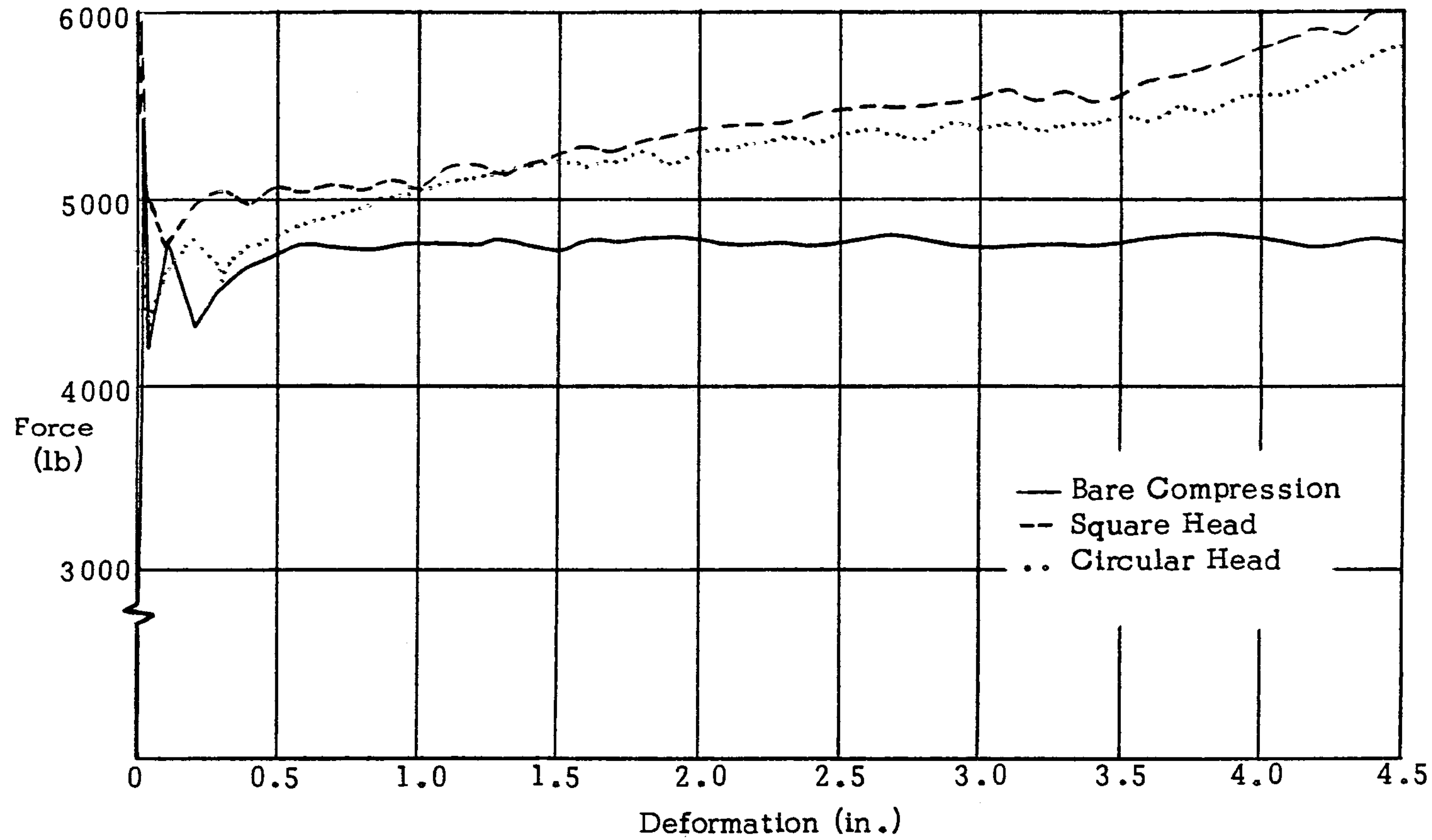

Figure 2. Static Test, 6 in. thickness x 9 in.^{2} area.

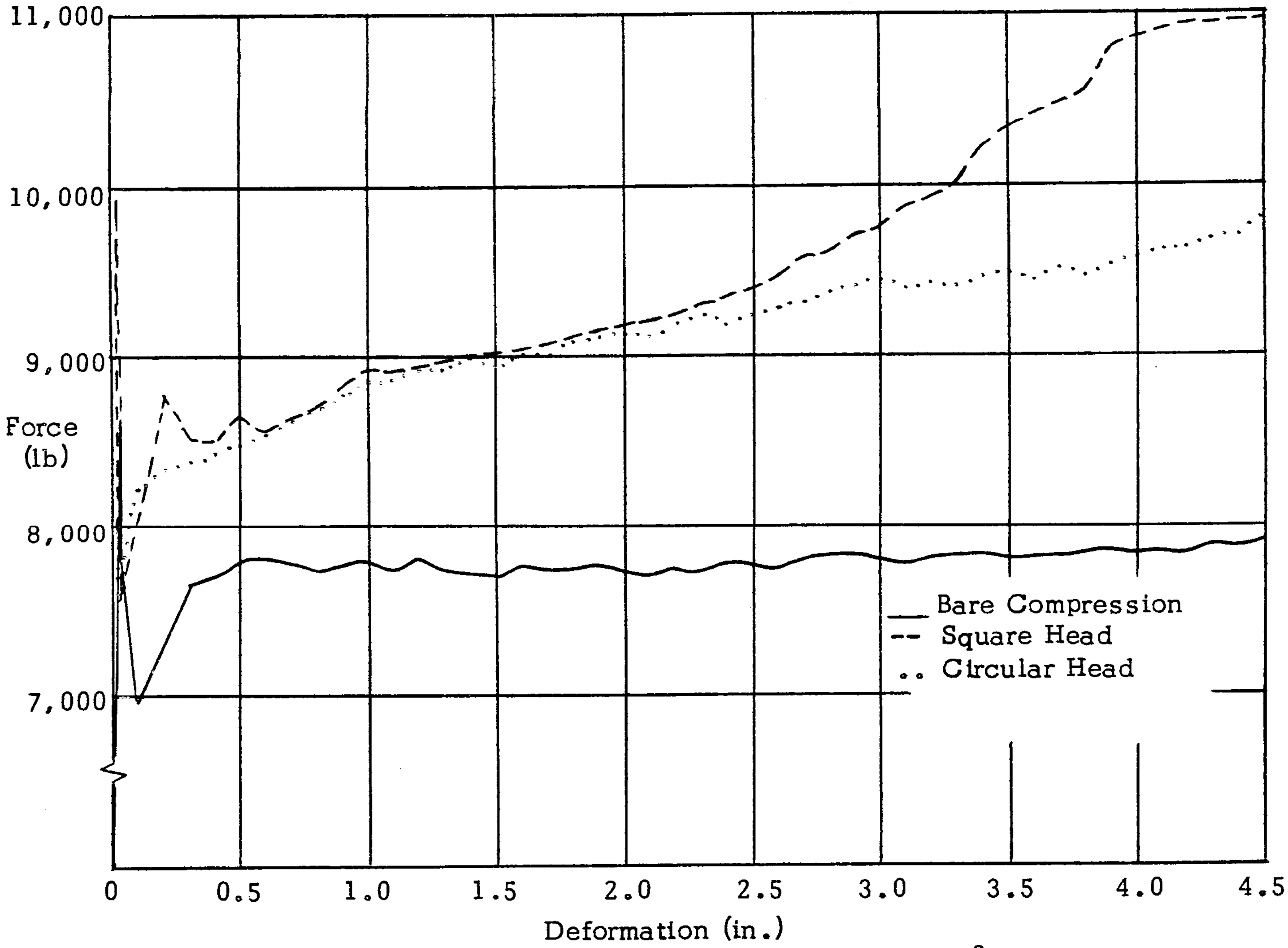

Figure 3. Static Test, 6 in. thickness x 16 in.^{2} area.

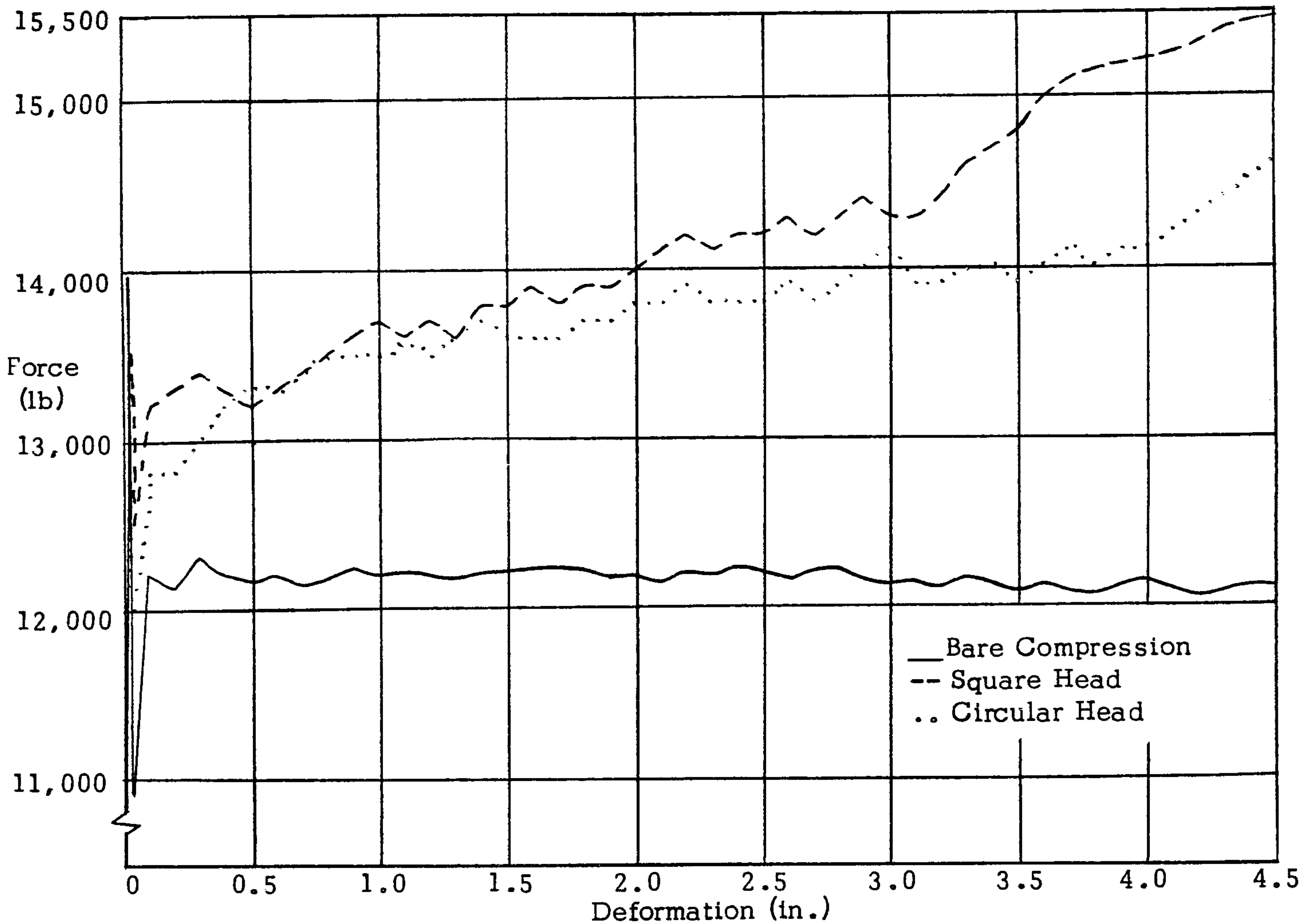

Figure 4. Static Test, 6 in. thickness x 25 in.^{2} area.

The use of aluminum honeycomb as an energy absorber has been limited to the compression of the entire area of the material under impact. An examination of the literature indicated that no work has been done to determine the effect on load level caused by the shearing of the cell walls during the crushing stroke by using an area in compression smaller than that of the specimen.

This investigation has a practical application for use on the shock-absorption system in the astronauts' couch of a vehicle such as the Apollo spacecraft. Since there is the possibility of a reduced number of occupants of the couch returning for an earth landing, there must be a capability of varying the amount of energy absorption desired for landing. By determing the effect on load level due to shearing of the cell walls, one may establish a predetermined area of material for the maximum load as well as the required area for a reduced load. The depth of the material will be determined by the acceleration loading computed for impact.

The material tested was 5052 aluminum honeycomb, 0.125-inch cell size, 0.0015-inch wall thickness.

II. Objectives

This investigation was conducted to determine experimentally the effect of variable geometry head loading on aluminum honeycomb core using a smaller area under compression than the entire specimen. It was the primary objective to determine what percentage of the crushing load was carried by the shear of the cell walls.

Since the guaranteed crush strength of the material is no closer than ± 20 per cent (3), it was necessary to establish the crush strength of the particular material through static testing. The results of the bare compression tests formed a basis to determine the primary objective.

Dynamic tests were also performed, using specimens similar to those of the static tests, since the capability of a material to absorb impact energy can best be evaluated from the dynamic crushing characteristics for that material (4). A secondary objective, therefore, was to prove the acceptability of static test results for dynamic testing.

III. Static Testing

A block of 5052 aluminum honeycomb with 0.125-inch cell seze and 0.0015-inch wall thickness was measured and weighed to determine the nominal density of 6.18 pounds per cubic foot. The thickness of the core for all specimens was 6 inches.

Specimens of 4, 9, 16, and 25 square inches in area were cut from the honeycomb block using a band saw. Exact dimensions were not obtained by this method. Since weight varied only with area, the density and thickness being constant, each specimen was weighed and the deviation from the precomputed weight per specimen noted. Bare compression test results were then scaled according to the deviation from the correct computed weight for that particular specimen.

Static tests were performed in a Baldwin Universal Testing Machine with a 60,000-pound capacity. Aluminum plates were placed on the top and bottom of each bare compression test specimen and a head travel of less than 0.5 inch per minute was used throughout the crushing stroke. Three specimens of each selected area were tested and data recorded at yield point and every 0.1 inch thereafter.

Square and circular heads, equal in area to that of the bare compression test specimens, were cut from 0.5-inch thick 1024 T4 aluminum plate. The equations used to determine the circular head diameter, which would give an area equal to that of the square head, are as follows:

$$A = \frac{\pi D^2}{4}$$

$$D^2 = \frac{4A}{\pi}$$

$$D = s\,\frac{4A}{\pi}$$

where A = area of square head

D = diameter of circular head

With this equation, the following areas and diameters were computed for the circular heads:

A_1 = 4 square inches $\quad$ D_1 = 2.257 inches

A_2 = 9 square inches $\quad$ D_2 = 3.385 inches

A_3 = 16 square inches D_3 = 4.512 inches

A_4 = 25 square inches D_4 = 5.641 inches

The square heads were sanded and the circular heads turned in a lathe to a tolerance of $\pm$ 0.002 inch.

Honeycomb block specimens, larger than the crushing head area, were placed on an aluminum plate in the testing machine. The square and circular heads were attached to a circular steel shaft 7 inches in length and 1.5 inches in diameter. The steel shaft was then driven through the honeycomb block producing both shear and compression in the specimen. Data were recorded at yield point and every 0.1 inch thereafter.

Several tests were conducted using the same head and these results were identical.

IV. Dynamic Testing

A limited number of dynamic tests were performed to determine the relationship between static and dynamic forces. These tests were accomplished in the guided drop-test facility which was designed and constructed in the Aerospace Structural Research Laboratory at Texas A&M University.

The equations used to calculate data for the dynamic tests were the same as in Enclosure 1.

The maximum and average accelerations were calculated from static test data using the compressive yield strength and average crushing force, respectively, for each specimen. Average crushing force for the square and circular head tests was determined using the trapezoidal rule for integration of the curves in Figures 1 through 4 and dividing by the stroke distance.

Specimens used in these tests were 6 inches in thickness as in the static tests. A crushing stroke of 4.5 inches was used to obtain maximum material deformation. A special steel shaft was made to attach to the bottom of the drop carriage. The square and circular heads were fixed to the shaft for the shearing portions of the dynamic tests.

The drop-test facility was designed to free-fall a known weight from a given distance which would impact on a stationary specimen. The lead weights on the drop carriage were varied according to the size of the specimen being tested. The variation in drop height resulted in impact velocities to from 18 to 30 feet per second.

An accelerometer was mounted on the top lead weight of the carriage to supply input voltage to a Tektronix Type 502 dual beam oscilloscope. Pictures were taken of the trace, which displayed acceleration versus time.

V. Results

Static Tests

The energy-absorbing capacity of aluminum honeycomb in bare compression is in direct proportion to the thickness and area of the honeycomb under load. Consequently, onee the average crushing stress for the material is established, the energy-absorbing capacity for the bare material varies linearly with the thickness as shown in Figures 5 through 8. The average crushing stress for 5052 aluminum honeycomb, 0.125-inch cell size, 0.0015-inch wall thickness, with a nominal density of 6.18 pounds per cubic foot, was 490 pounds per square inch.

When the effect of shearing of the cell walls by the square and circular heads was taken into account, an increase in compressive load of from 11 to 14 per cent was noted. The per cent increase varied with the depth of the crushing stroke.

Shear along the ribbon direction produced a clean break with the cell walls, but the heads tended to grab the material in the transverse direction and gather more material as the stroke increased. This effect accounts for the larger per cent increase in load toward the end of the crushing stroke.

The square heads produces a larger increase in load than the circular heads because of the greater length in contact with the transverse direction of the honeycomb. The perimeter of the variable geometry heads did not increase proportionally with the area, which resulted in a non-linear increase in the energy-absorbing capacity for each increase in head area. (See Figures 5 through 8.) The average force up to the point of deformation was used to plot the curves for the square and circular heads.

Dynamic Tests

Dynamic tests in the guided drop-test facility showed the average crushing stress of a static test to be indicative of

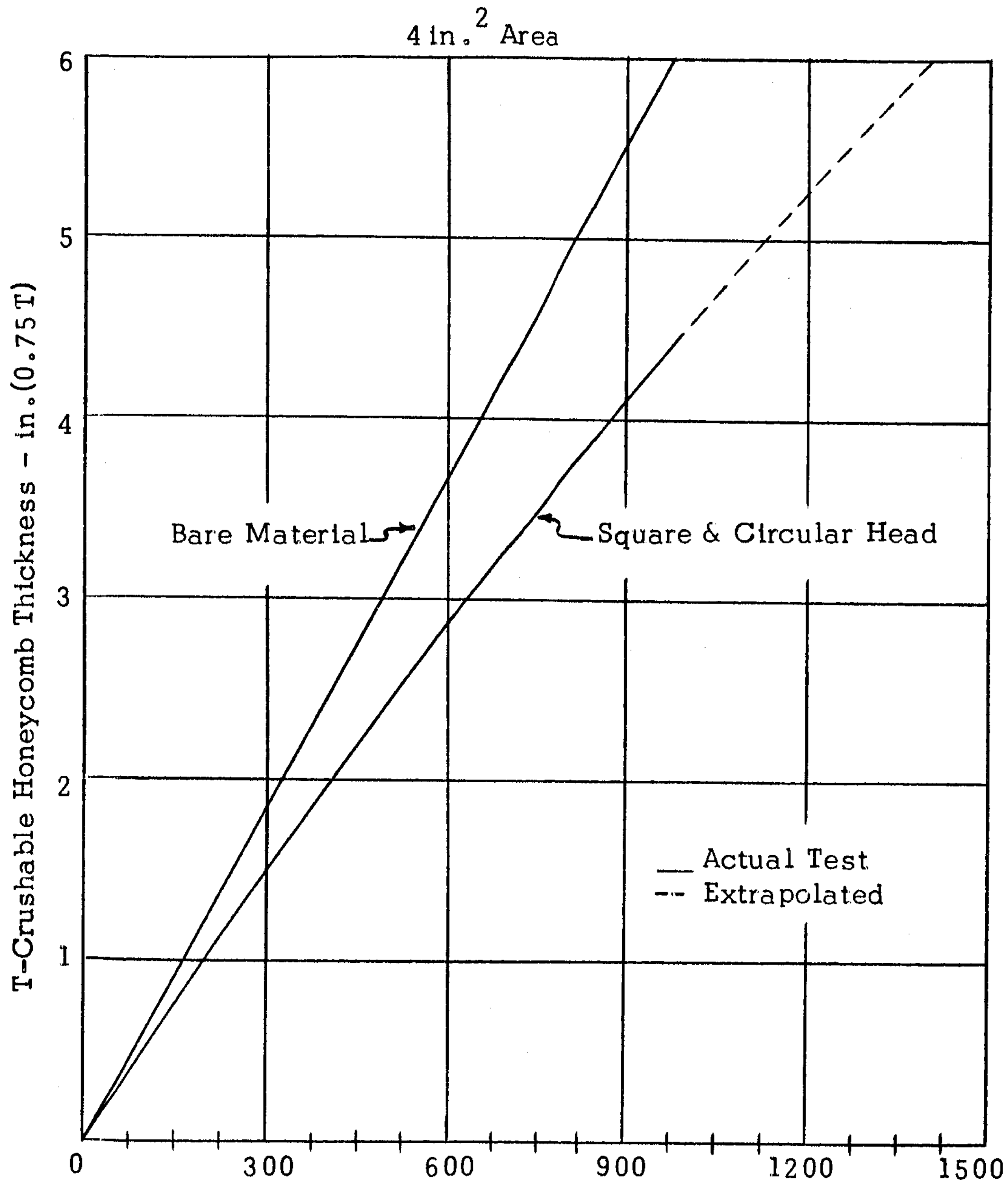

Figure 5. Energy-Absorbing Capacity, ft lbs

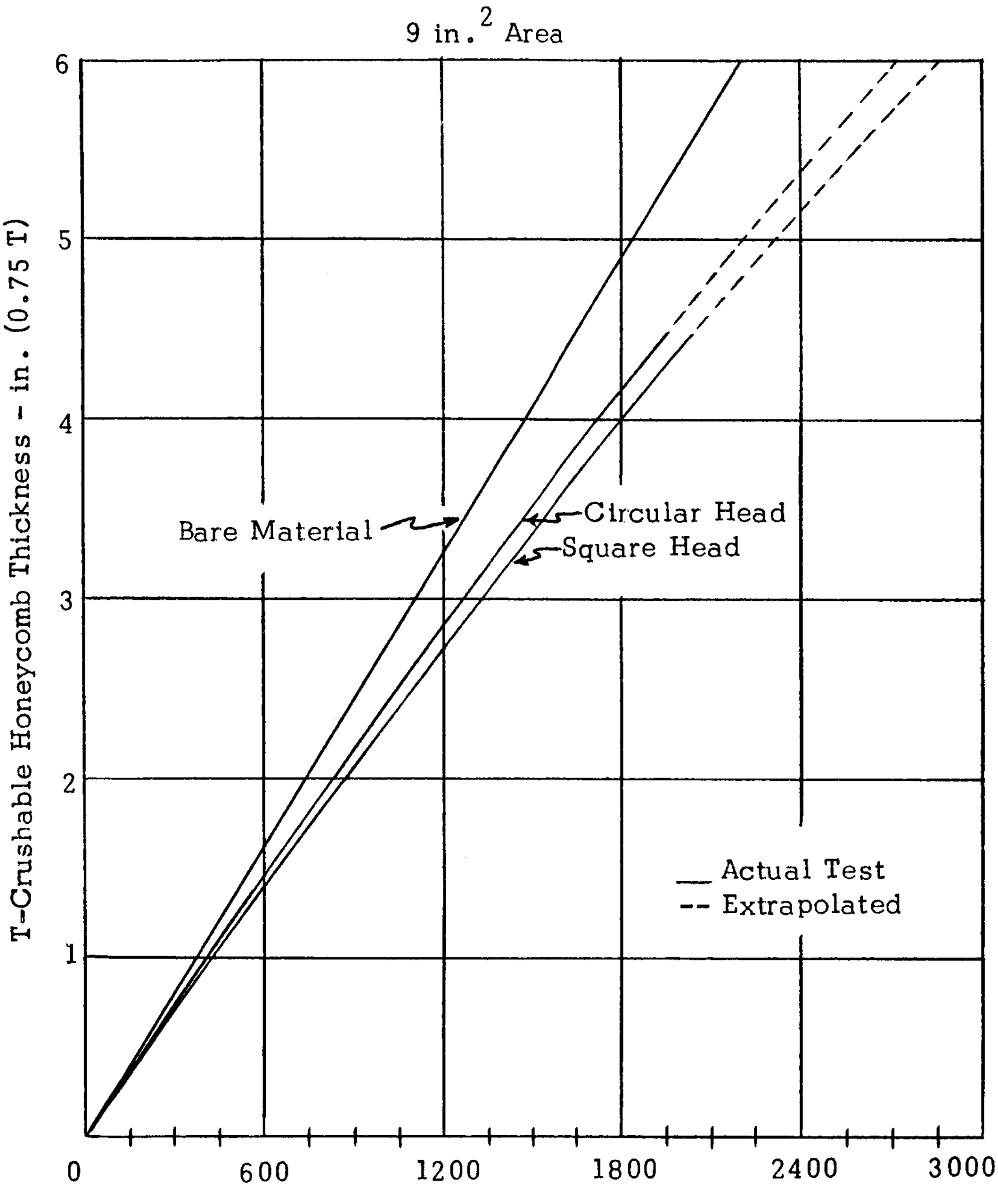

Figure 6. Energy-Absorbing Capacity, ft lbs

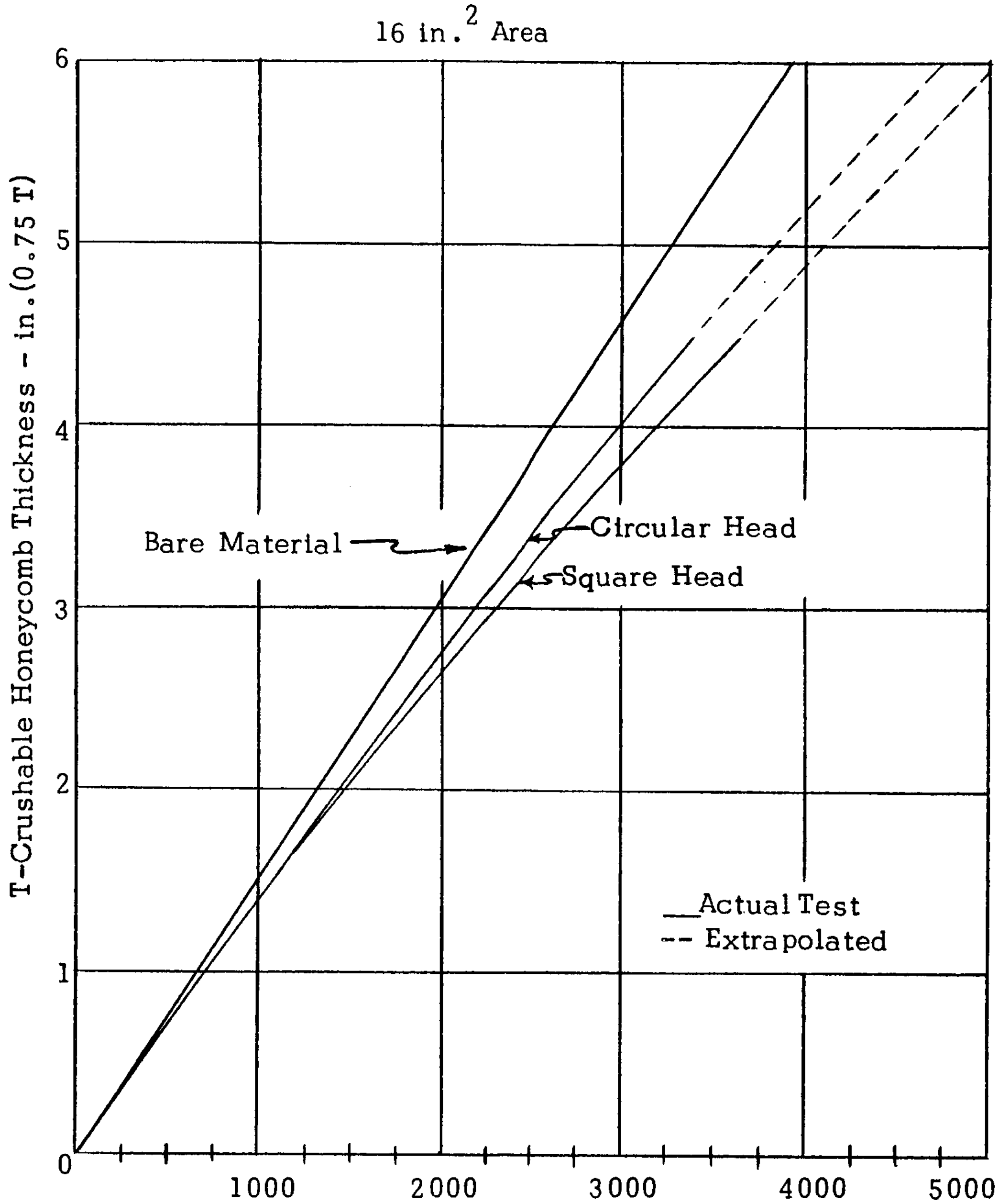

Figure 7. Energy-Absorbing Capacity, ft lbs

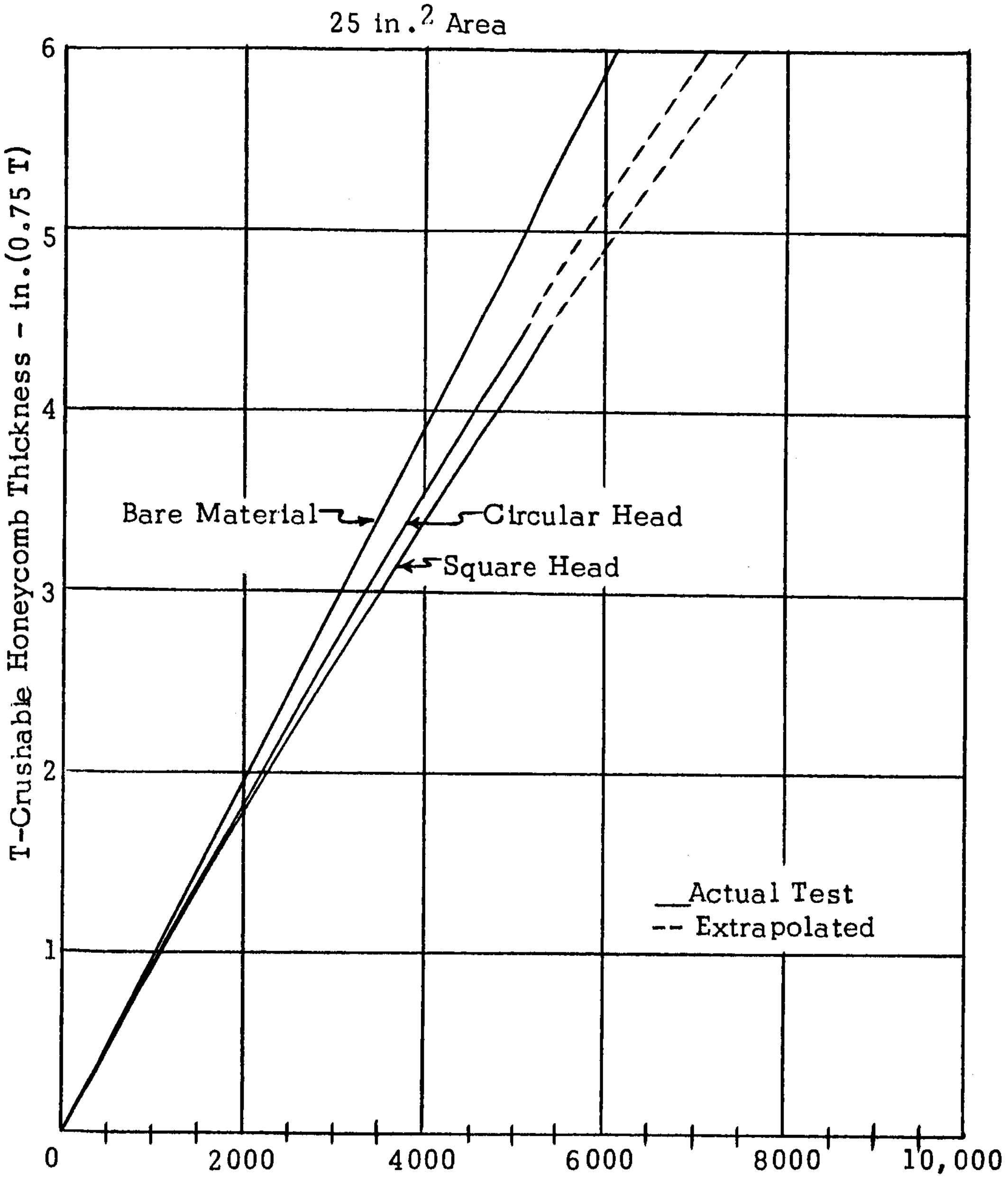

Figure 8. Energy-Absorbing Capacity, ft lbs

the average stress during a dynamic impact. Using impact velocities of from 18 to 30 feet per second, the maximum variation in crushing stroke was 0.1 inch. No rebound was detected visually during the tests.

VI. Application

The practical application of this investigation can best be illustrated by an example. The energy attenuation problem of the Apollo spacecraft returning for earth landing will be used. The couch support system is a separate system in itself and hence constitutes the energy-absorption problem.

The following assumptions are made for the purpose of calculating the amount of aluminum honeycomb required:

Weight of each astronaut	250 lbs.
Weight of couch	100 lbs.
Velocity at impact	20 ft. per sec.
Maximum G $\left(\frac{a}{g}\right)$	20

With three astronauts aboard, the kinetic energy at impact is:

$$KE = \frac{1}{2} mV_I^2$$

$$KE = \frac{1}{2} \frac{850}{32.2} (20)^2$$

$$KE = 5{,}280 \text{ ft lb}$$

Using a maximum G of 20, the minimum stroke distance is:

$$s = \frac{V_I^2}{2a}$$

$$s = \frac{20^2}{2(20)(32.2)}$$

$$s = 0.31 \text{ ft} = 3.72 \text{ in.}$$

Referring to Figure 8 and by using an area of 25 square inches of bare material, 5,280 foot pounds of kinetic energy can be dissipated with a stroke of 5.2 inches. This would result in an average G loading of:

$$G = \frac{V_I^2}{2sg}$$

$$G = \frac{(20)^2}{2(0.442)(32.2)}$$

$$G = 14.1$$

Since only 75 per cent of the honeycomb is usable for energy absorption, the total thickness of material required is 5.2(1.33) = 6.9 inches.

If only two astronauts return for landing, the total kinetic energy is:

$$KE = \frac{1}{2} mV_I^2$$

$$KE = \frac{1}{2} \frac{600}{32.2} (20)^2$$

$$KE = 3{,}730 \text{ ft lb}$$

Referring to Figure 7, this amount of energy can be absorbe. by using a circular head of 16 square inches in area through a stroke of 4.9 inched. The average G for the two astronauts would be

$$G = \frac{(20)^2}{2(0.408)(32.2)}$$

$$G = 15.2$$

If only one astronaut remains for earth landing, the total kinetic energy is:

$$KE = \frac{1}{2} mV_I^2$$

$$KE = \frac{1}{2} \frac{350}{32.2} (20)^2$$

$$\therefore KE = 2{,}170 \text{ ft lb}$$

Referring to Figure 6, this amount of energy can be absorbed using a circular head of 9 square inches in area through a stroke of 5.0 inches. The average G for this astronaut would be:

$$G = \frac{(20)^2}{2(0.407)(32.2)}$$

$$G = 15.3$$

Thus, it can be seen that this typical energy-absorption problem can be solved by using a piece of 5052 aluminum honeycomb 6.9 inches thick and 25 square inches in area. The acceleration for each case is well within the maximum. Three circular heads could be designed, the smaller heads fitted inside the larger, and by means of a keyway and cable, the appropriate head would be selected depending on the number of occupants.

VII. Conclusions and Recommendations

The data and conclusions in this experiment are valid only if the crushing takes place approximately parallel to the longitudinal cell axis. Up to 75 per cent of the original thickness of the material is usable for energy absorption. Nearly constant load levels are maintained during the crushing stroke and no appreciable rebound is encountered. Square heads have a less uniform increase in crushing stress than do circular heads because of gathering of the material along the transverse direction.

It is recommended that similar tests be conducted on aluminum honeycomb with different wall thicknesses to determine the variation in shear effect. Also, specimens of larger depth than 6 inches should be tested to determine the per cent increase in crushing stress after more material has been extracted from the cell sides by the shearing head.

Table I. Dynamic Test Data

Test	Predicted Deformation (in.)	Actual Deformation (in.)	Deviation (%)	Predicted Acceleration (g)	Actual Acceleration (g)	Deviation (%)
4 $in.^2$ Bare	4.5	4.45	1.11	14.9	14.0	6.0
9 $in.^2$ Bare	4.5	4.60	2.22	14.6	13.6	6.9
16 $in.^2$ Bare	4.5	4.50	0	27.3	24.6	10.0
25 $in.^2$ Bare	4.5	4.42	1.78	36.6	32.2	12.0
4 $in.^2$ Square Head	4.5	4.40	2.22	18.5	17.9	3.2
9 $in.^2$ Square Head	4.5	4.55	1.11	16.6	14.9	10.2
16 $in.^2$ Square Head	4.5	4.50	0	30.0	28.4	5.35
25 $in.^2$ Square Head	4.5	4.42	1.78	34.7	32.8	5.5
4 $in.^2$ Circular Head	4.5	4.4	2.22	18.5	16.4	11.5
9 $in.^2$ Circular Head	4.5	4.48	0.45	16.6	15.5	6.65
16 $in.^2$ Circular Head	4.5	4.4	2.22	29.8	26.4	11.4
25 $in.^2$ Circular Head	4.5	4.46	0.89	33.6	32.0	4.75

LITERATURE CITED

1. Turnbow, James W., Matlock, Hudson, Thompson, J. Neils, Characteristics of Paper Honeycomb Under Dynamic Loading, The University of Texas Structural Mechanics Research Laboratory, Austin, Texas, 1956.

2. Hexcel Products, Inc., Energy Absorption Properties of Aluminum Honeycomb, TSB-110, Hexcel Products, Inc., Berkeley, California, 1960.

3. Unpublished Report by A. C. Marshall, Energy Absorption Properties of Honeycomb, p. 2, Hexcel Products, Inc,, Berkeley, California, 1963.

4. Ali, Ahmin, Dynamic Stress-Strain Characteristics of Various Materials, p.11, The University of Texas Structural Mechanics Research Laboratory, Austin, Texas, 1957.

(See the February, 1964 Progress Report for a complete bibliography.)

SPACE TECHNOLOGY PROJECT NO. 9

SOLUTIONS OF ELASTICITY PROBLEMS USING BOUNDARY CONDITIONS OBTAINED EXPERIMENTALLY

SOLUTIONS OF ELASTICITY PROBLEMS USING BOUNDARY CONDITIONS OBTAINED EXPERIMENTALLY

Project Investigators:

Dr. J. G. H. Thompson
Professor of Mechanical Engineering

Mr. Jerrel Boyd Jones
Assistant Professor of Electrical Engineering

I. Introduction

The purpose of this project is to establish and evaluate techniques which rely on combinations of experimental and theoretical procedures to provide rapid solutions to complicated problems of plane stress.

The procedures under investigation are:

1. The establishment of a computer program which completely evaluates the state of stress at all points, corresponding to input data in the form of boundary conditions, and
2. The investigation of various experimental techniques for evaluating these boundary conditions.

These procedures are described in detail in the following sections.

II. Status

1. A computer program has been developed and is in the process of being further refined.
2. The applicability of a lateral extensometer as a device for determining the boundary conditions has been investigated.

Several new pieces of equipment have been designed and built which have materially improved the results obtained from the extensometer.

3. A new technique involving the use of conductive sheets is under development.

4. Preliminary studies are being made for extending the present work into the areas of multiply connected and three dimensional bodies.

III. Procedure

As was previously mentioned, the purpose of this work is to develop a technique for obtaining results for complicated plane stress problem using a combination of experimental and theoretical procedures. The approach that has been taken will be described here.

For any problem of plane stress involving simply connected bodies, Laplace's equation

$$\nabla^2\theta = 0$$

must be satisfied, where θ is given by

$$\theta = (\sigma_{xx} + \sigma_{yy}),$$

σ_{xx} and σ_{yy} being mutually perpendicular normal stresses at a point in the plane. Given the proper values of θ along the boundaries, the corresponding values of θ at any interior point can be determined by a relaxation process of Laplace's equation.

The values of θ on the boundary will first be evaluated experimentally. Several methods are under investigation, two of which show a great deal of promise and will be described in this report.

A computer program has been written which will then perform the relaxation process, solving for θ at a number of interior points. The program then determines the state of stress at a number of discrete points based on the calculated values of θ and boundary values of σ_{xx}, σ_{yy}, and σ_{xy} which were part of the input data.

IV. The Lateral Extensometer

One method of determining the appropriate values of θ on the boundary is to construct a model of the stressed member, apply the corresponding loads to the model, and measure the changes in thickness of the model along its boundary. This change in thickness is related to θ by the expression

$$\theta = k\left(\frac{\Delta t}{t}\right)$$

where t and t are the original thickness and the change in thickness and k is a lateral constant given by

$$k = -\frac{E}{\mu}$$

where E is Young's modulus and is Poisson's ratio.

Such models have been tested and the changes in thickness were measured with a Hiltscher Lateral Extensometer, having a sensitivity of 10^{-7}cm. It is felt that this device yields excellent results, but the acquisition of data is very slow and requires an experienced operator. This device will be used primarily as a check for values of θ obtained in other ways.

The extensometer applied at the side of a test specimen is shown in Figure 1.

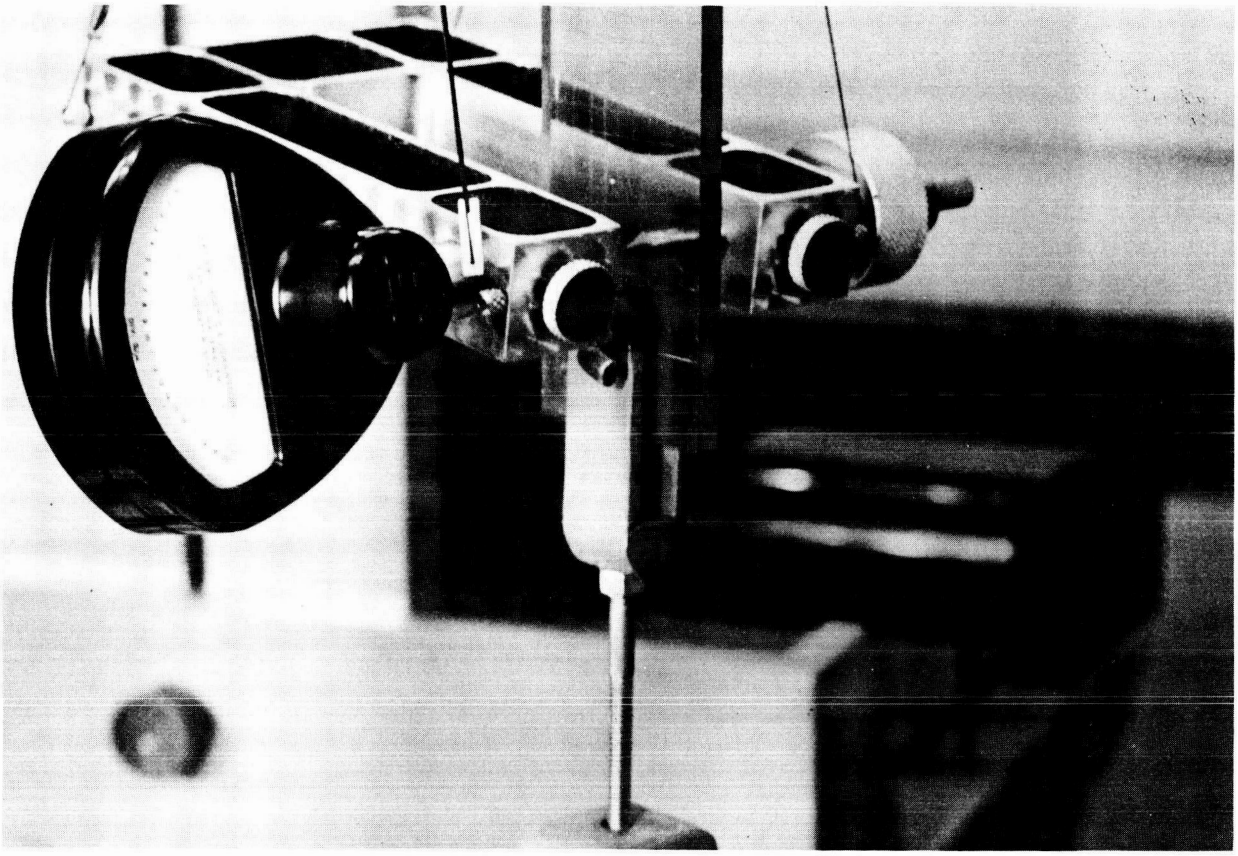

Figure 1. Close up of extersometer applied at side of test specimen.

V. The Conductive Sheet Analogy

The conductive sheet analogy experimentally determines the values of θ along the periphery of the part and at all desired interior positions in the part.

As stated earlier, θ satisfies Laplace's equation. In electromagnetic field theory, electric field problems which satisfy Laplace' equation are treated extensively. These are boundary value problems in a source-free region with conjugate function solutions. Two-dimensional electric fields are often simulated by a conduction current field in a resistive medium. In a conduction current field the scalar potential function, V, and its conjugate function, the current streamline function 1, both satisfy Laplace's equation. Thus one can see the basis for using a conducting sheet analogy in which irregularly shaped objects in plane stress may be represente by a corresponding sheet of conductive material having voltages applied such that the desired field is produced.

Most analogies of this type establish completely all boundary conditions to insure uniqueness of the field. In this present approach every effort is made to establish the unique field and this then enables one to determine values of θ on the periphery of the body being examined.

The over-all setup for the conducting sheet analogy is shown in Figure 2. This apparatus is represented schematically in Figure 7

Two distinct advantages are present in this refined measurement method. First, a highly linear potentiometer is used to set a

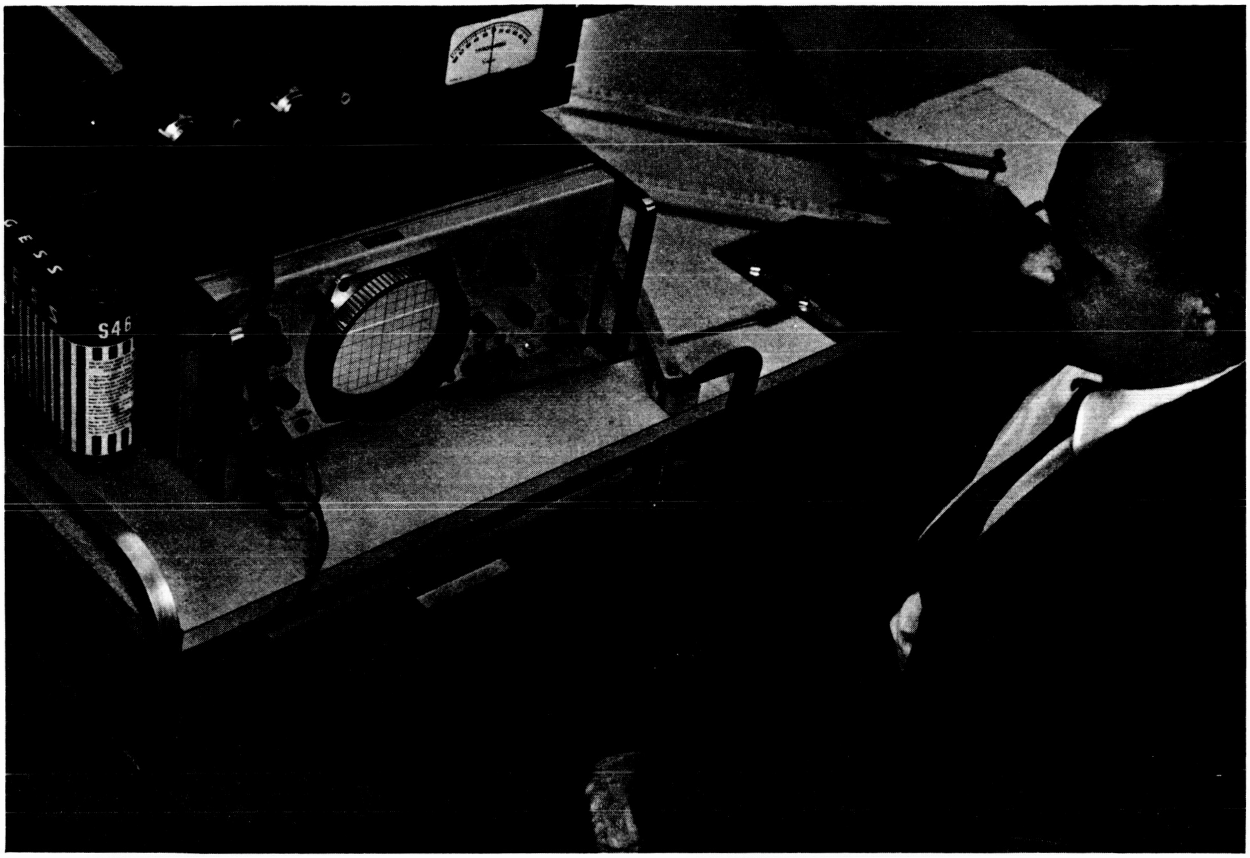

Figure 2. Plotting of equipotential lines on conducting sheet field mapping apparatus.

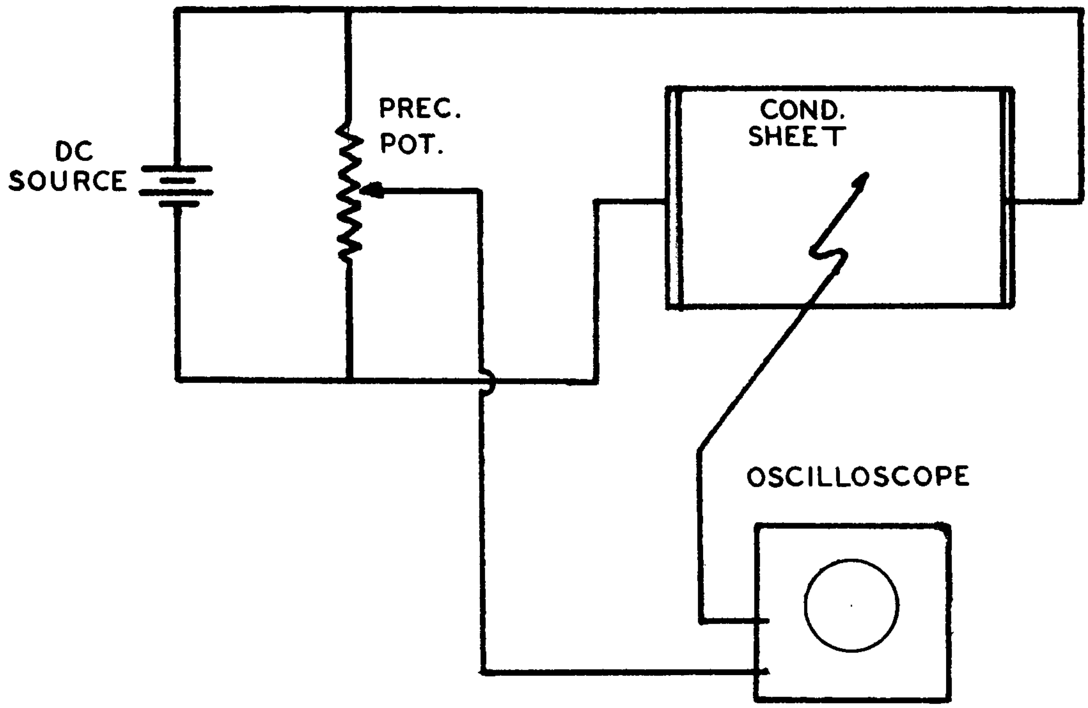

Figure 3. Schematic diagram of conductive sheet mapping apparatus.

reference level for the oscilloscope used as a detector. This heliopot establishes reference potentials on a percentage basis independent of supply voltage. The use of an oscilloscope as a d-c null-indicating device having high sensitivity and an extremely high input resistance increases the accuracy of measurements by insuring that the measuring instrument does not disturb the field to be explored.

Several novel approaches are used to establish the current density field on the conducting sheet. One of these involves the idea of conjugate functions where, for simple problems, conducting and insulated boundaries are interchanged. This enables one to obtain the streamlines directly and then rapidly compute values of θ. Any symmetry that the conducting field may possess is also used to simplify the establishment of the unique field. The principle of superposition is also applied to the scalar potential function in the sythesis of the desired field.

The preceding comments on the analogy considered that our electric field was within a source-free, isotropic, homogeneous, lossless medium. Our conduction current analog should also exhibit isotropy and homogeneity. However, commercially available conductive paper is not everywhere uniform and for this reason the resistivity measuring device shown in Figure 4 is employed. It consists of two copper buss bars spaced and insulated so as to measure the resistance (in ohms per square) of the conductive paper. When used with an ohmeter as shown in Figure 5, this device will enable one to measure

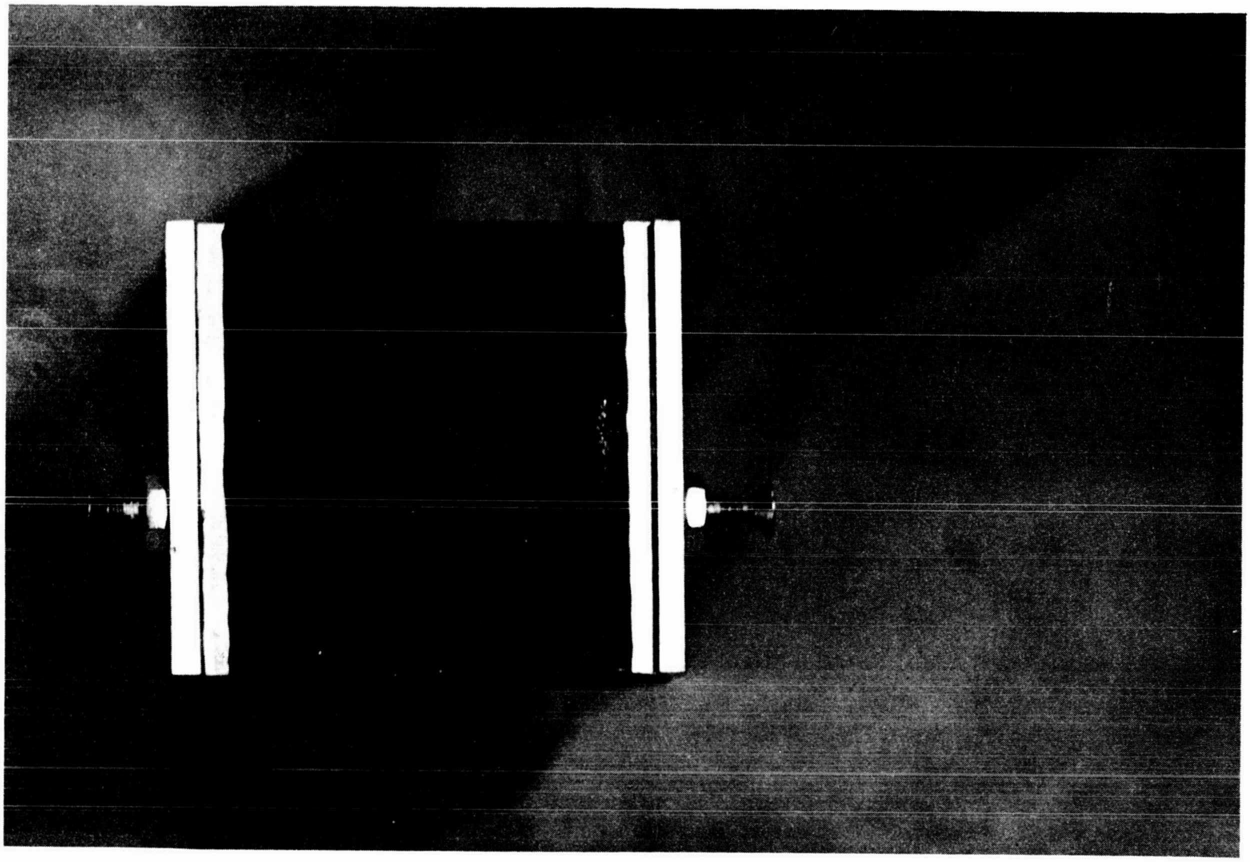

Figure 4. Close up of resistivity probe.

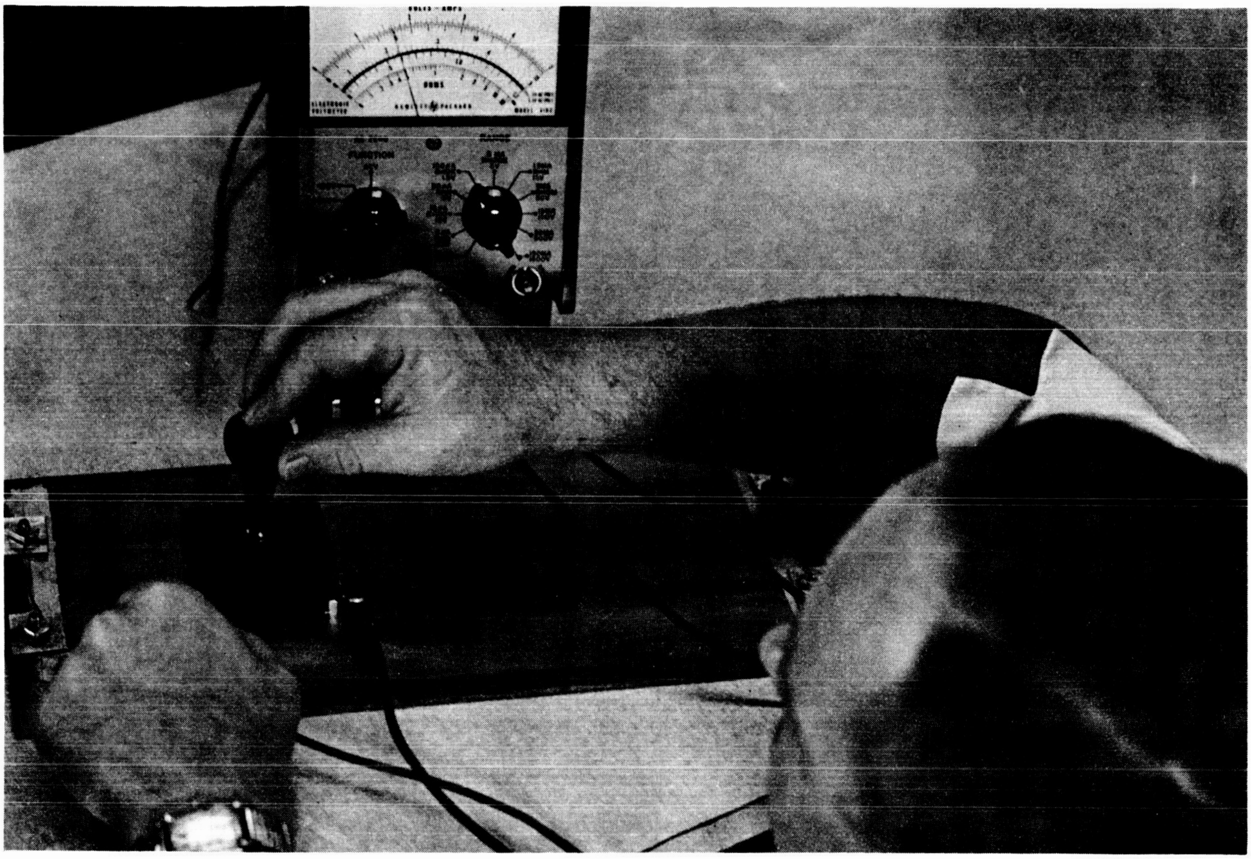

Figure 5. Operation of resistivity probe.

the uniformity of a conducting surface.

By initial measurements of voltage in a field, and by subsequent calculations, the values of θ may be obtained at all desired points of the field. We are, of course, particularly interested in determining θ along the periphery.

SPACE TECHNOLOGY PROJECT # 10

CHARACTERISTICS OF SOLID PROPELLANT OXIDIZER SUSPENSIONS

CHARACTERISTICS OF SOLID PROPELLANT OXIDIZER SUSPENSIONS

Project Investigators:

Dr. P. T. Eubank
Department of Chemical Engineering

Mr. B. F. Fort
Graduate Assistant

Mr. J. R. Brasington
Undergraduate Assistant

An experimental laboratory is under construction for research on the flow behavior of non-Newtonian liquids and suspensions.

Theoretically, the pressure drop as a function of the volumetric flow rate of a non-Newtonian fluid flowing in a circular pipe can be calculated exactly from the Rabinowitsch Equation if viscosity versus shear rate data exists for the fluid. Because the viscosity data may be accumulated at minimum expenditure of time and money, the conversion of viscosity data to pipe data is preferable to direct measurements. The conversion via the Rabinowitsch equation demands the evaluation of an integral. Numerical techniques and a digital computer are necessary to perform the integration.

Due to the numerical techniques, the computed pipe data may not be in agreement with experimental pipe data. For this reason, the method has not found widespread use. For most liquids, pipe data does not exist; converted viscosity data is considered unreliable due to errors that depend on the numerical techniques used.

It is the goal of this project to gain an understanding of the effect of numerical techniques on the data conversion outlined above. The procedure consists of:

1) Experimental measurement of viscosity as a function of shear rate for a non-Newtonian liquid or suspension.

2) Conversion of this data into computed pipe data using numerical techniques.

3) Experimental measurement of pressure drop versus volumetric flow rate in a pipe.

4) Comparison of the computed and experimental pipe data.

5) Selection of new numerical techniques if the above comparison proves unsatisfactory. Repeat Steps 2-5 until numerical methods are found that yield accurate computed pipe data.

6) Repetition of the above for other liquids. Attempt to discover numerical methods that yield accurate results with all liquids.

At the present time, a rotational Brookfield viscometer is being used for viscosity measurements (Step 1). Construction of the experimental, vertical pipe apparatus is near completion. Pressure drop as a function of time is measured by a precision quartz Bourdon tube pressure gage. Simultaneously, the volumetric flow rate, time trace may be found by weighing the liquid flowing from the pipe exit in a container. A calibrated load cell, connected under the loading platform holding the container, sends the weight, time trace to the recorder which is also following the pressure drop signal.

Conversion of literature viscosity data was performed by Mr. C. A. Osinski in a recent M.S. thesis. Also, preliminary experience was obtained in the use of various numerical techniques and how they affected the results (Step 2). Several digital computer programs were written that appear to give reasonable data conversion. However, only by experimental pipe measurement (Step 3) can the effect of numerical methods on the data conversion process be obtained quantitatively and efforts be made to minimize this effect.

SPACE TECHNOLOGY PROJECT # 11

MAGNETIC PROPERTIES OF SOLIDS

MAGNETIC PROPERTIES OF SOLIDS

Project Investigators

Dr. Charles F. Squire, Associate Dean for Science, Principal Investigator

Mr. Tom W. Adair, III, NASA Graduate Fellow

Mr. R. Zamecki, Graduate Fellow

Mr. E. Sharp, Graduate Fellow

I. Preface

With a major investment in equipment by Texas A&M University for a solid state-low temperature laboratory, and with modest funds from NASA for beginning experiments (together with a NASA fellowship for one graduate student), a new laboratory has been created which is known locally as the "NASA Low Temperature Laboratory." We describe in this progress report the work accomplished in the six months since getting NASA support and outline the vigorous program now in effect.

II. Introduction to Radiation Damage in Solids

When strong ultra-violet radiation, x-radiation, and other forms of energy flux (γ-rays, neutrons, protons, etc.) fall on a perfect crystalline solid, defects form which leave vacancies and interstitial positions may be occupied. The mechanism of defect formation presents many interesting problems[1] and experiments with

[1] A. B. Lidiard, Handbuch der Physik, Vol. 20, p. 246 (1957).

dielectric loss, nuclear magnetic resonance, and diffusion are used to obtain information. The contribution of defects to equilibrium properties such as thermal expansion, adiabatic compressibility, specific heat, etc. have been studied by Lawson[2] and others.[3] Theoretical studies[4] on the statistical mechanics of defect-containing solids have been of great interest. The practical problems of radiation damage at nuclear fission reactors, and other packaged nuclear energy sources of interest to NASA, are well known. We have made a new contribution to the field of radiation damage and this will now be briefly described. A detail paper has been submitted for publication by The Physical Review. We must seek further support for a vigorous pursuit of this promising work.

III. Magnetic Properties of Point Defects in Solid Lithium Fluoride

The new experimental observation in our laboratory concerning the magnetic properties of defects in single crystal LiF has been reported[5] by us before the American Physical Society. The magnitude of the magnetization observed in these measurements is a function of x-radiation damage producing point defects. Heat annealing the crystal can reduce the number of defects and hence reduce the

---

2 D. S. Tannhauser, L. J. Bruner, and A. W. Lawson, Phys. Rev. 102, 1276 (1956).

3 S. Mascarenhas, D. A. Wiegand, and R. Smoluchowski, Phys. Rev. 134, 481, (1964).

4 A. R. Allnatt and M. H. Cohen, J. Chem. Phys. 40, 1860, (1964).

5 C. F. Squire and T. W. Adair, Bull, Am. Phys. Soc. 9, p. 146 (1964).

observed magnetization, whereas x-radiation can increase the number of point defects and hence increase the observed magnetization. We now describe the observed magnetization on x-radiation damaged single crystal LiF of very high purity.

A right circular cylinder of a large crystal of LiF was hung along its axis of symmetry to form a simple torsion pendulum as shown in Figure 1. The crystal (3/4" diameter by 1" length) was located in a uniform and constant magnetic field at the center of a 12-inch diameter pole-face magnet. Under these conditions there would not be expected any torque arising from the diamagnetism of the specimen nor from its symmetrical shape. The experiments showed there was a torque. We summarize the following quantitative observations on several specimens of LiF:

A. The frequency of oscillation of the torsion pendulum always increased with applied magnetic field.

B. The frequency of oscillation is modulated as shown in Figure 1 by the direction which the external magnetic field makes with the crystalline axis of the specimen. The experimental curve in Figure 1 may be described by the equation:

$$\omega_B = \omega_o + \omega_1(B) + \omega_2(B) \cos 2(\theta-\phi)$$

where

- ω_B = angular frequency in a field B (radians/sec.)
- ω_o = angular frequency in zero field (radians/sec.)
- ω_1 = amplitude of increase of frequency (like a d-c bias)
- ω_2 = amplitude of modulation of frequency caused by angle between field direction and lattice axis.

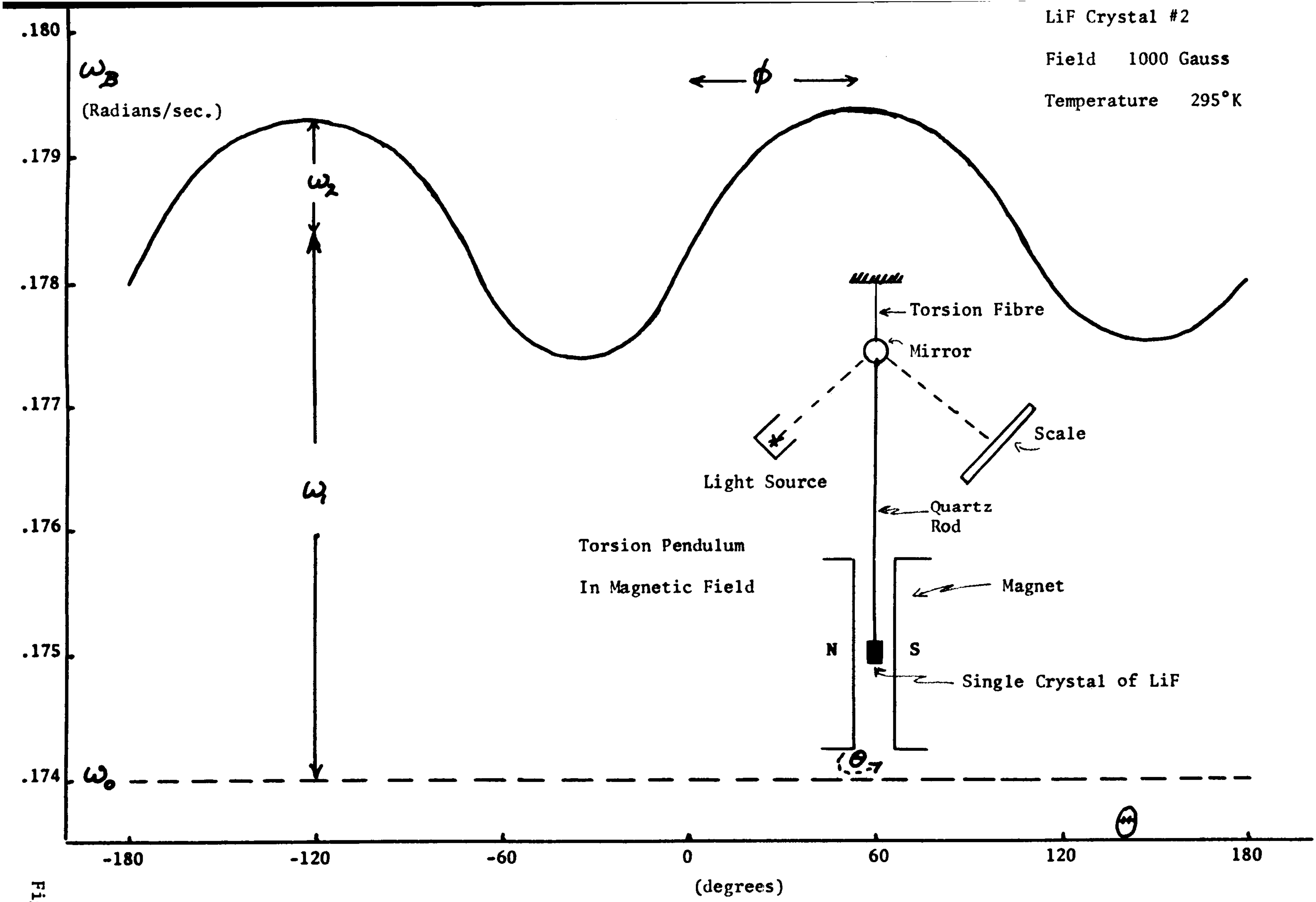

TORSION PENDULUM ANGULAR FREQUENCY
VS. MAGNETIC FIELD DIRECTION

Figure 1

ϕ = constant angle between some cubic face of the lattice structure and a fiducial mark on the cylinder specimen.

C. The values of ω_1 and of ω_2 depend upon the strength of the steady magnetic field, B. These quantities are independent of temperature in going from $300^{o}K$ down to $80^{o}K$. These quantities (ω_1 and ω_2) increase for a given specimen with soft x-ray radiation and they may be decreased with heat annealing above $500^{o}K$. Therefore they are functions of the number of lattice defects having a magnetic moment.

D. The magnetic moment produced by trapped electrons at some lattice defects (either at vacancies or at interstitials), the cooperative way in which these interact to give a net magnetization, M, which is locked to the crystalline lattice in a very special way--all of these are details which must be explored with further research.

Needless to say, great care has been taken to insure that the physical effects described are properties of the LiF specimen and not of the measuring equipment.

IV. Present Research Program on Magnetic Properties of Radiation Damaged at Low Temperatures.

The possibilities opened up for contributions to our basic understanding of lattice imperfections due to radiation damage are as follows:

A. Experimental studies on defect formation through radiation by x-rays, γ-rays, neutrons, and protons can be made with this new technique of magnetic studies. A program of intensive exploration with several graduate students and with use of our nuclear reactor is now going on. The radiation damage by a proton beam (of the energy encountered in space exploration--say, 50 MeV) will be explored when our new cyclotron facility is completed.

B. Quantitative exploration of soft x-ray produced defects in solid single crystals of LiF when bombarded at temperatures between $30^{o}K$ and $300^{o}K$. Speical equipment[6] has been purchased for these studies. A defect produced at low temperatures stays put in the lattice.

C. Exploration of the details of the magnetization effects discussed above. Studies in low magnetic fields of the Order 0 to 200 Gauss are planned using air coils[7] for small homogeneous fields. Extension to other alkali halides such as KCl and NaCl is proposed. The possibility of an integrating radiation detector would seem to exist.

V. <u>Present Research on Radiation Damage in Solids by Ultrasonic Velocity and Attenuation Studies.</u>

Our research know-how[8] has been developed along the lines of the measurement of ultrasonic velocity and attenuation of sound waves in solids as a function of temperature between $2^{o}K$ and $300^{o}K$.

---

6 Cryo-tip Refrigerators by Air Products & Chem. Co., (Allentown, Penna.)

7 M. E. Pittman and D. L. Waidelich, NASA Tech. Note D-2095.

8 C. F. Squire and co-authors including thesis work:
Phys. Rev., **106**, 1175 (1957).
Physica, **25**, 111 (1959).
Phys. Rev. **112**, 45 (1958).
Phys. Rev. **117**, 709 (1960).

From the velocity of longitudinal and of transverse waves, one can compute the elastic constants of simple, single crystals. These tensor-like quantities can be averages to give a measure of the elastic strength of the solid. Changes brought about by extensive radiation damage in the strength of a solid to resist elastic deformation are well known to many engineers and solid state scientists. With the possibility of starting with nearly perfect crystals and progressively producing point defects by radiation, we propose to examine (or re-examine in some cases) the effect on velocity and attenuation of 45 mc/sec. sound waves. As stated in the introduction, our objectives would be a deeper basic understanding of the mechanisms of defect formation.